SOIL DEGRADATION, THRESHOLDS AND DYNAMICS OF LONG-TERM CULTIVATION: FROM LANDSCAPE BIOGEOCHEMISTRY TO NANOSCALE BIOGEOCOMPLEXITY

A Dissertation

Presented to the Faculty of the Graduate School

of Cornell University

In Partial Fulfillment of the Requirements for the Degree of

Doctor of Philosophy

by

James Mukidza Kinyangi

January 2008

SOIL DEGRADATION, THRESHOLDS AND DYNAMICS OF LONG-TERM CULTIVATION: FROM LANDSCAPE BIOGEOCHEMISTRY TO NANOSCALE BIOGEOCOMPLEXITY

James Mukidza Kinyangi, Ph. D.

Cornell University 2008

In degrading tropical soils, carbon and nutrient exports represent a significant modification to global biogeochemical cycles. We assessed soil C and nutrient losses on 122 cultivated agricultural fields from three 100-yr chronosequence sites in western Kenya. During cultivation, C stocks and soil nutrients (N, P, K Ca and Mg) were rapidly lost from the surface soil after 15-36 years of continuous cropping. A lag phase was expressed in the half life kinetics between C decline and Ca and Mg rates. For all sites, crop C_4 –C gains offset between 15 to 34 % of the C losses but more than two thirds of the native forest C_3 –C was lost during 100 years of cropping. Heavy-textured Nandi soils cascaded from high to medium and low C stocks and nutrient equilibria, while medium-textured Kakamega soil, which already had lower nutrient contents instead transitioned from medium to low equilibrium of C stocks. By separating three SOM pools assigned to distinct soil functions as indicators of thresholds, we determined that nearly all C (13.6-24.3 g kg^{-1}) and N (1.5-3.1 g kg^{-1}) contents in the unstable and stable aggregate pools was lost 15 to 36 years after forest conversion. Long-term changes in the unstable and stable aggregate pool were characterized by rapid initial losses that reached equilibrium, a wide C:N ratio (19.3 and 18.3 respectively) and little $\delta^{15}N$ isotopic shift (<1.0 ‰). In contrast, the stable organomineral pools constituted large C and N contents which sustained

only gradual non-equilibrium decay behavior. This large pool had a narrow C:N ratio with a strong enrichment of $\delta^{15}N$ (1.7 to 3.5‰). Continuing C and N content decline at equilibrium were linear and the severe loss of stable aggregate C and N was an indicator of low stabilization of organic matter. The long-term cultivation loss of C and soil nutrients was therefore driven by land use changes from C and nutrient-rich tropical rain forest to low equilibria of C and nutrient-poor degraded soil

BIOGRAPHICAL SKETCH

James was raised the son of a farmer in the agricultural region of western Kenya. His mother was a career teacher. James developed early interest in learning and practicing agricultural skills. After high school he went on to enroll for a diploma in farm management at Egerton University in the rift valley region of Kenya. Upon completion, James worked for the government agriculture extension service, training farmers on how to manage land for better incomes. He also served as manager for the government demonstration farm in Kisumu, Kenya.

James went on to pursue a career in research as a technician working with the joint KEFRI-KARI-ICRAF project in Kenya. In 2000 he earned his Masters in Soil and Crop Science from Michigan State University. James then worked for TSBF-Afnet; a soil biology and fertility network in Nairobi, Kenya. He helped train national agricultural research scientists to model long term crop and soil data sets. This was in addition to conducting research on the applications of organic and inorganic inputs to agricultural soil. For his PhD at Cornell, James was part of the Biocomplexity in the Environment team of faculty and students studying the impact of degrading soils on rural poverty and the environment in Sub-Saharan Africa. His research was supervised by J. Lehmann. James is married to Millicent and they have 3 daughters, Sandra, Valessa, and Barbara.

To my wife Millicent, our three loving daughters, Sandra, Valessa and Barbara, my parents Richard and Dorcas, and to my brothers and sisters

For all your patience, it is truly deserved

ACKNOWLEDGMENTS

This study was funded by the Coupled Natural and Human Systems Program of the Bio-complexity Initiative of the NSF under grant BCS-0215890. The NEXAFS spectra were obtained from the National Synchrotron Light Source (NSLS), Brookhaven National Laboratory, at the Beam line X-1A1 developed by the research group of Janos Kirz and Chris Jacobsen at SUNY, Stony Brook, with support from the Office of Biological and Environmental Research, U.S. DoE under contract DEFG02-89ER60858, and the NSF under grants DBI-9605045 and ECS-9510499. The μ-FTIR spectra were obtained from the National Synchrotron Light Source (NSLS), Brookhaven National Laboratory, at the Beam line U-10B. Omnic Software support assistance was provided by Randy Smith. XPS measurements were conducted at the Wiley Environmental Molecular Sciences Laboratory.

I would like to sincerely recognize the guidance, counsel and support from my advisor, Johannes Lehmann, and to my committee, J Thies and A Pell. Thank you to the soil biogeochemistry laboratory group at Cornell. Also D Solomon, S Ngoze and B Liang. Many thanks to the great NSF-Cornell biogeocomplexity research group and particularly A Pell, L Verchot, S Riha and C Barrett. To the Rockefeller student group, staff at the World Agroforestry Center, thank you. Many thanks to Joseph Njeri, Lawrence Lanogwa and Wilson Okila for help in soil sample procurement. I also thank Brett Gleitsmann, Benjamin Amadalo, Lod Mise, Charles Mwoshi, Mr. Murgong, Hon. Daniel Otiende Mr. arap Maziwa and Mr Kima for maps and assistance in locating forest and agricultural sites, establishing land cultivation ages and reconstruction of land use histories. I acknowledge support from the Kenya government ministries of Agriculture, Livestock and Environment and Natural Resources in Nandi, Vihiga and Kakamega districts.

TABLE OF CONTENTS

BIOGRAPHICAL SKETCH iii
DEDICATION iv
ACKNOWLEDGMENTS v
LIST OF FIGURES viii
LIST OF TABLES xii

CHAPTER 1. STUDY BACKGROUND AND MOTIVATION 1
References 3

CHAPTER 2. LONG-TERM DEGRADATION AND EQUILIBRIUM DYNAMICS OF CARBON AND NUTRIENT LOSSES IN TROPICAL SOIL 4
Abstract 4
1. Introduction 5
2. Materials and methods 7
3. Results 16
4. Discussion 25
5. Conclusions 35
References 37

CHAPTER 3. LONG TERM CHANGES IN SOIL ORGANIC MATTER POOLS AS INDICATIORS OF THRESHOLDS IN TROPICAL AGROECOSYSTEMS 45
Abstract 45
1. Introduction 46
2. Materials and methods 48
3. Results 56
4. Discussion 63
5. Conclusions 72
References 74

CHAPTER. 4. MOLECULAR ALTERATTION OF MICROAGGREGATE ORGANIC MATTER AND MINERAL FORMS IN LONG TERM CULTIVATED SOIL. 81
Abstract 81
1. Introduction 82
2. Materials and methods 84
3. Results and discussion 87
4. Conclusions 103
References 105

CHAPTER 5.NANOSCALE BIOGEOCOMPLEXITY OF THE ORGANO-MINERAL ASSEMBLAGE IN SOIL: APPLICATION OF STXM MICROSCOPY AND C 1s-NEXAFS SPECTROSCOPY 114
Abstract 114
1. Introduction 115
2. Materials and methods 117
3. Results and discussion 124
4. Conclusions 142
References 144

CHAPTER 6.SUMMARY AND CONCLUSIONS 151

Appendix A 153

LIST OF FIGURES

Figure 2-1. Soil bulk density (ρ_b), changes to show the increase in the ρ_b of surface soils (0-0.10 m), as a result of conversion from native forest to cereal crop cultivation, n = 53. The exponential rise equations describe non-linear changes for, medium-textured Kakamega; $\rho_b = 0.76 + 0.44 \times(1\text{-}e^{0.06years})$; heavy-textured South Nandi $\rho_b = 0.56 + 0.53 \times(1\text{-}e^{0.22years})$ and heavy-textured North Nandi $\rho_b = 0.46 + 0.54 \times(1\text{-}e^{0.06years})$ sites. 8

Figure 2-2. Geographical locations of research sites across the study area for the Kakamega-Nandi forest margins and adjacent fields (+). The settlement corridor separating the once contiguous forest system is ~20 km wide. Sites to the Northeast margin of the South Nandi forest are part of the North Nandi chronosequence due to their similarity in elevation, temperature and rainfall. 12

Figure 2-3. Long-term effects of permanent cereal cropping on carbon (C) and nitrogen (N) stocks in surface (0-0.12 m, 0-0.11 m and 0.10 m) soil. Initial reference values are determined from the original native forest soil C stocks. Bars are ± 1 standard error of the mean for each age group of fields. For South Nandi n = 39; North Nandi n = 48 and Kakamega n = 35 19

Figure 2-4. Long-term shift in the isotopic compositions of $\delta^{13}C$ and $\delta^{15}N$ of cultivated (0-0.10 m) soils. Reference values of the $\delta^{13}C$ and $\delta^{15}N$ are from the source litter biomass of the original forest (-27.8 ‰, n = 4) and crop surface litter in cultivated soils are: South Nandi; -17.5 ‰, n = 39; North Nandi; 18.5 ‰, n = 48 and Kakamega; -19.7 ‰, n = 35. Bars are ± 1 standard error of the mean for each age group of fields. 20

Figure 2-5. Isotopic dynamics of forest and cereal crop sources of nitrogen (N) during long-term soil degradation. Changes in the N stocks (a), soil C/N ratio (b) and $\delta^{13}C$ (c) in relation to the $\delta^{15}N$ enrichment. 23

Figure 2-6. The long-term contribution of C_3, forest and C_4 cereal crop C sources to the soil C stocks during soil degradation. 24

Figure 2-7. Base cation ($mmol_c\ kg^{-1}$) dynamics of tropical soil following conversion from forest to continuous cereal cropping. 27

Figure 2-8. Effect of long-term cereal cropping on pH to show site differences in the soil buffering capacity. For heavy-textured North Nandi, the pH declined following exponential decay; $pH = 6.07 + 1.33e^{-0.063years}$. At the heavy-textured South Nandi and medium-textured Kakamega sites, a linear decrease in the pH is given by equations, $pH = 6.16e^{-0.0096years}$ and $pH = 6.10e^{-0.0057years}$ respectively. Significance levels are designated as (0.05*; 0.01** and <0.0001***). 28

Figure 3-1. Digital and light microscope images of soil from (a) native forest and (f) agriculture ecosystem as well as their respective surface litter fractions (b & g). After density and physical separation, free light fractions comprise recognizable plant debris (c, & h) whilst intra-aggregate fractions appear as finely divided, darker and more decomposed (d & i). The organomineral is darkest in color and represents the most highly decomposed C fraction (e & j) 55

Figure 3-2. Long-term changes of C contents in soil organic matter fractions of ecosystem sites (a) north Nandi, (b) south Nandi and (c) Kakamega, western Kenya. Model: $y = y_o + a \times exp^{-bx}$ (unstable, stable aggregate) and $y = a \times exp^{-bx}$ (stable organomineral) Significance level designated as 0.05*; 0.01** and <0.0001***. 58

Figure 3-3. Sources of C_3 forest and C_4 crop C (%) as a result of switching $\delta\ ^{13}C$ values in soil organic matter fractions of ecosystem sites (a) north Nandi, (b) south Nandi and (c) Kakamega, western Kenya 60

Figure 3-4. Long-term changes of N contents (g kg^{-1}) in soil organic matter fractions of ecosystem sites (a) north Nandi, (b) south Nandi and (c) Kakamega, western Kenya. Model: $y = y_o + a \times exp^{-bx}$ (unstable, stable aggregate) and $y = a \times exp^{-bx}$ (stable organomineral). Significance level designated as 0.05*; 0.01** and <0.0001***. 61

Figure 3-5. Isotopic $\delta\ ^{15}N$ values as a result of switching sources of N in soil organic matter fractions of ecosystem sites (a) south Nandi, (b) north Nandi and (c) Kakamega, western Kenya. 64

Figure 3-6. Semi-log plot of soil C and N losses and the equilibrium C:N ratio of organic matter fractions from forest (0-0.12 m) and agroecosystem sites (0-0.11 m, 0-0.10 m), western Kenya. 67

Figure 3-7. Declining total soil C and N concentration (g kg^{-1}) in whole soil of forest (0-0.12 m) and agroecosystem sites (0-0.11 m, 0-0.10 m), western Kenya. 70

Figure 4-1. Electron transitions in the molecular functional forms; (a), C 1s binding energy for C–C, C–H (284.6 eV), C–N, C–O (286.4 eV), C=O (287.6 eV) and COOH (289.1 eV); (b) O 1s binding energy for C=O interaction with kaolinite (531.8 eV) and (c) N 1s binding energy of aromatic amide (398.7 eV, 399.4 eV) and peptide N (399.8 eV). 90

Figure 4-2. Wide scan spectra of the surface electron transition in the binding energy of mineral elements, Al2p, Al2s, Si2p and Si2s of kaolinite. (a). The auger MgKLL and Ca2p transitions exhibit a double peak feature especially after 2 years of cultivation (b). Microaggregate surface Mg and Ca forms appear to be of organic origin as they are almost entirely degraded after 104-yr long-term alteration. 92

Figure 4-3. Absorbance chemigrams of infrared vibrational mode features unique to C bonding with N, O and H in kaolinitic mineral soil. Soil microaggregate physical video image (3a –iv, 3b –iv, 4c –iv) and chemical profile mapping (3a –ii, iii, v & vi; 3b –ii, iii, v & vi; and 3c –ii, iii, & v) show the distribution of C, N and kaolinite –OH forms. Figures correspond to (a) forest (b) 2-yr cultivation and (c) 104-yr old kaolinitic soil after long-term cultivation. The red (+) sign is a visual reference for organic matter "hot spots" 95

Figure 4-4. Infrared absorption bands assigned to organic matter and kaolinite –OH vibrations from the inner matrix (A) and outer surfaces (B) of microaggregates in kaolinite soil. Figures correspond to (a) forest (b) 2-yr cultivation and (c) 104-yr old kaolinitic soil after long-term cultivation. 97

Figure 4-5. Effect of long-term cultivation on kaolinite –OH outer to inner surface absorbance near 3695 cm^{-1} and 3622 cm^{-1} in relation to enrichment of C–OH (n = 9) and –CH (n = 10) molecular forms of MOM from "hot spots" mapped in Fig 4. Dotted line represents changes to outer to inner kaolinite –OH surface ratio of 1.0 100

Figure 5-1. Conceptual framework for the interplay between minerals, organic matter, and pore space determining the C stabilization in the soil organo-mineral assemblage. 125

Figure 5-2. STXM micrographs for an interior aggregate region taken below 281 eV (a) and above 290 eV (b) the carbon absorption edge. Contrast in the C and mineral density is shown in the ratio micrographs (c) calculated from –log [I/I*o*] where I = Σ (281 eV-282 eV) and I*o* = Σ (290 6 eV-291.5 eV). 126

Figure 5-3. STXM micrographs for an exterior aggregate region taken below 281 eV (a) and above 290 eV (b) the carbon absorption edge. Contrast in the C and mineral density is shown in the ratio micrographs (c) calculated from –log [I/I*o*] where I = Σ (281 eV-282 eV) and I*o* = Σ (290 6 eV-291.5 eV). 128

Figure 5-4. Cluster pixel plots of components 2 and 3 show spectral characteristics of mineral and organic matter, color-coded for each cluster (color legend on top axis). Yellow color represents mineral cluster pixels separated from cluster pixels of organic and organomineral complexes by the blue (a) and green (b) clusters of pore space pixels. Pixel separation with an OD gradient (axis component 2), distinguishes C chemical species in the organic or organo-mineral matter, and is noticeable only in (a) but not (b) on axis component 3. 130

Figure 5-5. Composition thickness maps of the main thematic regions in the interior of a micro-aggregate. Composition maps show bright white regions of minerals (a), organomineral complexes of carboxylic-C forms (b), organomineral coatings of aromatic, aliphatic-C forms (c), and particulate forms of aromatic-aliphatic-C (d). Red arrows show small nanometer pores in mineral matrix. Blue arrows point at small nanometer pores in organomineral complex. 131

Figure. 5-6. Spectral signatures of the composition thickness maps of the interior area shown in Figure 5, with both uncorrected PS-I*o* (a, b, c, and d) and CM-I*o* corrected spectra (e, f, g, and h). Spectra (a) and (e) refer to mineral and pore space signatures, respectively. Spectra b and c show elevated OD as a result of absorbance by mineral matter. Residual errors for the fitted spectra e, f, g and h are shown with their root variance, σ. 134

Figure 5-7. Composition thickness maps of the main thematic regions at the exterior of a micro-aggregate. Composition maps show bright white regions of minerals (a), organomineral complexes of carboxylic-C forms (b) and organomineral coatings of aromatic, carboxylic-C forms (c). Red arrows show small nanometer pores in mineral matrix. Blue arrows point at small nanometer pores in organomineral complex. 139

Figure 5-8. Spectral signatures of the composition thickness maps of the exterior area shown in Figure 7, with both uncorrected PS-I*o* (a, b and c) and CM-I*o* corrected spectra (d, e and f). Spectra (a) and (d) refer to mineral and pore space signatures, respectively. Spectra (b), (c), (e) and (f) show elevated OD as a result of absorbance by mineral matter. Residual errors for the fitted spectra (d), (e) and (f) are shown with their root variance, σ. 141

LIST OF TABLES

Table 2-1. Site physical and chemical characteristics of the surface soils (0-0.12 m) at three forest reference sites of the Kakamega-Nandi forest margins, western Kenya 10

Table 2-2. Non-linear regression for soil C (carbon) and N (nitrogen) degradation equilibria of tropical soil (0-0.12, 0-0.10 m) as a function of time under long-term cropping in western Kenya. Model; $y = y_o + a \times \exp^{-bx}$ 17

Table 2-3. Non-linear regression for N nitrogen sources and stock changes during long-term cropping in heavy-textured Nandi and medium-textured Kakamega highland soils (0-0.10 m), western Kenya. Model; $y = y_o + a \times (1 - \exp^{bx})$ 22

Table 2-4. Non-linear regression for soil P (mg kg^{-1}) and base cation ($mmol_c$ kg^{-1}) degradation equilibria in soil (0-0.10 m) during long-term cropping, western Kenya. Model; $y = y_o + a \times \exp^{-bx}$. and $^{\ddagger}y = a \times \exp^{-bx}$ 26

Table 3-1. Location and select properties of the reference forest ecosystem sites, western Kenya. 50

Table 3-2. Litter chemical characteristics (± s.e.) of organic matter inputs to forest and agroecosystem sites, western Kenya 57

Table 4-1. X-ray photoelectron spectroscopy (XPS) elemental composition, atomic mass ratios of aggregate surface and bulk soil 89

Table 4-2. Infrared (FTIR) peak assignment for carbon (C) and nitrogen (N) forms in soil 94

Table 5-1. Relationships between aggregate features, optical densities (OD) and the C compositional expression from spectral signal dominance of the interior and exterior regions of a soil microaggregate 123

Table 5-2. Photon energy (eV) peak resonance assignment for organic C functional forms obtained from near edge absorption fine structure (NEXAFS) spectroscopy 137

CHAPTER 1

STUDY BACKGROUND AND MOTIVATION

The loss of soil ecosystem function leads to permanent land-use changes brought about by soil degradation (Sanchez, 1983). These changes affect not only the global C balance but also the ability of local farmers to make decisions about soil organic matter management. The interplay between long-term agriculture and the agroecosystem responses to productivity in a changing climate is one of the key challenges threatening the human population. In the tropical forest margins of western Kenya, slash and burn agriculture is a common farming practice.

In these forest margins, transformations of C and nutrient losses are the direct effect of continuous cultivation without adequate soil amendments. For non-degraded soils, organic matter quality controls the ecological function of C as a source of energy for microbial populations and mineralization of N (Verchot et al., 2006) which in turn affects microbial biomass When native forest soils degrade, their rehabilitation through nutrient replenishments may be achieved using organic amendments. However, where land use includes continuous crop production, these soils continue to suffer widespread nutrient deficiencies of N, P and base cations, Ca, Mg and K (Hartshorn et al., 2006) the soil response to recovery may be a function of their degraded status. Therefore, we need to better understand the long-term degradation pathways by examining the dynamic linkage between the rate processes determining the equilibrium dynamics of degrading C stocks and declining nutrient contents since forest conversion.

Global estimates of changes in the soil stocks of C and N are inferred from their content in soil organic matter (SOM) but long-term turnover is often simulated from model calculations (Six et al., 2002) after accounting for the residence times of

different C pools. To some extent, these calculations allow us to investigate the biochemical controls of C and N pool transformations but model estimates often fail to account for differences in C stabilization due to the physical order of the soil organomineral assemblage which determines accessibility of the decomposing SOM (Gregorich et al., 2006). For this reason, conceptual model approaches may not be appropriate in explaining functional relationships in the long-term degradation of SOM.

Through fractionation, the removal of organic matter particles in discrete compartments that have distinct chemical reactivity permits us to draw inferences about their ecosystem function as soil ecological indicators of thresholds following land use change (Liefield et al., 2005). Since soils are a part of the ecological system we hypothesize that thresholds can be deduced from sudden and abrupt changes in non-linear trends (Groffman et al., 2006) which describe different ecosystem equilibria. Therefore we can assess long-term changes to C and N stocks in SOM pools as indicators of thresholds in tropical degrading soil to determine the effect of organic matter loss on agroecosystem functions

Long-term stabilization of soil organic matter (SOM) is controlled by structural configurations in the organo-mineral assemblage of soil microaggregates (Tisdall, 1996) Current soil aggregation models explain organomineral interaction through correlation between mineral surface area. The usefulness of such correlations in predicting the functional distribution of soil C remains undemonstrated. In this study, we additionally propose to use synchrotron microspectroscopy to probe the carbon chemistry and its spatial molecular evolution in kaolinitic soil from native Kakamega-Nandi forests and long-term agricultural cultivation sites.

REFERENCES

Gregorich, E.G., M.H. Beare, U.F. McKim, J.O. Skjemstad. 2006. Chemical and biological characteristics of physically uncomplexed organic matter. Soil Sci. Soc. Am. J. 70:975–985.

Groffman, P. M., J. S. Baron, T. Blett, A. J. Gold, I. Goodman, L.H. Gunderson, B. Levinson, M. Palmer, H.W. Paerl, G.D. Peterson, N. LeRoy Poff, D.W. Rejeski, J.F. Reynolds, M.G. Turner, K.C. Weathers, and J. Wiens. 2006. Ecological thresholds: the key to successful environmental management or an important concept with no practical application? Ecosystems 9:1–13.

Leifeld, J., and I. Kögel-Knabner. 2004. Soil organic matter fractions as early indicators for carbon stock changes under different land-use? Geoderma 124:143–155.

Hartshorn, A. S., O. A. Chadwick, P. M. Vitousek, and P. V. Kirch. 2006. Prehistoric agricultural depletion of soil nutrients in Hawai'i. Proceedings of the National Academy of Sciences of the United States of America 103; 11092–11097.

Sanchez, P. A. 1983. Soil fertility dynamics after clearing a tropical rainforest in Peru. Soil Science Society of America Journal 47: 1171–1178.

Six, J., R.T. Conant, E.A. Paul, and K. Paustian. 2002. Stabilization mechanisms of soil organic matter: Implications for C-saturation of soils. Plant Soil 241:155–176.

Tisdall, J.M., and J.M. Oades. 1982. Organic matter and water-stable aggregates in soils. J. Soil Sci. 33: 141–163.

Verchot, L. V., L. Hutabarat, K. Hairiah, and M. van Noordwijk. 2006. Nitrogen availability and soil N2O emissions following conversion of forests to coffee in Southern Sumatra. Global Biogeochemical Cycles 20, GB4008, doi:10.1029/2005GB002469.

CHAPTER 2

LONG-TERM DEGRADATION AND EQUILIBRIUM DYNAMICS OF CARBON AND NUTRIENT LOSSES IN TROPICAL HIGHLAND SOIL

Abstract

In degrading tropical soils, carbon (C) and nutrient exports represent a significant modification to global biogeochemical cycles. We assessed soil C and nutrient losses on 122 cultivated agricultural fields from three chronosequence sites in western Kenya, following <3, 3-9, 10-22, 23-34, 35-57, 58-83 and 84-114 years since forest conversion. Medium-textured Kakamega and heavy-textured North and South Nandi forest soils have accumulated large C (4.2 to 7.3 kg m^{-2}) and N (0.5 to 0.7 kg m^{-2}) stocks in their surface soil to a depth of 0.12 m. During cultivation, C stocks and soil nutrients (N, P, K Ca and Mg) were rapidly lost from the surface soil in the initial 15-36 years of continuous cereal cropping. The expression of a lag phase in the half life kinetics indicated uncoupling effects between C decline and Ca and Mg rates of loss following forest conversion. Soil pH of the native forest sites was near neutral (6.0 to 7.5) and appeared well buffered against acidity at North Nandi. During cultivation, soils at South Nandi and Kakamega sites showed a small linear increase in acidity (≤ 1.0 pH unit change). At the degradation equilibrium, C and N stocks at the heavy-textured North Nandi site were two-fold higher than at both heavy-textured South Nandi and medium-textured Kakamega sites. For all sites, crop C_4 –C gains offset between 15 to 34 % of the C losses but more than two thirds of the native forest C_3 –C was lost during 100 years of cropping. We demonstrate that degrading heavy-textured tropical highland cultivated soils cascade from high to medium and low C stocks and nutrient equilibria, while medium-textured soil, which

already has lower nutrient contents; instead transitions from medium to low equilibrium of C stocks. During this process, the biogeochemistry of C and soil nutrients was driven by land use changes from C and nutrient-rich tropical rain forest to different equilibria of uncoupled C and nutrients in degraded soils.

1. Introduction

The loss of soil ecosystem function leads to permanent land-use changes brought about by soil degradation (Murdiyarso and Wasrin, 1995; Sanchez, 1983; Post and Kwon, 2000), Establishment of permanent agriculture from native tropical forest conversion can be described as a three step process (Woomer et al., 1994). After forest harvest, cultivation accelerates the depletion of soil organic matter (SOM), as nutrients held in decomposing forest litter are mineralized (Juo and Manu, 1996; Conant et al., 2004). After the initial rapid mineralization, soil nutrients may be taken up by crops or lost from the soil ecosystem through other pathways such as leaching or erosion (Townsend et al., 1995; Hughes et al., 2000). The nutrients involved during the phases of rapid mineralization and crop uptake or loss to the systems are primarily from litter biomass previously accumulated from the native forest vegetation. Before deforestation, the initial state reflects the original equilibrium between organic and inorganic nutrient fluxes within the landscape (Palm et al., 1996). Nutrient cycling in litterfall and SOM is frequently assessed to explain the biogeochemistry of tropical forest ecosystems (Edwards, 1982; Vitousek, 1984). A general assertion is that nutrient cycling in tropical lowland forests is limited by N while highland forests are limited by P (Davidson et al., 2004; Tanner et al., 1998).

Transformations of C and nutrient losses are the direct effect of continuous cultivation without adequate soil amendments. In non-degraded soils, organic matter quality and clay mineralogy control the ecological function of C as a source of energy

for microbial populations and mineralization of N (Verchot et al., 2006) which in turn affects microbial biomass (Lal, 2004). In addition, SOM is also an important source of variable negative charge and buffer capacity (Sollins et al., 1988), of inorganic nutrients (Vitousek and Sanford, 1986). When tropical soils degrade, their rehabilitation through nutrient replenishments is primarily achieved when organic C and N is incorporated in crop biomass (Smith, 2005). However, where land use includes continuous crop production, these soils continue to suffer widespread nutrient deficiencies of N, P and base cations, Ca, Mg and K (Hartshorn et al., 2006). In tropical agriculture, questions remain whether long-term C and N recovery in SOM can be achieved with sole additions of organic resources, which appear to be influenced by other nutrient elements (van Groenigen et al., 2006).

In tropical rain forests, soil C and N stocks are maintained through annual inputs of leaf litter fall and root turnover (McGrath et al., 2000) and the nutrients required for tree growth are derived from recycled elements, from mineralization of forest litter and also from atmospheric inputs. The amounts of biomass and mineral nutrients returned to the soils are much lower in agricultural cropping systems than in forests (Palm et al., 1996). For organic matter losses, C may be respired as CO_2 or exported in leachate as dissolved organic and inorganic C (Johnson et al., 2006). After deforestation and burning, the inorganic N (Matson et al., 1987) and base cation status of tropical soils are often elevated particularly for K (Edwards, 1982). In the moist tropics, these nutrients are vulnerable to leaching from the surface soils when their flux exceeds the capacities for soil retention and crop uptake (Krull et al., 2002).

Human settlements profoundly modify elemental cycles by mining nutrients to support agricultural production (Hartshorn et al., 2006). The rate and extent of nutrient depletion of a particular soil depends on its mineralogical composition, pH and CEC conditions, as well as other mitigating climatic factors (Austin and Vitousek, 1998). In

forest soils, mineralization and immobilization reactions may support close coupling of C and nutrient cycling (Wang et al., 2007) whereas the removal of forest biomass causes large nutrient losses due to uncoupling effects following conversion (Johnson et al., 1997). Tropical soils may therefore continue to sustain close coupling between C and nutrient losses during long-term degradation, (Richter et al., 2000). In this study, our objective was to investigate the dynamic linkage between the rate processes determining the equilibrium dynamics of degrading C stocks and declining nutrient contents since forest conversion. In this approach we also examined whether a close coupling exists, where the long-term decline in soil C stocks is associated with other soil nutrient losses following tropical deforestation.

2. Materials and Methods

2.1 Experimental Study Sites

Three chronosequences of soil degradation were established with 122 agricultural fields on highly weathered soils covering 800 km^2, along the Kakamega and Nandi forest margins in Kenya (Figure. 1). Both forest ecosystems form the eastern boundary of the once contiguous rainforest and they are among the last remnants of pristine tropical rainforests currently existing in this intensely cultivated region (Lung et al., 2006; Solomon et al., 2007). The natural vegetation of both forest ecosystems is derived from tropical rainforest species, including *Aningeria altissima* (A. Chev.), *Milicia excelsa* (Welw. C.C. Berg), *Antiaris toxicaria* (Lesch) and *Chrysophyllum albidum* (G. Don). At higher elevation, there are species of montane forests including *Olea capensis* (L.) and *Croton megalocarpus* (Hutchinson).

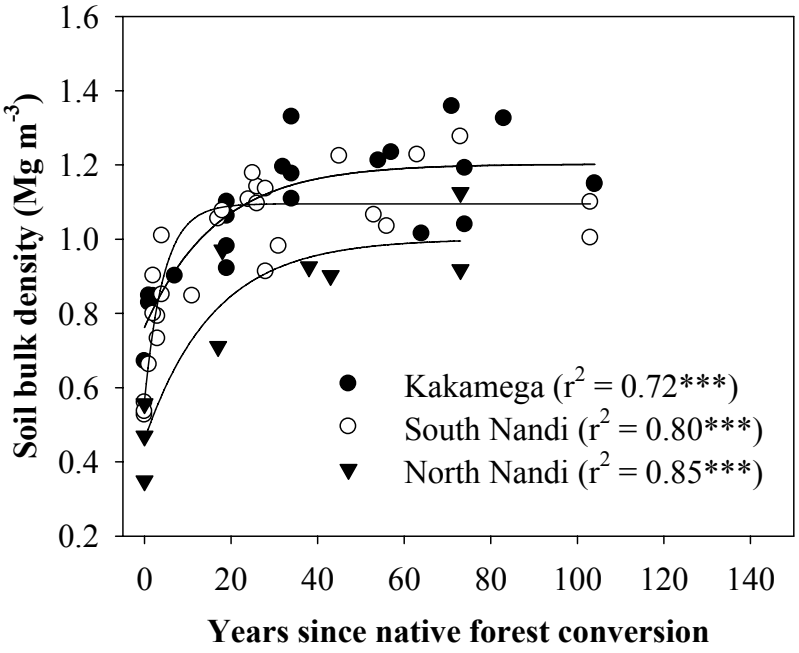

Figure. 2-1. Bulk density (ρ_b), changes to show the increase in the ρ_b of surface soils (0-0.10 m), as a result of conversion from native forest to cereal crop cultivation, *n* = 53. The exponential rise equations describe non-linear changes for, medium-textured Kakamega; $\rho_b = 0.76 + 0.44 \times(1\text{-}e^{\ 0.06years})$; heavy-textured South Nandi $\rho_b = 0.56 + 0.53 \times(1\text{-}e^{\ 0.22years})$ and heavy-textured North Nandi $\rho_b = 0.46 + 0.54 \times(1\text{-}e^{\ 0.06years})$ sites.

The Kakamega-Nandi forest ecosystem is developed on kaolinitic Acrisols (FAO-UNESCO-ISRIC, 1988) or Ultisols (Soil Survey Staff, 1998). The parent material of the native forest is composed of granite, including some precambrian gneisses supporting Luvisols (Werner et al., 2007) at lower elevations and other undifferentiated basement system rocks at higher elevations (Jaetzold and Schmidt, 1983). These soils are dominated by Si and Al contents of kaolinite in the B horizon (Krull et al., 2002). The Al:Fe ratios suggest that the dominant clays contain large proportions of alumino-silicate minerals as well as Al and Fe oxides (Table 1). The long-term climate data from Kaimosi and Kibiri recording stations which are adjacent to the forest margins show that the chronosequence sites which were located between 1500-2000 m above sea level (a.s.l.), have a mean annual temperature (MAT) of 18.0 °C to 21.0 °C and a mean annual precipitation (MAP) of ~ 2000 mm (Table 1) (Jaetzold and Schmidt, 1983). The elevation data were confirmed by GPS readings (Garmin e-Trex® unit). The soils from Kakamega sites were medium-textured soils (sand, 390 g kg^{-1}) and included fields situated between 1500 -1700 m a.s.l. (Bleher et al., 2005; Lung and Schaab, 2006). South Nandi sites were grouped between 1600 – 1800 m a.s.l. forming a transition between the lower Kakamega and upper North Nandi forests. The North Nandi sites were situated between 1800-2000 m a.s.l. (Brooker et al., 2004). Both North and South Nandi chronosequence sites were located on heavy-textured soils (clay+silt, 730 and 840 g kg^{-1} respectively, Table 1).

2.2 Agricultural conversion along the chronosequence

Specific age classes of designating when native forests were converted to agriculture were determined from historical community settlement patterns over the last century (Morgan, 1963).

Table 2-1. Site physical and chemical characteristics of the surface soils (0-0.12 m) at three forest reference sites of the Kakamega-Nandi forest margins, western Kenya

Chronosequence site	South Nandi, Chepkumia	North Nandi, Kiptuiya	Kakamega, Kibiri
Location	00º 09’ 34"N 34º 57’ 37"E	00º 13’ 31"N 35º 00’ 27"E	00º 10’ 06"N 34º 51’ 40"E
Elevation (m.a. s. l) †	1750	1969	1596
MAT (ºC) ‡	19.0	18.0	21.0
MAP (mm yr^{-1}) ¥	2024	2119	2040
Soil type*	humic Acrisol	humic Acrisol	ferric Acrisol
Soil properties			
Clay+Silt (g kg^{-1})	840	730	610
Sand (g kg^{-1})	160	270	390
Bulk density (Mg m^{-3})	0.67	0.71	0.83
pH (water, 1:2.5)	6.2	7.4	6.1
CEC ($mmol_c$ kg^{-1}) #	331	248	99
Total elements			
Fe (g kg^{-1})	52.9	30.7	35.7
Al (g kg^{-1})	65.2	42.6	58.4
Ca (g kg^{-1})	5.7	10.7	2.3
Mg (g kg^{-1})	1.1	1.4	1.0
K (g kg^{-1})	8.2	9.4	13.9
P (mg kg^{-1})	1087	1116	568
Zn (mg kg^{-1})	146	96	158
Al:Fe	1.2	1.4	1.6
Al:P	64	38	103
Fe:P	52	28	63

†Elevation in meters above sea level. Long-term ¥mean annual precipitation and ‡Mean annual temperature records for nearby stations; Kaimosi (Chepkumia), Kaimosi FTC (Kiptuiya) and Forest station (Kibiri). *Soil description adapted from Kenya Soil Surv.: Explorat. Soil Map and Agro-clim. Zone Map of Kenya, Scale 1:1 000 000. *Exploratory Soil Survey Report E 1*, Nairobi, 1982 and cited in *Jaetzold and Schmidt*, (1983). # Sum of base cations Ca^{2+}, $Mg^{2+}$and K^{+} calculated from Mehlich 3 extraction.

Times of conversion were inferred from data available from records of the Kenya government from the Department of Forests, the Ministry of Agriculture Extension Service and the Soil Survey as well as from oral interviews with officials of local institutions and from county council records. Within each site, there were distinct population settlement patterns where newly acquired fields were excised from sections of the native forest for agriculture (Bleher et al., 2005). For appropriate statistical analysis and model treatment, we needed replicated chronosequences with the following number of years since native forest conversion: <3, 3-9, 10-22, 23-34, 35-57, 58-83 and 84-114 years. These sites supported historical settlements of Luhya and Nandi communities who have cultivated the southern and eastern margins of the Kakamega-Nandi forests since the 1890s (Bleher et al., 2005; Lung and Schaab, 2006). The traditional food crops of the Luhya include cereals, grain legumes and root tubers, which, distinguishes them from the Nandi who integrate livestock farming (Jaetzold and Schmidt, 1983; Lung and Schaab, 2006). For the past 100 or more years, millet, sorghum and maize have been grown on the Luhya's land, usually two crops per year (Crowley and Carter, 2000). At the Nandi locations, cereal crops were combined with off-season grazing of livestock (Jaetzold and Schmidt, 1983; Anderson, 1986). By matching the community settlements, we ensured that these ethnic differences did not confound our interpretation of the C and nutrient loss data. Sample collection from the various conversion sites was restricted to areas with similar soil texture, altitude range and precipitation. In all cases, only fields known to have received little or no addition of fertilizer or manure were included in the study.

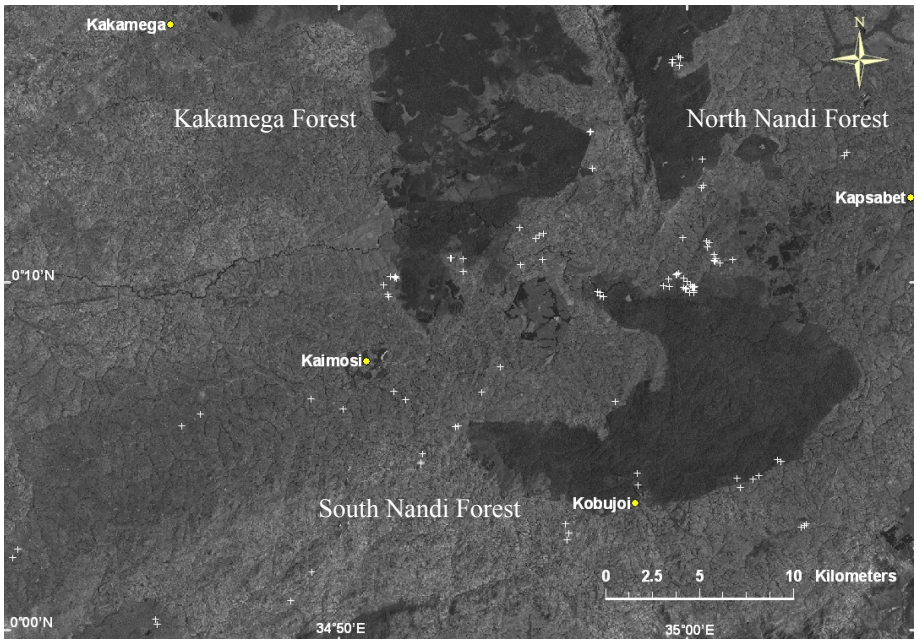

Figure. 2-2. Geographical locations of research sites across the study area for the Kakamega-Nandi forest margins and adjacent fields (+). The settlement corridor separating the once contiguous forest system is ~20 km wide. Sites to the Northeast margin of the South Nandi forest are part of the North Nandi chronosequence due to their similarity in elevation, temperature and rainfall

2.3 Soil sampling and analysis

Soil samples were collected from 10 random locations in agricultural fields where cereal sorghum (*Sorghum bicolor* L.), finger millet (*Eleusine coracana* (L.) Gaertn), and maize (*Zea mays* L.) crops were historically cultivated. Nine undisturbed native forest reference sites were sampled to permit comparison of the cultivated plots with the original forest and to establish the equilibria of soil C, N and other nutrients prior to native forest conversion. Due to tillage compaction in newly converted fields, we adjusted the soil sampling depth in order to correct for the differences in mass of the core sample by first determining 0.05 m incremental bulk density of the soil for 5 forest and 48 agricultural parcels (Figure. 2). From these measurements, we estimated that a sampling depth of 0 to 0.12 m in the forest, 0 to 0.11 m in the recently converted sites and 0 to 0.1 m for all other sites represented an equal mass of soil used in calculations to quantify stocks of organic and inorganic elements. We reported the stocks in kg m^{-2} after multiplying the total elemental concentrations by the soil core mass.

From each time of conversion, available P and inorganic base cations Ca, Mg and K were determined on 3 fields using the Mehlich 3 extraction procedure (Mehlich, 1984). To 3.0 g of air-dried soil, 30 mL of Mehlich 3 solution was added, and the soil extraction mixture was shaken for 5 min on a reciprocating shaker. The solution was filtered through Whatman 42 (ash less 110 mm diameter) in two steps in order to trap organic particles since soils from native forests contained high organic matter contents. The filtrate (2 mL) was analyzed for available P, Ca, Mg and K on an inductively coupled plasma atomic emission spectrometer (ICP-AES, Spectro CIROS, CCD, Germany).

For total elemental contents, 0.5 g soil was digested in 9 mL of concentrated nitric acid and 3 mL hydrofluoric acid for 15 min and heated using a microwave oven.

Elemental composition of the digest was analyzed by ICP-AES according to procedure EPA 3052 (US EPA, 1996). Total C and total N were determined by dry combustion on a Europa ANCA-GSL CN analyzer (PDZ Europa Ltd., Sandbach, UK), after the soil was finely ground using a Mixer Mill (MM301, Retsch, Germany). Natural abundance $\delta^{15}N$, and the $\delta^{13}C$ for the same sample was determined on a coupled Europa 20-20 continuous flow isotope ratio mass spectrometer (PDZ Europa Ltd., Sandbach, UK) following combustion at 1000°C. The $\delta^{15}N$ values were expressed relative to atmospheric N_2, while the $\delta^{13}C$ values were expressed relative to the Vienna-Pee Dee Belemnite (V-PDB) standard. In addition, $\delta^{13}C$ and $\delta^{15}N$ of 4 surface litter samples from forest and 9 cereal cropping sites were determined to record the initial stable isotopic composition of the organic matter sources.

Because soils with a pH > 5.5 are close to 100% base saturation (Magdoff and Bartlett, 1985; Magdoff et al., 1987) we estimated the CEC ($mmol_c\ kg^{-1}$) from the calculated amounts of base cations(Ca^{2+}, Mg^{2+} and K^{+}) extracted by Mehlich 3. It was assumed that for pH ≥ 6.0, the contribution of acidity to CEC was minor (Magdoff and Bartlett, 1985). In the pH range 4.2 to 8.3, Wang et al. (2004) determined from 317 soils that Mehlich 3 extractable cations are well correlated to those estimated from NH_4–Ac buffered at pH 7.0 (Ca, Mg = 1:1 and K = 1.1:1).

2.4 Statistical modeling

Long-term C and nutrient degradation was estimated from non-linear regression. Equation and curve fitting routines were calculated in SigmaPlot for Windows 2002, Version 8.0®. The C and N decay and P, K, Ca and Mg loss data were fitted using a three parameter single exponential decay/loss model:

$$y = y_o + a \times \exp^{-bx} \qquad \text{Eq. (1)}$$

where,

y_o = C, N, P, K, Ca and Mg equilibrium level

a = C, N degradation (kg m^{-2}) and P (mg kg^{-1}), K, Ca and Mg ($mmol_c$ kg^{-1}) loss

b = rate of loss

x = time (years)

In fitting the exponential decay function, we used the initial conditions of the forest soil equilibrium to derive the long-term soil C and N decay attributable to agricultural cultivation. For the kinetics of C and N decay and P, K, Ca and Mg loss, the estimated number of years required for one half of the original stock to decay ($t_{½}$) was calculated from the inverse of the exponential decay;

$$t_{½} = \ln (0.5)/b \qquad \text{Eq. (2)}$$

The long-term dynamics of the isotopic composition in the natural abundance of ^{13}C and ^{15}N were expressed as an enrichment value, ev, relative to reference soil and plant $\delta^{13}C$ and $\delta^{15}N$ where crop source incorporation was less negative, $\delta^{13}C$ and more positive, $\delta^{15}N$. These data were fitted using an exponential function assuming that δ signature changes are buffered at the new soil degradation equilibrium, expressed as:

$$y = y_o + a \times (1 - \exp^{bx}) \qquad \text{Eq. (3)}$$

y_o = initial isotopic composition (‰)

a = enrichment in $\delta^{13}C$ and $\delta^{15}N$ (‰)

b = rate of isotopic enrichment

x = time (years)

2.5 Soil C sources

To estimate the proportion of remaining C stocks (C_s) from forest C_3 and crop -derived C_4-C sources, we used the mixing model approximation (Solomon et al., 2002; Huggins et al., 2007) after we first determined that the maximum $\delta^{13}C$ difference between forest litter and cereal crop litter $\delta^{13}C$ was 13.8 ‰. For all sites, we

adjusted the forest $\delta^{13}C$ values in order to account for the initial difference between forest litter $\delta^{13}C$ (27.8 ± 0.7 ‰) and forest soil $\delta^{13}C$ (25.8 ± 0.3 ‰). According to Högberg (1997), this signature variation does not arise from C_4-C source incorporation but rather from the enrichment of microbial metabolites with the heavier isotope during decomposition. The C stocks were partitioned from the following mixing equation:

$$\text{cereal crop } C_4\text{-C} = C_{cc} = ((\delta_{nfs} - \delta_{cs}) / (\delta_{nfl} - \delta_{cl})) \times C_s \quad (4)$$

$$\text{native forest } C_3\text{-C} = C_{nf} = (C_s - C_{cc}) \quad (5)$$

where,

C_{cc} = cereal crop C_4-C, C_{nf} = native forest C_3-C, δ_{nfs} = $\delta^{13}C$ of forest soil, δ_{cs} = $\delta^{13}C$ of cultivated soil approaching degradation equilibrium. δ_{nfl} = $\delta^{13}C$ of litter in forest and δ_{cl} = $\delta^{13}C$ of litter in crop land.

3. Results

3.1 Characteristics of native forest reference sites

Surface of soils (0-0.12 m) from the native forest sites of the Nandi and Kakamega forests contained 4.2 to 7.4 kg C m^{-2} and 0.50 to 0.7 kg N m^{-2} reflecting their high organic C and N contents (Table 2). The $\delta^{13}C$ composition of the Nandi-Kakamega forest surface soils (-26 ‰) indicates only a slight enrichment in the heavier isotope from the initial surface litter value (-28 ‰). At the forest sites, the ^{15}N contents in surface soils ($\delta^{15}N$ of 5.3 ± 0.8 ‰) were significantly higher than in the forest litter (2.9 ± 0.8‰).

3.2 Long -term C and N stock changes

The decline in C and N was most rapid during the initial 25-36 years at Nandi and 15 years at Kakamega, after which the stocks approached equilibrium.

Table 2-2. Non-linear regression for soil C (carbon) and N (nitrogen) degradation equilibria of tropical soil (0-0.12, 0-0.10 m) as a function of time under long-term cropping in western Kenya. Model; $y = y_o + a \times \exp^{-bx}$

Chronosequence site	Parameter	Stable isotopic shift		Organic matter content	
		$\Delta\ ^{13}C$	$\delta\ ^{15}N$	C	N
Heavy-textured South Nandi	y_o	-25.7	5.6	1.8	0.2
	a	7.2	1.8	4.3	0.5
	b	0.12	0.14	0.06	0.07
	p-value	0.005	0.02	<0.0001	<0.0001
	r^2	0.88	0.86	0.98	0.98
Heavy-textured North Nandi	y_o	-25.4	4.8	4.0	0.4
	a	8.3	1.7	3.3	0.3
	b	0.34	0.13	0.16	0.16
	p-value	<0.0001	0.01	0.02	0.014
	r^2	0.99	0.90	0.80	0.82
Medium-textured Kakamega	y_o	-26.4	5.4	2.0	0.2
	a	6.7	1.5	2.2	0.3
	b	0.19	0.09	0.25	0.29
	p-value	0.0001	0.07	0.003	0.0006
	r^2	0.97	0.74	0.90	0.95

Of the declining amounts, equilibrium contents were determined from the time when greater than 90% of the C and N stock losses had been exceeded. Starting from the forest equilibrium state, agricultural cultivation resulted in an exponential decline of C and N stocks of the forest surface soils at all three chronosequence sites (Figure. 3). At the medium-textured site, equilibrium stocks of 2.0 kg C m^{-2} indicated that 2.2 kg C m^{-2} has decayed in surface soil during continuous cereal crop cultivation. At the Nandi sites, the onset of C losses was more rapid at North Nandi ($b = 0.16$, $p = 0.02$) as opposed to the South Nandi site ($b = 0.06$, $p < 0.0001$). The N loss rate ($b = 0.16$; $p = 0.014$) was more than two times higher in North Nandi compared to South Nandi sites ($b = 0.07$; $p = <0.0001$). In comparison to the Nandi sites, C stock decay rates were 2 to 3 times faster at Kakamega but N loss rates barely surpassed those measured at Nandi (Table 2).

3.3 $\delta^{13}C$ and $\delta^{15}N$ isotopic composition

Under native forest conditions, the surface organic litter, originating from forest C_3 vegetation ($\delta^{13}C$ of -27.8 ± 0.7 ‰) was depleted in the heavier N isotope ($\delta^{15}N$ of 2.1± 0.2 ‰) The initial forest surface soil $\delta^{13}C$ values ranged from -26.4 ‰ to -25.4 ‰ (Table 2, Figure 4). Immediately after deforestation, the isotopic composition of the SOM was similar to that of the C_3 surface litter inputs (27.8 ‰). Also, the $\delta^{13}C$ values of surface crop litter from cultivated fields (-18.9 ± 2.3 ‰) were similar to the $\delta^{13}C$ of all three sites when approaching the soil C equilibrium (-18.5 ‰, South Nandi; -17.1 ‰, North Nandi, -19.7 ‰, Kakamega). The two heavy-textured sites differed in their C/N in relation to N mineralization during degradation (Figure. 5b). For North Nandi sites, C/N was not significantly correlated to the ev of $\delta^{15}N$ (Table 3). At the South Nandi site, 87% of the variation in C/N was associated with the ev shift of 0.7 ‰

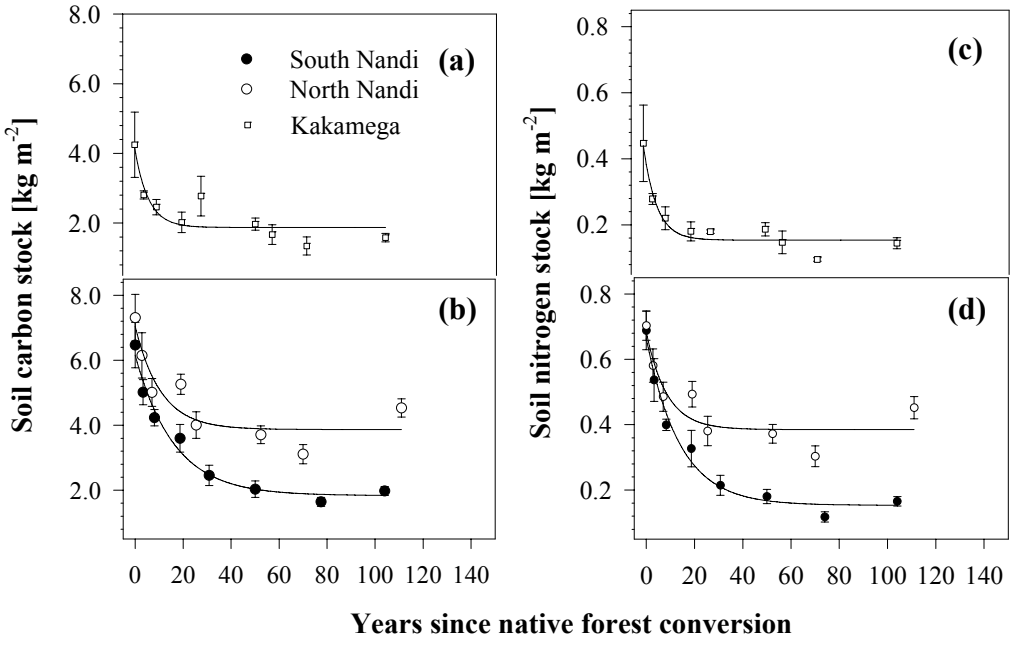

Figure. 2-3. Long-term effects of permanent cereal cropping on carbon (C) and nitrogen (N) stocks in surface (0-0.12 m, 0-0.11 m and 0.10 m) soil. Initial reference values are determined from the original native forest soil C stocks. Bars are ± 1 standard error of the mean for each age group of fields. For South Nandi n = 39; North Nandi n = 48 and Kakamega n = 35

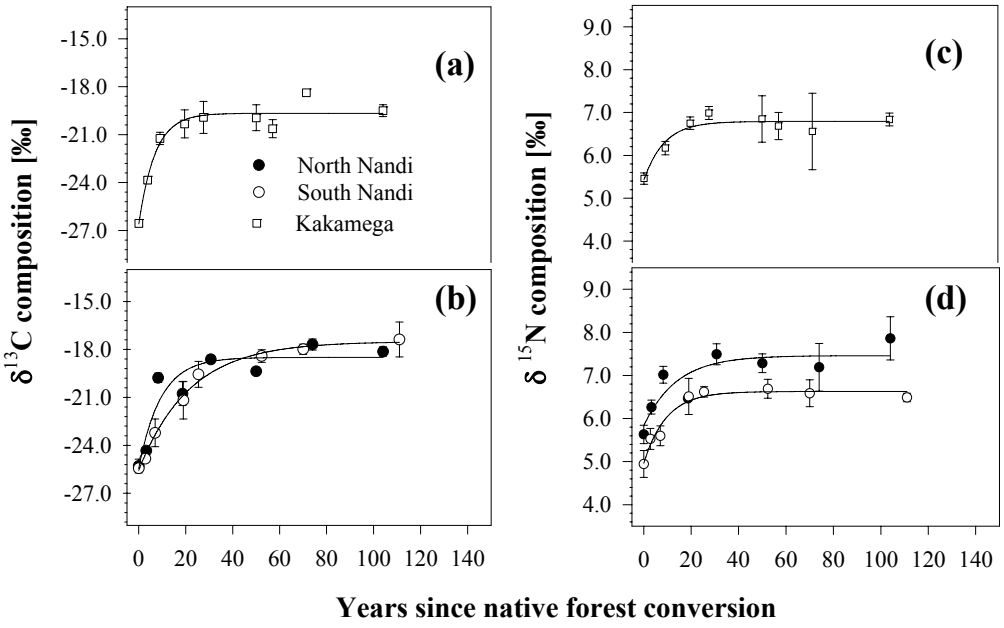

Figure. 2-4. Long-term shift in the isotopic compositions of $\delta^{13}C$ and $\delta^{15}N$ of cultivated (0-0.10 m) soils. Reference values of the $\delta^{13}C$ and $\delta^{15}N$ are from the source litter biomass of the original forest (-27.8 ‰, *n* = 4) and crop surface litter in cultivated soils are: South Nandi; -17.5 ‰, *n* = 39; North Nandi; 18.5 ‰, *n* = 48 and Kakamega; -19.7 ‰, *n* = 35. Bars are ± 1 standard error of the mean for each age group of fields.

As the chronosequence sites approached the C degradation equilibrium, $\delta^{13}C$ estimates of partitioning C sources between C_{nf} and C_{cc} organic matter inputs (Eqs. 4 and 5) showed that a significant proportion of the remaining C was derived from the original C_{nf} organic matter (Figure. 6). Comparing the two heavy-textured sites, North Nandi sustained a soil C loss of 3.3 kg m^{-2} but gained more than twice the new crop C during long-term cultivation (Figure 6).

3.4 P, Ca^{2+}, Mg^{2+}, and K^{+}, nutrient losses

In the Nandi and Kakamega ecosystems, long-term cereal crop cultivation appeared to profoundly modify nutrient availability from the original forest litter (Table 4). Among all sites, there was variation in the amounts of extractable P and rates of loss of extractable base cations. Over the entire 100-yr cultivation period, variations in available P (Figure. 7a) showed a significant decline and the loss rate was nearly three times faster than the decline rate for C and N at South Nandi (Table 4). For North Nandi, the P loss rate (b = 0.09) was about 30% less than the C and N decay rate. However, this rate of loss was not significant (p = 0.206). Moreover, only half of the variation in the loss dynamics of P (r^2 = 0.47) is explained by the exponential model. As soil nutrient degradation approached equilibrium, the Ca^{2+} contents were an order of magnitude greater than P, Mg^{2+} and K^{+}. For all sites, Ca^{2+} occupied more than two thirds of the total base complex. At the heavy-textured Nandi sites, 100 to 190 $mmol_c$ kg^{-1} Ca was lost from surface soils over the 100 year period. Less than one quarter of the original Ca amount (40-50 $mmol_c$ kg^{-1}) was retained as soil nutrient contents stabilized towards the equilibrium. However, at the medium-textured site, the already low base cation amounts were further diminished by a large and immediate flux of all base cations from the surface soil.

Table 2-3. Non-linear regression for N nitrogen sources and stock changes during long-term cropping in heavy-textured Nandi and medium-textured Kakamega tropical highland soils (0-0.10 m), western Kenya. Model; $y = y_o + a \times (1 - exp^{bx})$

			Intercept		Slope		Model
Isotopic shift	Site	*n*	estimate	p-value	estimate	p-value	r^2
$\delta^{15}N$ vs N	South Nandi	7	7.7	<0.0001	-2.9	0.022	0.61
	North Nandi	8	8.0	<0.0001	-4.2	0.009	0.71
	Kakamega	8	7.4	<0.0001	-4.2	0.041	0.53
$\delta^{15}N$ vs C/N	South Nandi	7	-0.71	0.61	0.70	0.002	0.87
	North Nandi	8	0.15	0.99	0.56	0.664	0.03
	Kakamega	8	2.59	0.36	0.35	0.193	0.26
$\delta^{15}N$ vs $\delta^{13}C$	South Nandi	8	11.0	0.0001	0.20	0.017	0.64
	North Nandi	8	10.2	<0.0001	0.20	0.004	0.78
	Kakamega	8	9.9	0.0003	0.17	0.04	0.53

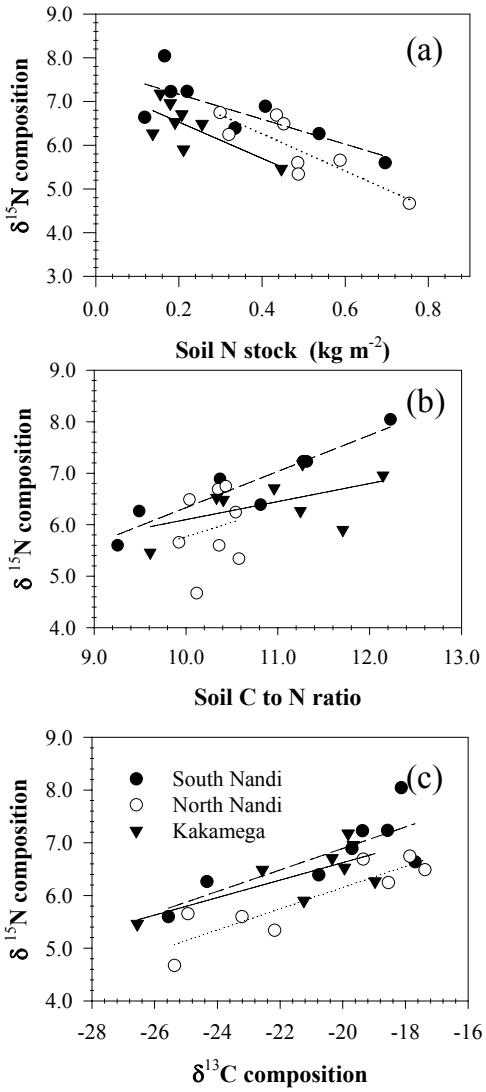

Figure. 2-5. Isotopic dynamics of forest and cereal crop sources of nitrogen (N) during long-term soil degradation. Changes in the N stocks (a), soil C/N ratio (b) and $\delta^{13}C$ (c) in relation to the $\delta^{15}N$ enrichment.

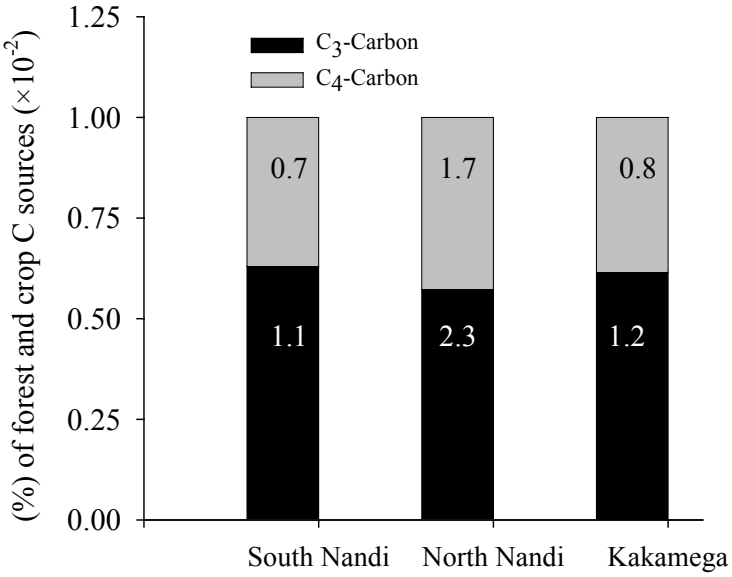

Equilibrium C stock (kg m^{-2})	1.8	4.0	2.0
Initial forest C stock (kg m^{-2})	6.1	7.3	4.2

Figure. 2-6. The long-term contribution of C_3, forest and C_4 cereal crop C sources to the soil C stocks during soil degradation.

3 5 Cation exchange capacity and pH

In recently cultivated fields, the CEC estimated as the sum of base cations Ca^{2+}, Mg^{2+} and K^{+} was highest at heavy-textured South Nandi (271 ± 39 $mmol_c\ kg^{-1}$), intermediate at North Nandi (154 ± 19 $mmol_c\ kg^{-1}$) but very low at the medium-textured Kakamega site (31 ± 5 $mmol_c\ kg^{-1}$). With reference to the initial amounts in recently cultivated fields (Figure. 6), there were significant losses in CEC at all 3 sites (South Nandi, 73.0 ± 25 $mmol_c\ kg^{-1}$; North Nandi, 96.0 ± 13 $mmol_c\ kg^{-1}$; Kakamega 16.0 ± 4 $mmol_c\ kg^{-1}$).

Out of the 30 fields with a cultivation history of 25 years or less, only 23% had pH values in the slightly acid range 5.5 to 6.0 (Figure. 7). For those fields with cultivation histories exceeding 20 years (39), 74% had pH values ≤ 6.0. Model estimates showed a non-linear increase ($r^2 = 0.72$, $p < 0.0001$) in the H^{+} concentration for North Nandi sites and the pH reached an equilibrium value of 6.1 (Figure. 8). The linear increase in the H^{+} concentration was not buffered at heavy-textured South Nandi and medium-textured Kakamega sites ($r^2 = 0.42$, $p = 0.0028$ and $r^2 = 0.46$, $p = 0.0001$ respectively), and the soil continued to generate acidity.

4. Discussion

4.1 Forest reference sites

In the tropics, large C stocks and nutrient contents accumulate in the surface soils from the long-term deposition of litter biomass under natural forest conditions (Houghton and Hackler, 2006; Hairiah et al., 2006).

Table 2-4. Non-linear regression for soil P (mg kg^{-1}) and base cation ($mmol_c$ kg^{-1}) degradation equilibria in soil (0-0.10 m) during long-term cropping, western Kenya. Model; $y = y_o + a \times exp^{-bx}$. and $^{‡}y = a \times exp^{-bx}$

Chronosequence site	Parameter	Mehlich 3 extractable soil P and base cations			
		P	K	Ca	Mg
Heavy-textured South Nandi	y_o	4.3	5.5	41.3	10.0
	a	28.4	19.6	492.1	117.5
	b	0.60	0.26	0.52	0.67
	p-value	0.001	<0.0001	0.0001	<0.0001
	r^2	0.57	0.82	0.84	0.74
Heavy-textured North Nandi	y_o	11.1	–	38.6	16.6
	a	32.2	6.8‡	101.4	19.8
	b	0.19	0.0019	0.03	0.05
	p-value	0.005	0.24	0.0004	0.02
	r^2	0.40	0.07	0.51	0.30
Medium-textured Kakamega	y_o	6.5	0.9	–	3.8
	a	3.0	1.6	22.7‡	5.2
	b	0.18	0.16	0.009	0.10
	p-value	0.78	0.064	0.088	0.227
	r^2	0.02	0.25	0.13	0.14

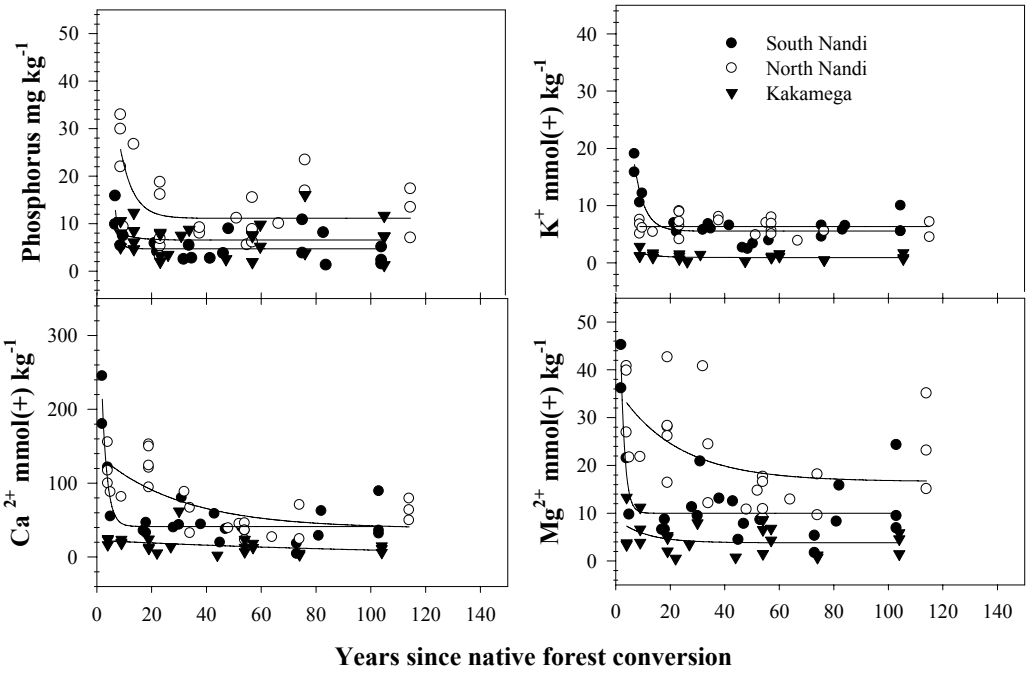

Figure. 2-7. Base cation ($mmol_c\ kg^{-1}$) dynamics of tropical soil following conversion from forest to continuous cereal cropping

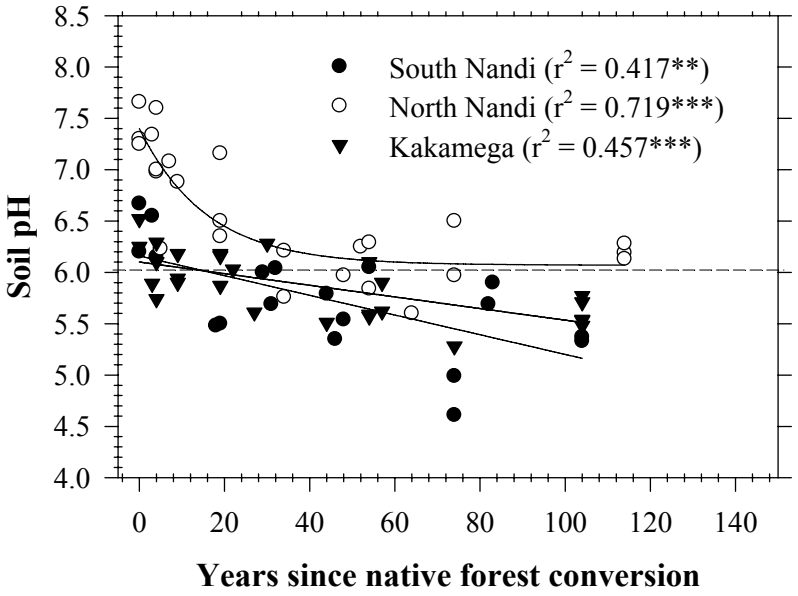

Figure. 2-8. Effect of long-term cereal cropping on pH to show site differences in the soil buffering capacity. For heavy-textured North Nandi, the pH declined following exponential decay; $pH = 6.07 + 1.33e^{-0.063years}$. At the heavy-textured South Nandi and medium-textured Kakamega sites, a linear decrease in the pH is given by equations, $pH = 6.16e^{-0.0096years}$ and $pH = 6.10e^{-0.0057years}$ respectively. Significance levels are designated as (0.05*; 0.01** and <0.0001***).

Tropical rain forests develop on nutrient poor soils (Vitousek, 1984; Vitousek and Sanford, 1986) but the long-term accumulation of organic matter slows decomposition thereby increasing the C and N content of soil (Murty et al., 2002), especially in highland forests experiencing low mean annual temperature (Raich, 2006). Since many such tropical highland as well as lowland forests develop on nutrient-poor substrate, they tend to exhibit a rich nutrient economy with close coupling between C and other element cycles (Vitousek and Sanford, 1986). Given the large C and N stocks accumulation and nutrient contents (Table 2, Table 4) in the surface soil, the heavy-textured higher elevation Nandi forest sites show little nutrient limitation, near neutral pH and high CEC. Medium-textured lower elevation Kakamega forest sites, with half the total soil P content and a low CEC are clearly P-limited (Table 4). From an inventory of the forest soils at 5 sites Werner et al., (2007) show that differences in soil texture cause a large variation in the pH, C and N concentrations of the litter layer, 0-0.05 m and 0.05-0.2 m soil depth of the Kakamega forest. Nandi forests are therefore organic matter and nutrient-rich whereas the lower elevation Kakamega forest is comparatively organic matter rich but nutrient poor.

4.2 Carbon and N losses following forest conversion

We inferred the initial decay rate dynamics in from the time required to degrade half of the soil C and N stocks (Eq. 2), after estimating their degradation equilibrium from Eq. 1. Half-life decay rates show that it takes 2 to 3 times longer to reach equilibrium at the heavy-textured Nandi sites than at the medium-textured Kakamega sites. In both heavy and medium textured soils, the half life of the C and N stocks was 5-11 and 2-10 years, respectively. For a similar study, Zach et al. (2006) found half lives of about 10 years, revealing a lack of C stabilization in SOM fractions. Therefore, a large fraction of the available C pool is lost 11 years upon

cultivation. However, from a decay rate constant (b = 0.18, p = 0.09), we estimated that one half of the soil C stock was already lost 4 years after forest conversion. The soil C decomposition rate is similar to that for N (b = 0.19; p = 0.01). On a P-limited lowland forest, Matson et al. (1987) reported that an immediate N flush after deforestation and crop uptake account for less than 20% of total N stocks. Therefore, differences in N stocks may probably originate from the initial N losses after deforestation and from limitations due to the poor availability of other soil nutrients such as P. Due to large C accumulations in the top in the forest litter and surface soil at Kakamega forest, large losses of N_2O to the atmosphere occur at the onset of rains representing a significant N loss pathway (Werner et al., 2007)

4.3 Long-term changes in the isotopic composition of organic matter

The $\delta^{13}C$ of the degrading sites of intermediate age represented a mixture between crop litter inputs and the residual forest derived C that was being enriched in ^{13}C as a result of differential loss during decomposition. These changes in the $\delta^{13}C$ and $\delta^{15}N$ values can be attributed to a progressive enrichment of the heavier C isotope in the SOM arising from either decomposition (Boutton et al., 1998; Glaser et al., 2001), or fresh inputs of C_4 crop litter (Solomon et al., 2002). Over the entire cultivation period, a shift in the input and decay rates of the SOM showed an ev of 7 to 8 ‰ in $\delta^{13}C$ and an ev of 1.4 to 1.7 ‰ in $\delta^{15}N$ (Figure. 3). Kramer et al. (2003) argue that increases in $\delta^{15}N$ values represent the progressive decomposition and associated N mineralization rather than a selective preservation of organic matter constituents. For these sites, the $\delta^{13}C$ ev indicated that progressive decomposition and the mineralization of soil N was overriding the enrichment of $\delta^{15}N$ from N in forest and cropland litter (Table 3). In North Nandi sites, there was low variation in the C/N ratio and it was difficult to detect a relationship with $\delta^{15}N$ signature changes.

For both isotope signatures, the rate of enrichment (Eq 3) could be expressed as a ratio ($\delta^{13}C$ to $\delta^{15}N$) in order to better understand the C and N cycling between the three chronosequence sites (data not shown). Using this ratio, the relative rate of C and N decomposition appeared to be similar for South Nandi site (0.9) whereas these ratios were more than 2 times higher for the North Nandi and Kakamega sites. This may suggest that the initial C losses at heavy-textured North Nandi and medium-textured Kakamega sites involved losses of available C in forest litter. In contrast, slow decomposing forms of organic matter in forest litter dominated C losses at the South Nandi site. This indicated that there were site differences in both the form and quality of C and N lost upon cultivation. Vitousek et al. (1979) proposed that N immobilization such as in structural litter biomass, can delay losses of leachable N, which could be the case at the heavy-textured South Nandi (Figures. 4a, 4b). By correlating the $\delta^{13}C$ and $\delta^{15}N$ signature changes (Table 3), we estimated whether the observed long-term N input changes originated from internal C cycling dynamics or from inputs of new C_4 carbon (Figure. 4c). For all three sites, 53-71% of the variation in the composition of $\delta^{13}C$ could be accounted for by a positive linear increase in the $\delta^{15}N$, indicating that the long-term enrichment of N was from decomposing SOM (Table 3) and to a less extent from crop litter. This loss processes has been described by Cleveland et al. (2006), who showed that high rainfall leads to N decline in the structural litter layer of organic matter in tropical rain forests, whereas Johnson et al. (2006) suggest that leaching of dissolved organic matter may be more important than direct C loss as CO_2. An inverse relationship between N stocks and changes in the ev of $\delta^{15}N$, confirmed that the increase in the $\delta^{15}N$ enrichment (Figure. 4a) was driven by N loss dynamics to a greater extent at the Nandi sites (slope = -4.2) than at the medium-textured Kakamega sites (slope = -2.85).

4.4 Equilibrium sources of soil C

Despite the rapid loss of C_{nf} in the surface soils (5.0 kg m^{-2} at both heavy-textured Nandi and 3.0 kg m^{-2} at the medium-textured Kakamega sites), modest gains of C_{cc} appeared to only offset 13 % and 34% of the loss at South and North Nandi, respectively. At the medium-textured Kakamega, the gain from C_{cc} replaced 26% of the total C_{nf} loss. In a recent review of studies examining C stock degradation upon conversion of tropical rain forest to agriculture, Murty et al. (2002) concluded that for studies correcting for bulk density but not C_{cc}, approximate C and N losses average 24 and 15% respectively. In 0-20 cm soil depth of annual crop fields, Palm et al. (2004) estimate that these C losses could be as high as 50% of the original native forest. The losses at Kakamega-Nandi forest chronosequence sites fall in between values reported from the two studies. Additionally, these equilibrium estimates need to be interpreted with caution since we assumed that the ev in $\delta^{13}C$ shift was entirely due to new C_{cc}. Because the ev in the forest soil (-2.0 ‰ ± 0.3) is attributed to decomposition, it is possible to argue for adjustment to the ev by correcting for the shift in the $\delta^{13}C$. Adjustment to the signature shift would result in lower estimates of incorporation of new C_{cc} (22% at South Nandi, 25% at North Nandi and 28% for Kakamega). But still, about one third or less of the remaining C_s was new C_{cc} and its incorporation was neither influenced by differences in soil texture nor by the crop history, possibly due to low crop biomass inputs during long-term cropping.

4.5 Soil nutrient losses and pH changes during long-term cultivation

In contrast to the C and N rates of decomposition, the rapid rate of loss for P from the surface soil was attributable to crop uptake. At South Nandi, the P loss rate surpasses by 5 times the N rate of loss, meaning that its rate of loss exceeds crop uptake for the existing yield goals (Table 2, Table 4). We suspect that labile fractions

of P, co-mineralized with C and available in solution may have been lost through erosion and leaching of organic P forms. In tropical soils, a larger fraction of the available P pool is retained as organic P (Sanchez, 1983), which increases not only P availability but also renders phosphates susceptible to transport in leachate as well as runoff (Neill et al., 2001; Markewitz et al., 2001). Following conversion, the equilibrium soil P contents were extremely low for both moderately fertile North Nandi and poorly fertile South Nandi and Kakamega (Table 4).

Other soil nutrient data were fitted to the exponential model using values from the recently cultivated fields as the initial data points because deforestation often included burning woody biomass which could elevate the base status of newly cultivated land (McGrath et al., 2001; Palm et al., 1996). Even for ecosystems that are recovering from soil nutrient degradation, Ca removals by uptake and leaching far exceed supply from mineral dissolution (Richter et al., 1994). Since kaolinite clays do not support high CEC (Sollins et al., 1988), we argue that long-term base cation losses could be attributed to the leaching and crop export of Ca^{2+} from cultivated soils, which accumulated from decomposition of forest litter biomass. At the Kakamega forest sites, the accumulation of C in litter mass is estimated to range between 9.2 to 15.0 kg C m^{-2} (Werner et al., 2007). Therefore, forest and agricultural crop litter inputs may be a more important source of Ca especially when the parent soil materials are inherently poor in their Ca mineral composition.

In the heavy-textured Nandi soils, both sites sustained nearly similar long-term equilibrium base amounts (Figure. 6). The difference in CEC could be explained by the equilibrium Mg^{2+}, which contributed 16.6 $mmol_c$ kg^{-1} at North Nandi, 10.0 $mmol_c$ kg^{-1} at South Nandi and only 3.8 $mmol_c$ kg^{-1} at the Kakamega site (Table 4). Upon conversion, accompanying alterations in pH and CEC are expected to affect nutrient availability for cropping systems (Jaiyeoba, 2003). In the Kakamega-Nandi forest

margins, pH and CEC changes were driven mostly by the loss in extractable base cations from surface soils. In Kakamega forest, a previous study found that up to half of the CEC in the 0.1-0.2 m depth of the upper B horizon (50 to 100 $mmol_c$ kg-1) could be associated with organic matter (Krull et al., 2002).Upon forest conversion and given the rapid initial nutrient loss, Ca and Mg appear to be the first limiting nutrients for crop production particularly at South Nandi and their deficiency could affect subsequent responses to N and P (Vitousek, 1984). At South Nandi, differences in the lag phase of Ca and Mg half lives compared to the C decline (-7.5 and -8.5 years, respectively) pointed to their immediate limitation to crop production. With higher equilibrium C and N stocks, there was better nutrient retention at North Nandi as it took a period of 9 and 22 years after deforestation for Mg and Ca to become limiting. Kakamega sites remained nutrient limited and overall, lag effects represented uncoupling between long-term C degradation and nutrient loss processes.

Since both Kakamega and Nandi forest sites are developed under moist tropical highland conditions (Glenday, 2006), decaying forest litter yields organic acids which decompose into carbonates (Sollins et al., 1988; Markewitz et al., 2001). At pH $\geq$ 6.0, carbonates (CO_3^{2-}) accept protons (H^+) to form bicarbonate (HCO_3^-) ions causing a more effective buffer around its pKa (~ 6.1). Since the equilibrium C contents were higher at North Nandi, an increased yield of organic acids may partly explain why the pH changes were buffered at North Nandi but not at the South Nandi and Kakamega sites. In which case, the CEC associated with organic matter dependent charge may be influenced through bicarbonate ion formation from root and microbial respiration (Johnson et al., 1997; Markewitz et al., 2004). In addition, since there was no documented use of fertilizer on these fields, the continuous removal of base cations at the most intensively cultivated sites is only gradual and the resulting acidification

did not exceed 1.0 pH unit. This indicated that the long-term pH changes might as well be buffered at both South Nandi and Kakamega sites.

5. Conclusions

Land use conversion and abundant precipitation enhance rapid C stock and nutrient loss rates in the Kakamega-Nandi tropical highland forests. Changes in the isotopic composition of organic matter suggest that C held in pools with varying turnover times was related to the long-term availability of N. Soil C and N stocks were uncoupled to soil nutrient contents in cultivated soil, where differences existed in the lag phase between their losses from surface soil. Close coupling arises from organic matter mineralization-immobilization for C and N whereas uncoupling occurred after soil nutrients were released and became susceptible to rapid leaching out of surface soils. For all sites, organic matter dependent charge compensated for the loss in cation charge, providing buffering capacity to reduce pH decline at heavy-textured North Nandi sites and permitting only gradual modest acidification at heavy-textured South Nandi and medium-textured Kakamega sites.

Upon cultivation, C stocks and soil nutrients at equilibrium depended on the organic matter content and quality of the tropical forest soils, as well as on the land use history of nutrient mining that occurred over a 100-year period of cultivation. Distinct equilibria of soil C and nutrient loss were evident depending on differences in soil texture and crop land use histories. Although loss pathways differed among organic (C, N) and inorganic elements (P, Ca, Mg, K), the degrading heavy-textured Nandi soils cascade from high to medium and low C stocks and nutrient equilibria, while medium-textured Kakamega soil instead transitions from medium to low equilibrium of C stocks. These data provide important information about biogeochemical characteristics of degrading soil in a highland tropical ecosystem. Our

knowledge of these processes should lead to a better understanding of the long-term nutrient losses as well as the nature and timing of C and nutrient repletion required to reverse soil degradation and its implication for global cycles of elements in terrestrial and aquatic ecosystems

REFERENCES

Anderson, D. 1986. Stock theft and moral economy in colonial Kenya. Journal of the International African Institute 56: 399-416.

Austin, A. T., and P. M. Vitousek. 1998. Nutrient dynamics on a precipitation gradient in Hawai'i, Oecologia 113: 519-529.

Bleher, B., D. Uster, and T. Bergsdorf. 2006. Assessment of threat status and management effectiveness in Kakamega forest, Kenya. Biodiversity and Conservation 15: 1159–1177.

Boutton, T. W., S. R. Archer, A. J Midwood, S. F. Zitzer, and R. Bol. 1998. $\delta^{13}C$ values of soil organic carbon and their use in documenting vegetation change in a subtropical savanna ecosystem. Geoderma 82: 5–41.

Brooker, S., S. Clarke, J. K. Njagi, S. Polack, B. Mugo, B. Estambale, E. Muchiri, P. Magnussen, and J. Cox. 2004. Spatial clustering of malaria and associated risk factors during an epidemic in a highland area of western Kenya. Tropical Medicine and International Health 9: 757–766.

Cleveland, C. C., and A. R. Townsend. 2006. Nutrient additions to a tropical rain forest drive substantial soil carbon dioxide losses to the atmosphere. Proceedings of the National Academy of Sciences of the United States of America 103: 10316–10321.

Crowley, E. L., and S. E. Carter. 2000. Agrarian change and the changing relationships between toil and soil in Maragoli, western Kenya (1900–1994). Human Ecology 28: 383–414.

Davidson, E. A., C.J.R. de Carvalho; I.C.G. Vieira, R. de O. Figureueiredo, P. Moutinho, F. Y. Ishida, M. T. P. dos Santos, J. B. Guerrero, K. Kalif, and R. T. Saba. 2004. Nitrogen and phosphorus limitation of biomass growth in a tropical secondary forest. Ecological Applications 14: S150–S163.

Edwards P. J. 1982. Studies of mineral cycling in a montane rain forest in new Guinea: V. Rates of cycling in throughfall and litter fall, Journal of Ecology 70: 807–827.

FAO-UNESCO-ISRIC. 1988. Revised legend, FAO-Unesco soil map of the world. World Soil Resources Reports 60: 119 pp

Glaser, B., R. Bol, W. Amelung, N. Preedy and W. Zech. 2001, Short-term sequestration of slurry-derived carbon and nitrogen in temperate grassland soil using $\delta^{13}C$ and $\delta\ ^{15}N$ natural abundance. Journal of Plant Nutrition and Soil Science 164: 467–474.

Glenday, J. 2006. Carbon storage and emissions offset potential in an East African tropical rainforest. Forest Ecology and Management 235: 72-83.

Hairiah, K., H. Sulistyani, D. Suprayogo, Widianto, P. Purnomosidhi, R. H. Widodo, and M. van Noordwijk. 2006. Litter layer residence time in forest and coffee agroforestry systems in Sumberjaya, West Lampung. Forest Ecology and Management 224: 45–57.

Hartshorn, A. S., O. A. Chadwick, P. M. Vitousek, and P. V. Kirch. 2006. Prehistoric agricultural depletion of soil nutrients in Hawai'i. Proceedings of the National Academy of Sciences of the United States of America 103; 11092–11097.

Högberg, P. 1997. ^{15}N natural abundance in soil–plant systems. New Phytologist 137, 179–203.

Houghton, R. A., and J. L. Hackler. 2006. Emissions of carbon from land use change in sub-Saharan Africa. Journal of Geophysical Research, 111, G02003, doi:10.1029/2005JG000076.

Huggins, D. R., R. R. Allmaras, C. E. Clapp, J. A. Lamb, and G. W. Randall. 2007. Corn-soybean sequence and tillage effects on soil carbon dynamics and storage. Soil Science Society of America Journal 71: 145–154.

Hughes, R. F., J. B Kauffman, and V. J. Jaramillo. 2000. Ecosystem-scale impacts of deforestation and land use in a humid tropical region of Mexico. Ecological Applications 10: 515–527.

Jaetzold, R., and H. Schmidt. 1983. Farm management handbook of Kenya, Vol. 2 Natural conditions and farm management information, Part A. west Kenya. MALD, Kenya.

Jaiyeoba, I. A. 2003. Changes in soil properties due to continuous cultivation in Nigerian semiarid savannah. Soil and Tillage Research 70: 91–98.

Johnson, D. W., R. B. Susfalk, and R. A. Dahlgren. 1997. Nutrient fluxes in forests of the eastern Sierra Nevada mountains, United States of America. Global Biogeochemical Cycles 11: 673–681.

Johnson, M. S., J. Lehmann, E. G. Couto, J. P. Novaes-Filho, and S. Riha. 2006. DOC and DIC in flowpaths of Amazonian headwater catchments with hydrologically contrasting soils. Biogeochemistry 81: 45–57.

Juo, A. S. R., and A. Manu. 1996. Chemical dynamics in slash-and-burn agriculture. Agriculture Ecosystems and Environment 58: 49–60.

Kramer, M G., P. Sollins, R. S. Sletten, and P. K. N. Swartd. 2003. Isotope fractionation and measures of organic matter alteration during decomposition. Ecology 84, 2021–2025.

Krull, E.S., E.A Bestland,., and W.P Gates. 2002. Soil organic matter decomposition and turnover in a tropical Ultisol: Evidence from $\delta^{13}C$, $\delta^{15}N$ and geochemistry. Radiocarbon 44: 93–112.

Lal, R. 2004. Agricultural activities and the global carbon cycle. Nutrient Cycling in Agroecosystems 70: 103–116.

Lung, T., and G. Schaab. 2006. Assessing fragmentation and disturbance of west Kenyan rainforests by means of remotely sensed time series data and landscape metrics. African Journal of Ecology 44: 491–506.

Magdoff, F. R., and R. J. Bartlett. 1985. Soil-pH buffering revisited. Soil Science Society of America Journal 49: 145–148.

Magdoff, F.R., R. J. Bartlett, and D. Ross. 1987. Acidification and pH buffering of forest soils. Soil Science Society of America Journal 51: 1384–1386.

Markewitz D., E. A. Davidson, R. O. Figureueiredo, R. L Victoria. and A.V Krusche. 2001. Control of cation concentrations in stream waters by surface soil processes in an Amazonian watershed. Nature 410: 802–805.

Markewitz, D, E, Davidson, P, Moutinho, and D Nepstad. 2004. Nutrient loss and redistribution after forest clearing on a highly weathered soil in Amazonia. Ecological. Applications 14; S177–S199.

Matson P A., P. M. Vitousek, J. J. Ewel, M. J. Mazzarino, and G. P. Robertson. 1987. Nitrogen transformations following tropical forest felling and burning on a volcanic soil. Ecology 68: 491–502.

McGrath, D A., M. L. Duryea, N. B. Comerford and W. P. Cropper. 2000. Nitrogen and phosphorus cycling in an Amazonian agroforest eight years following forest conversion. Ecological Applications 10: 1633–1647.

McGrath, D. A., C. K Smith, H. L. Gholz, and F. A. Oliveira. 2001. Effects of land-use change on soil nutrient dynamics in Amazonia, Ecosystems 4: 625–645.

Mehlich, A. 1984. Mehlich 3 soil test extractant: a modification of Mehlich 2 extractant. Communications in Soil Science and Plant Analysis 15: 1409–1416.

Morgan, W. T. W. 1963 The 'White highlands' of Kenya. Geographical Journal, 129: 40–155.

Murdiyarso, D, and U. R. Wasrin. 1995. Estimating land use change and carbon release from tropical forests conversion using remote sensing technique. Journal of Biogeography 22: 715–721

Murty, D., M. F. Kirschbaum, R. E. McMurtrie, and H. McGilvary. 2002. Does conversion of forest to agricultural land change soil carbon and nitrogen? A review of the literature. Global Change Biology 8: 105–123.

Neill, C., M. C. Piccolo, P. A. Steudler, J. M. Melillo, B. Feigl, and C. C. Cerri. 1995. Nitrogen dynamics in soils of forests and active pastures in the western Brazilian Amazon Basin. Soil Biology and Biochemistry 27: 1167-1175.

Neill, C., L. A. Deegan, S. M. Thomas, and C. C. Cerri. 2001. Deforestation for pasture alters nitrogen and phosphorus in soil solution and stream water of small Amazonian watersheds. Ecological Applications 11: 1817–1828.

Palm, C. A., M. J. Swift, and P. L. Woomer. 1996. Soil biological dynamics in slash-and-burn agriculture. Agriculture, Ecosystems and Environment 58: 61–74.

Palm, C., T. P Tomich, M. van Noordwijk, S. Vosit, J. Gockowski, J. Alegre, and L. Verchot. 2004. Mitigating GHG emissions in the humid tropics: case studies from the alternatives to slash-and-burn program (ASB). Environment Development and Sustainability 6: 145-162.

Post, W. M., and K. C. Kwon. 2000. Soil carbon sequestration and land-use change: processes and potential. Global Change Biology 6: 317–327.

Raich, J. W. 2006. Temperature influences carbon accumulation in moist tropical forests. Ecology 87: 76–87

Richter, D. D., D. Markewitz, C. G. Wells, H. L. Allen, R. April, P. R. Heine, and B. Urrego. 1994. Soil chemical change during three decades in an old-field loblolly pine (Pinus taeda L.) ecosystem. Ecology 75: 1463–1473.

Sanchez, P. A. 1983. Soil fertility dynamics after clearing a tropical rainforest in Peru. Soil Science Society of America Journal 47: 1171–1178.

Soil Survey Staff. 2003. Keys to soil taxonomy, 9th ed., USDA-Soil Conservation Service, Pocahontas Press, Blacksburg, VA.

Sollins, P., G. P. Robertson, and G. Uehara. 1988. Nutrient mobility in variable- and permanent-charge soils. Biogeochemistry 6: 181–199.

Solomon, D., J. Lehmann, J. M. Kinyangi, W. Amelung, I. Lobe, A. Pell, S. Riha, S. Ngoze, L. Verchot, D. Mbugua, J. Skjemstad, and T. Schäfer. 2007. Long-term impacts of anthropogenic perturbations on dynamics and speciation of organic carbon in tropical forest and subtropical grassland ecosystems. Global Change Biology 13: 1–20.

Solomon, D., F. Fritzsche, J. Lehmann, M. Tekalign, and W. Zech. 2002. Soil organic matter dynamics in the subhumid agroecosystems of the Ethiopian highlands: Evidence from natural ^{13}C abundance and particle-size fractionation. Soil Science Society of America Journal 66: 969-978.

Tanner, E.V.J., P.M. Vitousek, and E. Cuevas. 1998. Experimental investigation of nutrient limitation of forest growth on wet tropical mountains. Ecology 79; 10-22

Townsend, A. R., P. M. Vitousek, and S. E. Trumbore. 1995. Soil organic matter dynamics along gradients in temperature and land use on the island of Hawaii. Ecology 76: 721–733.

U S, E P A. 1996. Method 3052: Microwave assisted acid digestion of siliceous and organically based sediments, In Test methods for evaluating solid waste, physical/chemical methods – SW-846, US EPA, Washington, DC, USA.

van Groenigen, K. J., J. Six, B. A. Hungate, M. de Graaff, N. van Breemen, and C. van Kessel. 2006. Element interactions limit soil carbon storage. Proceedings of the

National Academy of Sciences of the United States of America 103: 6571–6574

Verchot, L. V., L. Hutabarat, K. Hairiah, and M. van Noordwijk. 2006. Nitrogen availability and soil N2O emissions following conversion of forests to coffee in Southern Sumatra. Global Biogeochemical Cycles 20, GB4008, doi:10.1029/2005GB002469.

Vitousek PM, J. R Gosz, C. C Grier, J. M Mellilo, W. A Reiners and R. C Todd .1979. Nitrate losses from disturbed ecosystems. Science, 204: 469–474

Vitousek, P. M. 1984. Litterfall, nutrient cycling, and nutrient limitation in tropical forests. Ecology 65: 285–298

Vitousek, P. M., and R. L. Sanford, Jr. 1986. Nutrient cycling in moist tropical forest. Annual Review of Ecology and Systematics 17: 137–167.

Wang, J. J., D. H. Harrell, R. E. Henderson, and P. E. Bell. 2004. Comparison of soil-test extractants for phosphorus, potassium, calcium, magnesium, sodium, zinc, copper, manganese, and iron in Louisiana soils. Communications in Soil Science and Plant Analysis 35: 145–160.

Wang, Y. P., B. Z. Houlton, and C. B. Field. 2007. A model of biogeochemical cycles of carbon, nitrogen, and phosphorus including symbiotic nitrogen fixation and phosphatase production. Global Biogeochemical. Cycles 21, GB1018, doi:10.1029/2006GB002797.

Werner, C., R. Kiese, and K. Butterbach-Bahl. 2007. Soil-atmosphere exchange of N2O, CH4, and CO2 and controlling environmental factors for tropical rain forest sites in western Kenya. Journal of Geophysical Research 112, D03308, doi:10.1029/2006JD007388.

Woomer, P. L., A. Martin, A. Albrecht, D. V. S. Reseck, amd H. W. Scharpenseel. 1994. The importance and management of soil organic matter in the tropics,

edited by P. L. Woomer, and M. J. Swift, 243 pp. The biological management of tropical soil fertility, J. Wiley, Chichester, UK.

Zach, A., H. Tiessen, and E. Noellemeyer. 2006. Carbon turnover and Carbon-13 Natural abundance under land use change in semiarid savanna soils of La Pampa, Argentina. Soil Science Society of America Journal 70: 1541–1546

CHAPTER 3

LONG-TERM CHANGES IN SOIL ORGANIC MATTER POOLS AS INDICATORS OF THRESHOLDS IN TROPICAL AGROECOSYSTEMS

Abstract

We hypothesize that the net contribution of tropical agroecosystems to the global C balance is subject to threshold behavior. We determined thresholds of carbon (C) and nitrogen (N) loss in soil organic matter (SOM) pools from three agroecosystem chronosequence sites that were developed on Ultisols in western Kenya. By separating three SOM pools assigned to distinct soil functions as indicators of thresholds, we determined that nearly all C (13.6-24.3 g kg^{-1}) and N (1.5-3.1 g kg^{-1}) stocks in the unstable and stable aggregate pools were lost 15 to 36 years after forest conversion. Since between 60-90% of the C and N remained in the soil organomineral pool, this fraction degraded slowly, losing large stocks of C (19.9-50.8 g kg^{-1}) and N (2.2-5.3 g kg^{-1}) over a longer time scale. In all cases, the rate of loss between pools differed by an order of magnitude, primarily because of changes in SOM quality (C:N ratio). The C:N ratio changes caused differences in the rate of decay between pools without affecting the long-term decline in C and N stocks. The long-term changes in the unstable and stable aggregate pool were characterized by small C and N stocks, rapid initial losses that reached equilibrium, a wide C:N ratio at the agroecosystem equilibrium phase (19.3 and 18.3 respectively) and little $\delta^{15}N$ isotopic shift (<1.0 ‰). In contrast, the stable organomineral pools constituted large C and N stocks which sustained only gradual non-equilibrium decay behavior. This large pool had a narrow C:N ratio with a strong enrichment of $\delta^{15}N$ (1.7 to 3.5‰). Continuing C and N stock decline at equilibrium were linear and the severe loss of stable aggregate C and N was an indicator of low stabilization of organic matter. By using a threshold loss

equilibrium deficit indicator (EQD) we propose that only recoveries matching the C and N loss and input stocks into the stable organomineral pool can shift the soil degradation threshold in response to organic matter inputs under tropical agriculture

1. Introduction

The potential for carbon (C) and nitrogen (N) sequestration in soil is determined by land use controls (Bronick and Lal. 2005; Zingore et al., 2005) and their total ecosystem budget reflects a long-term balance in pools and fluxes (Houghton et al., 2005). Global estimates of changes in the soil stocks of C and N are inferred from their content in soil organic matter (SOM) but long-term turnover is often simulated from model calculations (Six et al., 2001; Del Gado et al., 2003; Wander 2004) after accounting for the residence times of different C pools (Trumbore, 1993). To some extent, these calculations allow us to investigate the biochemical controls of C and N pool transformations but model estimates often fail to account for differences in C stabilization due to the physical order of the soil organomineral assemblage which determines accessibility of the decomposing SOM (Gregorich et al., 2006). For this reason, conceptual model approaches may not be appropriate in explaining functional relationships in the long-term degradation of SOM (Smith et al., 2002).

Through fractionation, the removal of organic matter particles in discrete compartments that have distinct chemical reactivity permits us to draw inferences about their ecosystem function as soil ecological indicators following land use change (Liefield et al., 2005). For instance, the free light fraction organic matter is isolated from free as well as dissassemblage of organic particles released from stable-unstable aggregates (Sollins et al., 1996). This fraction is the most biologically active (Gregorich et al., 2006) and its ecological significance arises from its role in soil

health and ecosystem functioning e.g. nutrient cycling (Doran et al., 1996; Kettler et al., 2001). It originates from direct inputs of non-structural soluble C and structural plant litter as well as atmospheric deposits good correlation with CO_2 respiration since energy reserve for biota (Sollins et al., 1996). Intra-aggregate organic matter, usually occluded by unstable macroaggregates and stable microaggregates is liberated by disruption from agricultural cultivation (Six et al., 2002, 2004). It forms a key niche that is inhabited by the decomposer community (Carter, 2002) and provides the interface between mineral components and free C in soil. The intra-aggregate fraction is transformed through physical dissassemblage and modifications to the quality of C incorporated during its life cycle (Six et al., 2004.) The residual organomineral assemblage is involved in the long-term C storage (Sollins et al., 1996)

The role of aggregation in the formation of stable and unstable assemblages is suggested to be the key driving mechanism for the association between organic matter and the soil mineral matrix (Tisdall and Oades, 1986; Carter, 2002). In native forest ecosystems, where equilibria exist in long-term C and N loss (Kinyangi et al., unpublished), C transfers between organic matter pools is regulated through aggregation processes (Blanco-Canqui and Lal. 2004). In addition, decomposition of the C pool is controlled by the rate and quality of organic matter deposition (Joffre et al., 2001). Carter, (2002) propose the need to develop a critical level of desired organic matter content but perhaps a threshold approach would better indicate loss of a functional role in relation to the non-linear changes of C between pools since fractions are critical drivers of C cycling in soil. Irreversible threshold change points in property and function are better valid assessments since fractions are sensitive indicators of land use change (Leifeld and Kögel-Knabner. 2004).

Soils are part of the ecological system (Whitkamp, 1971). The ecological importance of soil degradation remains unknown particularly as it relates to the loss of

critical soil ecological processes (Brown et al., 1999) or the degradation in the quality of the soil ecosystem property such as nutrient availability (Andrews et al., 2004). In degrading soil, we hypothesize that thresholds can be deduced from sudden and abrupt changes in non-linear trends (Groffman et al., 2006) which describe different equilibrium C and N contents in light and intra-aggregate organic matter fractions. In turn, these changes occur at such a large scale as to cause non-equilibrium alterations in the large organomineral fractions. Therefore our objectives were i) to assess long-term changes to C and N stocks in SOM pools as indicators of thresholds in tropical degrading soil and ii) to determine the effect of different soil as well as crop C and N sources on threshold behavior during long-term agriculture and iii) determine the effect of organic matter loss on agroecosystem function

2. Materials and methods

2.1 Experimental study sites

Three sites of degrading soil were established and consisted of forest and agricultural fields along the intensely cultivated margins of the Kakamega and Nandi forests in western Kenya. Two of these sites were located in higher elevation Nandi area on heavy textured soils while a third site was located at lower elevation Kakamega, on medium textured soil. Site chemical and physical properties of the ecosystem sites are presented in Table 1 and a full documented account of the forest and agriculture ecosystems, including a description of the longterm degradation of C stocks and nutrient losses has been reported by Kinyangi et al., (unpublished data). In brief, the natural vegetation of both forest ecosystems is derived from tropical rainforest species, including *Aningeria altissima* (A. Chev.), *Milicia excelsa* (Welw. C.C. Berg), *Antiaris toxicaria* (Lesch) and *Chrysophyllum albidum* (G. Don). At the

higher elevation Nandi sites, there are species of montane forests including *Olea capensis* (L.) and *Croton megalocarpus* (Hutchinson).

The forest ecosystems are developed on kaolinitic Acrisols (FAO-UNESCO-ISRIC, 1988) or Ultisols (Soil Survey Staff, 2003), derived from granite as well as other undifferentiated basement systems of parent rock formations (Jaetzold and Schmidt, 1983). Long-term climate data were obtained from Kaimosi and Kibiri recording stations which are adjacent to the forest margins (Table 1). All forest sites were located between 1500-2000 m above sea level (a.s.l.), with a mean annual temperature (MAT) ranging between 18.0 °C to 21.0 °C and a mean annual precipitation (MAP) of ~ 2000 mm (Table 1) (Jaetzold and Schmidt, 1983).

The three chronosequence sites of forest and agricultural cultivation were identified using landsat TEM images by observing change in land use patterns since forest conversion (Glenday, 2006). Together with data from the Kenya government Department of Forest, Ministry of Agriculture Extension Service, Soil Survey, and oral interviews with local institutional personnel and county council records, we previously described specific land use conversion categories that correspond to historical cropping patterns that influenced long-term C and nutrient losses (Kinyangi et al., unpublished data). For the purpose of this study we pooled soil sampled from the following categories; forest, <3, 4-19, 20-54, 55-81, 82-114 years of agricultural cultivation. Among agroecosystem sites, these chronosequence ages provided a gradient of time since native forest conversion and in all cases, only soils from agricultural fields for which there was no documented history of the addition of fertilizer and manure were sampled.

Table 3-1. Location and select properties of the reference forest ecosystem sites, western Kenya.

Ecosystem sites	Kakamega[a], Kibiri	North Nandi[b], Kiptuiya	South Nandi[c], Chepkumia
Location	00 º 10’ 06"N 34 º 51’ 40"E	00 º 13’ 31"N 35 º 00’ 27"E	00 º 09’ 34"N 34 º 57’ 37"E
Elevation [m.a. s. l]	1596	1969	1750
MAT. [ºC]	21.0	18.0	19.0
MAP ¥ [mm yr^{-1}]	2040	2119	2024
*Soil type	Ferr. Acrisol	Hum. Acrisol	Hum. Acrisol
Soil properties			
Clay+Silt [g kg^{-1}]	610	730	840
Sand [g kg^{-1}]	390	270	160
Bulk density‡ [Mg m^{-3}]	0.83	0.71	0.67
pH [water, 1:2.5]	6.1	7.4	6.2
#CEC [$mmol_c$ kg^{-1}]	99	248	331
Carbon [kg m^{-2}]	4.2	7.3	6.1
[1] Equilib. C [kg m^{-2}]	2.0	4.0	1.8
Nitrogen [kg m^{-2}]	0.5	0.7	0.7
[2] Equilb. N [kg m^{-2}]	0.2	0.4	0.2

Source: Kinyangi et al.,unpublished data

†Elevation in meters above sea level. Long-term ¥mean annual precipitation and ‡Mean annual temperature records for nearby stations; Kaimosi tea estates (Chepkumia), Kaimosi FTC (Kiptuiya) and Forest station (Kibiri). # Sum of base cations Ca^{2+}, $Mg^{2+}$and K^{+} calculated as charge ($mmol_c$ kg^{-1}) from Mehlich 3 extraction procedure. [1, 2] Equilibrium C and N stocks at 15[a], 25[b] and 36[c] years since forest conversion.

2.2 Soil sample collection

Soil samples were collected from 10 random locations in agricultural fields of the agroecosystem sites where cereal sorghum (*Sorghum bicolor* L.), finger millet (*Eleusine coracana* (L.) Gaertn), and maize (*Zea mays* L.) crops were historically cultivated without a known history of fertilizer addition. Due to tillage compaction in new agricultural fields, we adjusted the soil sampling depth in order to correct for the differences in mass of the core sample (Kinyangi et al., unpublished data). From bulk density measurements, we estimated that a sampling depth of 0 to 0.12 m in the forest, 0 to 0.11 m in new sites and 0 to 0.1 m for all other agroecosystem sites represented an equal mass of soil used to quantify C and N stocks. Nine undisturbed forest ecosystem reference sites were sampled to permit comparison of the cultivated plots with the native forest and to establish the equilibria of soil C and N stocks in the organic matter fractions prior to native forest conversion.

2.3 Organic matter fractionation

We applied a combined density and physical disruption energy to separate three pools of organic matter (Sohi et al., 2001). Each sample of 15.0 g air dried soil was added to 0.09 L of NaI solution, prepared to a density of 1.8 Mg m^{-3} (determined by hydrometer). Six 0.25 L polycarbonate centrifuge bottles were swirled by hand for 30 s to allow particles of SOM released from the breakdown of unstable aggregates to float off. The downward sedimentation of heavy particles was accelerated by centrifuging the bottles at 8000 × *g* for 30 min. Floating free light fraction was recovered from each bottle, together with the NaI solution, using a trimmed 25. mL plastic pipette (Sohi et al., 2001). This set-up was attached to a vacuum flask and a water aspirator suction line via 6-mm diameter tubing in order to exhaust the fraction contents. Free light fraction was isolated by decanting the contents of the vacuum

flask over a glass fiber filter (type GF/A, 47 mm diameter, 1.6 μm retention; Whatman) in a vacuum filtration unit (Millipore). Retained fraction material was rinsed thoroughly with deionised water using a wash bottle and a separate collector in order to remove soil mineral and salt contaminants. The receiver apparatus filter platform and threads of the filtration unit were rinsed in de-ionized water and dried before re-assembling the alternate collector for the next sample extraction.

In a second step, we isolated intra-aggregate light fraction from particles of SOM located within stable aggregates, which were released by re-suspending the contents of the centrifuge bottles and sonicating (Misonix XL 2020, Farmingdale, NY) for 5 min. Soil suspensions in the centrifuge bottles were dispersed by adjusting the probe horn (9.5 mm diameter) submersion to 19 mm depth. Actual calorimetric energy transfer was 0.25 kW, measured by temperature (ºC) change in 100 mL cold water over 5 min. (Sohi et al., 2001), then verified after 5 sample runs. Sonication resulted in energy inputs of 1.50 kJ g^{-1} soil. Because of the heat generated, the centrifuge bottles in were cooled in 1.0 L ice-packed beakers. After centrifugation, the intra-aggregate light fraction was recovered using the same procedure as described for free light fraction. In the last step, the residual organomineral fraction was recovered following 3 runs of centrifugation (8000× *g*, 15 min.) with deionised water to flush the excess NaI salt.

Total C and N were determined by dry combustion after fine grinding soil using a Mixer Mill (MM301, Retsch, Germany). Samples were analyzed for C and N contents with a Europa ANCA-GSL CN analyzer (PDZ Europa Ltd., Sandbach, UK). The C and N content was calculated after multiplying the C or N concentration (mg kg^{-1}) of the fraction with the dry weight yield of fraction per kg soil. Natural abundance ^{15}N, and the ^{13}C for the same samples were determined on a coupled Europa 20-20 continuous flow isotope ratio mass spectrometer (PDZ Europa Ltd.,

Sandbach, UK) following combustion at 1000°C. The $\delta^{15}N$ values were expressed relative to atmospheric N_2. The $\delta^{13}C$ values were expressed relative to Vienna-Pee Dee Belemnite (V-PDB). In addition, $\delta^{13}C$ and $\delta^{15}N$ values of 4 surface litter samples from forest and 9 crop litter samples from agroecosystem sites were determined to record the initial isotopic composition of the native forest C_3 and agroecosystem C_4 organic matter inputs. Based on the fraction chemical and physical attributes (Sohi et al., 2001), we use organic matter fraction and pool terms interchangeably to denote unstable pool (free light fraction), stable aggregate pool (intra-aggregate fraction) and stable organomineral pool (organomineral fraction).

2.4 Statistical modeling

Because C and N are key determinants of soil function, their long-term losses were estimated from non-linear regression, using model equation and curve fitting routines of SigmaPlot for Windows (SPSS Inc. 2004). The unstable and stable aggregate organic matter pool C and N loss data were fitted to a 3-parameter single exponential decay model:

$$y = y_o + a \times \exp^{-bx} \qquad \text{Eq. 1}$$

where, y_o = C, and N stocks at equilibrium, a = C and N stock loss, b = loss rate constant, x = time in years

For the organomineral pool, we tested the hypothesis that there is a continuous draw-down on the soil C and N stocks (Eq 2) based on the assumption that its decomposition does not equilibrate during a period of 100 years. Using data from the heavy-textured South Nandi site, we determined that an exponential decay function explained 10% more variation in the non-linear loss of C stocks in the stable organomineral pool (linear model; $r^2 = 0.80$, $p = 0.0164$; non-linear model, $r^2 = 0.90$, $p = 0.004$). Therefore we fitted:-$y = a \times \exp^{-bx}$ Eq. 2

Equation1 assumes equilibrium while Eq. 2 tests for non-equilibrium behavior. For all three agroecosystem chronosequences, Kinyangi et al., (unpublished data) established that the long-term soil degradation was characterized by an initial period of rapid losses of C and nutrients in recently cultivated sites (< 15 to 36 years) followed by a C loss equilibrium phase in fields that had been cultivated over a longer timescale (> 15 to 36 years and up to 104-114 years). For agricultural fields, C loss equilibrium was approached when ≥ 90% of the total soil C stocks (kg m^{-2}) were degraded after forest conversion. From the exponential model, the period of rapid C decline was determined as 25 years at north Nandi, 36 years at south Nandi and 15 years at Kakamega sites.

2.5 C and N sources

To estimate the proportion of remaining C content (C_s) from C_3 forest and cereal crop -derived C_4 C sources, we used the mixing model approximation (Solomon et al., 2002; Collins et al., 1999). First, we determined the maximum $\delta^{13}C$ range between forest litter and cereal crop litter $\delta^{13}C$ which was 13.8 ‰. Surface crop litter contained proportions of C_3 C derived from weeds in the cereal crop plots so its $\delta^{13}C$ value (-14.0 ±0.5 ‰) is nearly 1-2 ‰ more depleted than values typical of C_4 C. The C contents were partitioned following the equation:

$$\text{cereal crop } C_4\text{-}C = C_{cc} = [(\delta_{nfs} - \delta_{cs}) / (\delta_{nfl} - \delta_{cl})] \times C_s \quad \text{Eq. 3}$$

$$\text{native forest } C_3\text{-}C = C_{nf} = [C_s - C_{cc}] \quad \text{Eq. 4}$$

where $\delta_{nfs} = \delta^{13}C$ of forest soil, $\delta_{cs} = \delta^{13}C$ of cultivated soil approaching equilibrium $\delta_{nfl} = \delta^{13}C$ of forest litter and $\delta_{cl} = \delta^{13}C$ of crop litter

Figure. 3-1. Digital and light microscope images of soil from (a) native forest and (f) agricultural ecosystem as well as their respective surface litter fractions (b & g). After density and physical separation, free light fractions comprise recognizable plant debris (c, & h) whilst intra-aggregate fractions appear as finely divided, darker and more decomposed (d & i). The organomineral is darkest in color and represents the most highly decomposed C fraction (e & j)

The source of N was inferred from the change in the difference between the $\delta^{15}N$ enrichment value of the SOM fraction, from that of surface litter under forest and agroecosystem sites.

3. Results

3.1 Forest and agriculture ecosystems: litter properties.

The composition of forest surface and light fraction litter was dominated by recognizable coarse organic fragments of structural woody and non-structural leafy biomass (Figure 1b, c). In contrast, agroecosystem crop residues (Figure 1g) were finely divided into light fraction litter (Figure 1h). At the forest ecosystem sites, the surface litter N content was 2.9 ± 0.3 % N which appeared higher that the N content of surface litter from recently (< 15-36 years) cultivated agricultural fields of the agroecosystem sites (2.1± 0.3 % N). These values were 2 to 3 times higher than the maize litter N content (1.06% N) although the $\delta^{15}N$value of surface litter from agricultural fields was more depleted in the heavier isotope (Table 2). The surface litter chemistry at the agroecosystem sites was more similar to the maize crop litter both in the C (281 ± 37 g kg^{-1} vs 247 ± 51 g kg^{-1}) and N (14.4 ± 2.5 g kg^{-1} vs 10.6 ± 2.4 g kg^{-1}) contents as well as in the isotopic $\delta^{13}C$ (-14.0 ± 0.5 ‰ vs -13.2 ± 0.3 ‰) and $\delta^{15}N$ (4.5 ± 0.5 ‰ vs 4.3 ± 0.2) signatures. There were no significant differences in the C:N ratio of forest (13.0 ± 1.4 % N) and agroecosystem litter (15.2 ± 1.3 % N).

3.2 Soil organic matter: C stocks

The decay coefficients showed that Nandi soils sustained the largest loss in the proportion of the initial C contents for both unstable and stable aggregate pool (Figure 2a, b). The decline in C content from both organic matter pools was much less and represented a small fraction of the initial C content at Kakamega sites (Figure 2c).

Table 3-2. Litter chemical characteristics (± s.e.) of organic matter inputs to forest and agroecosystem sites, western Kenya

Ecosystem sites	Carbon	Nitrogen	$\delta^{13}C$	$\delta^{15}N$	C:N
	----(g kg^{-1})----		---(‰)---		
Forest litter					
Surface, *n* = 4	371 (12)	29.3 (2.7)	-27.8 (0.7)	2.9 (0.8)	13.0 (1.4)
Agriculture litter					
< 15-36 yrs, *n* = 5	305 (32)	20.6 (3.4)	-19.7 (1.3)	5.1 (0.8)	15.2 (1.3)
> 15-36 yrs, *n* = 4	281 (37)	14.4 (2.5)	-14.0 (0.5)	4.5 (0.5)	19.2 (1.9)
Maize, *n* = 2	247 (51)	10.6 (2.4)	-13.2 (0.3)	4.3 (0.2)	23.5 (0.6)

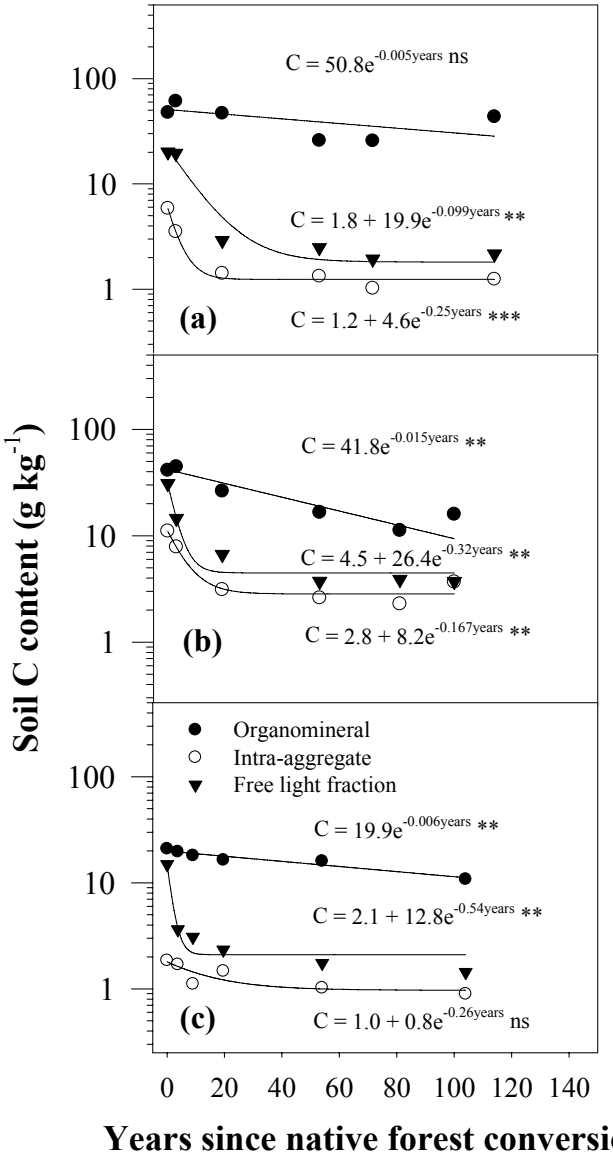

Figure. 3-2. Long-term changes of C contents in soil organic matter fractions of ecosystem sites (a) north Nandi, (b) south Nandi and (c) Kakamega, western Kenya. Model: $y = y_o + a \times \exp^{-bx}$ (unstable, stable aggregate) and $y = a \times \exp^{-bx}$ (stable organomineral) Significance level designated as 0.05*; 0.01** and <0.0001***.

For Nandi sites the C rate of loss constant of the unstable pool (-0.01) was two and a half times lower than the C rate of loss of the stable aggregate pool (-0.25) and the C contents remaining during the C loss equilibrium phase were higher at south Nandi than at both north Nandi and Kakamega sites (Figure 2a, b & c). At south Nandi, the C rate of loss in the stable organomineral pool was two and a half times higher than at Kakamega and the decline continued without approaching equilibrium. The rate of C loss for this fraction was not significant at the north Nandi sites. For all agroecosystem sites, the overall C degradation from unstable pool was high, ranging from 71-82% of the initial C content. For the stable aggregate pool, C changes at the Nandi sites (59-64%) were nearly twice as much as the loss (28%) that occurred at the Kakamega sites.

3.3 Soil organic matter: C sources

At the C loss equilibrium, a shift was recorded in the isotopic composition of the organomineral fractions (Figure 3) which resulted in the enrichment of $\delta^{13}C$ values of between 4.0 to 7.7 ‰ at the Nandi sites and a slightly narrower range of between 1.7 to 2.3 ‰.at the Kakamega sites. At north Nandi the $\delta^{13}C$ values of the unstable and stable aggregate pool were more similar to the $\delta^{13}C$ signature of mixed sources of C_3/C_4 sources of C from agricultural fields. The $\delta^{13}C$ signature for the same fractions at south Nandi (-15.0‰) and the free unstable pool at north Nandi (-12.4‰) appeared to consist entirely of C_4 sources of C (Figure 3). In the Kakamega soil, only the stable aggregate pool consists of C_4 sources of C whereas the unstable and stable organomineral pool contain mixed C_3/C_4 sources of C. All organomineral fractions and the free light fraction at north Nandi retained a mixture of C_3/C_4 sources of C with $\delta^{13}C$ values ranging between -18‰ to -20‰.

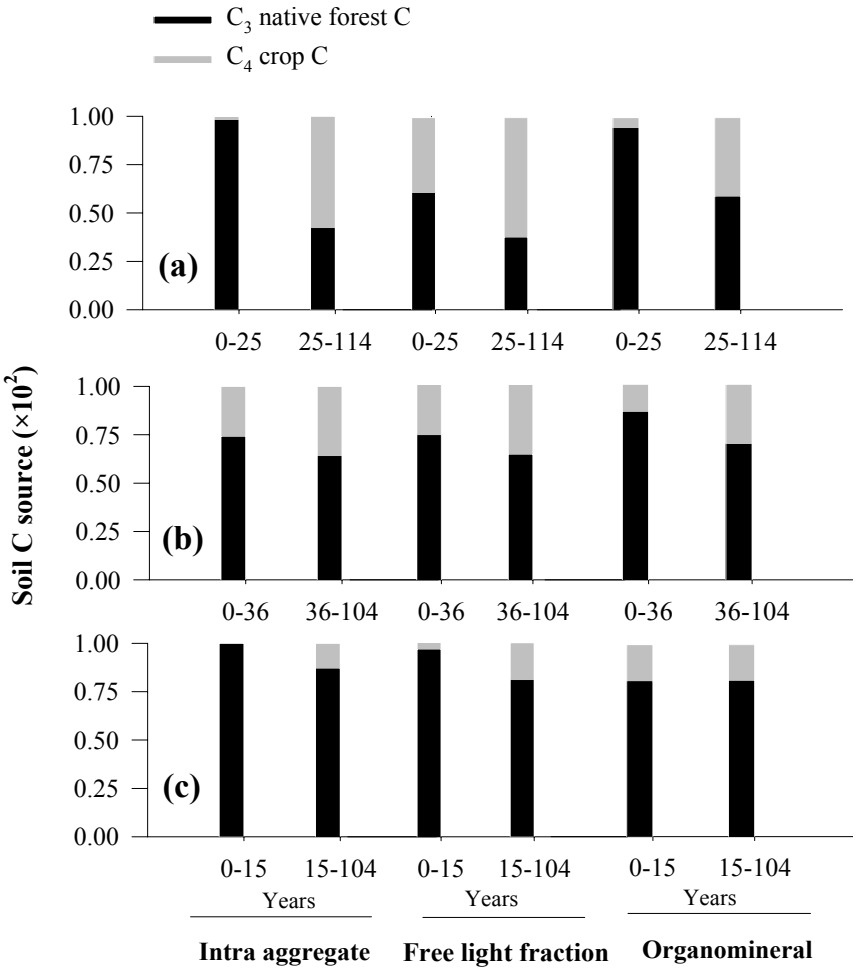

--------σ^{13}C values (‰)----------

(a)	-22.7	-15.0	-20.8	-12.4	-23.8	-18.3
(b)	-24.8	-20.0	-24.7	-18.7	-22.5	-18.5
(c)	-25.2	-23.5	-16.9	-14.4	-22.3	-19.8

Figure. 3-3. Sources of C_3 forest and C_4 crop C (%) as a result of switching δ ^{13}C values in soil organic matter fractions of ecosystem sites (a) north Nandi, (b) south Nandi and (c) Kakamega, western Kenya

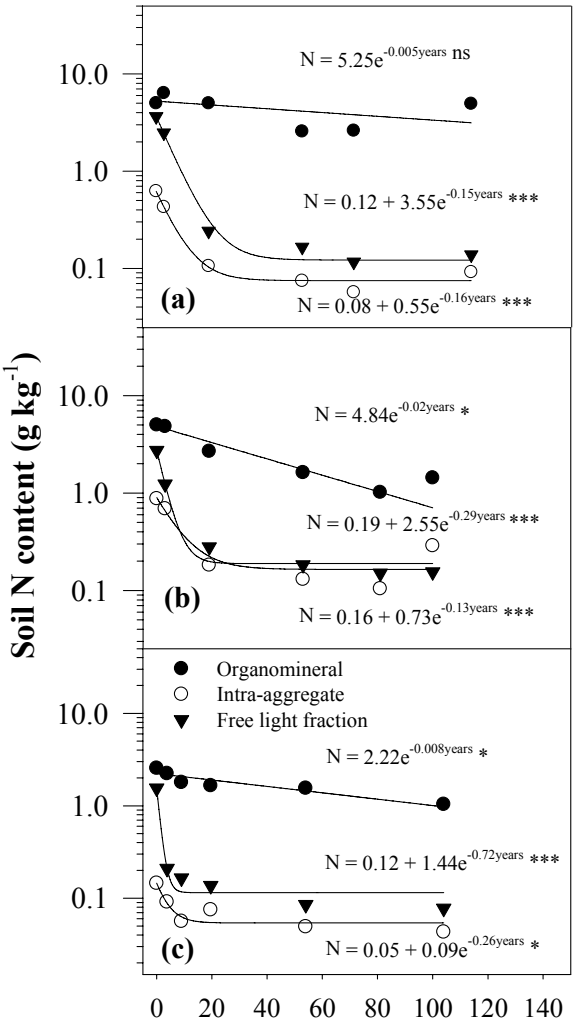

Figure. 3-4. Long-term changes of N content (g kg^{-1}) in soil organic matter fractions of ecosystem sites (a) north Nandi, (b) south Nandi and (c) Kakamega, western Kenya. Model: $y = y_o + a \times exp^{-bx}$ (unstable, stable aggregate) and $y = a \times exp^{-bx}$ (stable organomineral). Significance level designated as 0.05*; 0.01** and <0.0001***.

3.4 Soil organic matter: N stocks

For all agroecosystem sites, we observed an exponential decline in N content of the free light and intra-aggregate organic matter. (Figure 4a, b & c). In the unstable pool the rate of loss at Kakamega (-0.72) was nearly five-fold higher than north Nandi (-0.15) and two and a half times greater than the rate of loss at north Nandi (-0.29). At the C loss equilibrium, with the exception of south Nandi, the remaining N content in the stable aggregate organic matter (0.05-0.08 g kg^{-1}) were less than half of the N content retained in the unstable pool (0.12-0.19 g kg^{-1}). The largest changes to the stable organomineral pool were observed at south Nandi (Figure 4b). For all sites, the overall N changes from unstable pools were high, ranging from 81% of the initial to as much as 92% N decline between the initial rapid loss period (< 15 to 36 years) and the C loss equilibrium phase (> 15 to 36 years). For Nandi sites the N loss from the stable aggregate pool ranged between 42 to 72% of initial N content and these changes are nearly similar to N decline (42%) at the Kakamega sites.

3.5 Soil organic matter: N sources

There was little shift in the $\delta^{15}N$ composition of the free and stable aggregate pool at south and north Nandi sites (Figure 5). Small changes ranging from 0.2-0.3 ‰ were also recorded at Kakamega. At all agroecosystem sites the signature changes for these fractions were within variation of 1.0 ‰. The $\delta^{15}N$ signature changes of the stable organomineral pools showed a large difference (1.7-3.5 ‰) and the overall enrichment in the $\delta^{15}N$ values indicated depletion in the heavier isotope during fractionation. In contrast, the $\delta^{15}N$ values of the unstable pool and stable aggregate pool were relatively enriched in the heavier isotope fraction, particularly for south Nandi and Kakamega sites during the rapid sol degradation phase (Figure 5a, c)

4. Discussion

4.1 Forest and agriculture ecosystems.

The surface litter characteristics were a good indicator of the quality of organic matter inputs to forest and agroecosystem sites (Table 1). The C content of the forest litter (37.1% C) was slightly lower than the expected range for plant material and it varied in the forms of wood and leaf debris (Figure 1b). Its N concentration (2.90% N, n = 4)exceeded the N content in leaves (1.90% N, n=78) reported for tropical forest sites (Martinelli et al., 1999) but was similar to N content of the litter layer (1.6-2.2%) at Kakamega forest (Werner et al., 2007). These values were also higher compared to the N content of leaves from 4 tropical forests (0.4-1.1%N) in Indonesia (Anderson et al, 1983). The agroecosystems were dominated by N from surface crop litter (5.1 ‰). Furthermore, the C content of crop litter from agroecosystem sites were significantly lower than forest litter and had a large enrichment in the $\delta^{13}C$ values of between 8.1 to 13.8 ‰. Also the $\delta^{15}N$ value of forest litter (2.9 ±0.8) was significantly depleted compared to the maize litter signature (4.3 ±0.2) presumably due to the contribution of biological N fixation in forest. Litter N may also be derived from fixed N, since leguminous trees are common in tropical forests (Pons et al., 2006) and the isotopic signal was closer to 0.0 even though the agricultural fields had no known fertilization history and N fixation was expected to decrease during cultivation (Cleveland et al., 199). Because the likely interference of mineral particles to the unstable and stable aggregate pool is negligible (Sollins et al., 2006) we conclude that long-term agriculture results in alteration of the agroecosystem litter chemistry as organic matter sources switch from diverse forest C_3 to crop monoculture of C_4 dominated inputs. In addition, some C losses occur before crop litter is incorporated to soil and this loss increases in agricultural fields (Table 2) compared to forest ecosystems.

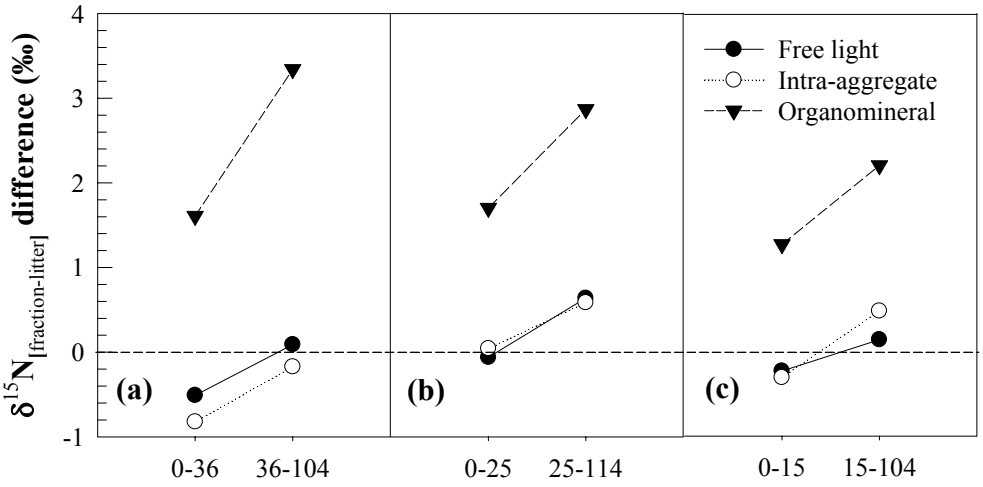

			--------σ15N values (‰)----------			
Organomineral	6.7	7.8	6.8	7.4	6.4	6.7
Free light	4.3	4.3	5.1	5.1	4.8	5.0
Intra-aggregate	4.6	4.6	5.0	5.1	4.9	4.6

Figure. 3-5. Isotopic δ ^{15}N values as a result of switching sources of N in soil organic matter fractions of ecosystem sites (a) south Nandi, (b) north Nandi and (c) Kakamega, western Kenya.

4.2 Declining soil C and N stocks

There was an exponential decline in the contents of C and N of all free light and intra-aggregate fractions at all three chronosequence sites. Compared to the stable organomineral pool, a large proportion of the initial C and N content in unstable and stable aggregate pool were lost during the 15 to 36-yr period of rapid C decline. During this period, and in both fractions, the non-linear loss of C and N content upon forest conversion occurred primarily from decomposition of litter accumulated during forest rather than cereal crop farming. Due to the heterogeneity in the quality and therefore decomposability of these litter substrates, there is non-linearity in the rate of C and N loss (Figure 2, Figure 4). In our previous work, we studied changes in the chemical composition of organic matter from the same ecosystem sites and found that much of the chemically labile C such as plant-derived carbohydrates was lost upon forest conversion. At the C loss equilibrium only subtle changes occurred in the C functional group chemistry (Solomon et al. 2007). These changes in the litter chemistry appear to control the non-linear decline in C and N content, particularly during the rapid C loss phase (< 15 to 36-yr period)

The loss of N from the unstable (93-97%) and stable (82-87%) aggregate pools was highest at the Nandi ecosystem sites but the lower equilibrium N content at north Nandi (0.08 g kg^{-1}) and Kakamega (0.05 g kg^{-1}) reflect a poor contribution of aggregate stabilization of N. Soil aggregate stabilized organic matter is enriched in C substrates (Gregorich et al., 2006) that help to bind organomineral particles but its wide C:N ratio (Sohi et al., 2001) indicates that it may be a poor source of N. At all sites, C and N losses in the stable organomineral pools were an order of magnitude higher than the unstable and aggregate stable pools and the loss rate kinetics showed that their degradation continued over the entire 100-yr period without approaching equilibrium. In long-term degrading Australian soils, Dalal and Mayer, (1986)

attribute the development of an equilibrium phase after 70 years of cereal cropping to a reduction in C loss from physical protection of organic matter by soil aggregates. Western Kenya soils are dominated by Ultisols that have low activity kaolinite and high proportions of mineral Fe and Al oxides (Krull et al., 2002). Based on the immediate decline and the extremely low equilibrium C and N contents (Figure 2, Figure 4) in the stable aggregate pools, we are unable to conclude if physical protection of aggregate associated organic matter was significant in stabilizing C and N. However, we note that Kakamega soils not only have lower C and N equilibria but also reach these equilibria much faster than Nandi soils.

4.3 Changing sources of soil C and N

The changes in the $\delta^{13}C$ composition can be attributed to a progressive isotopic enrichment of the SOM from either decomposition (Bernoux et al., 1998) and associated enrichment of the heavier isotope (Kramer et al., 2003) as well as source additions of fresh litter inputs with different isotopic contents (Högberg, 1997; Solomon et al., 2002). At north Nandi, C_4 C contribution at the C loss equilibrium to the stable organomineral pool was large (12.9 g C kg^{-1}), which accounted for 41% of the total C pool but replaced only half of the losses from unstable pool (19.3 g C kg^{-1}) and stable aggregate pool (4.6 g C kg^{-1}). In the Kakamega soils, C_4 C contribution to the organomineral pool was lower (2.7 g C kg^{-1}) representing 19.0% of the total C pool. This input compensated for less than one quarter of the loss sustained from the unstable pool (12.8 g C kg^{-1}) and stable aggregate pool (0.8 g C kg^{-1}). Similarly for soil at south Nandi, the effect of low C_4 C input (4.4 g C kg^{-1}) comprising 30% of the total C pool was insufficient to offset large losses from the unstable pool (26.4 g C kg^{-1}) and stable aggregate pool (8.2 g C kg^{-1}).

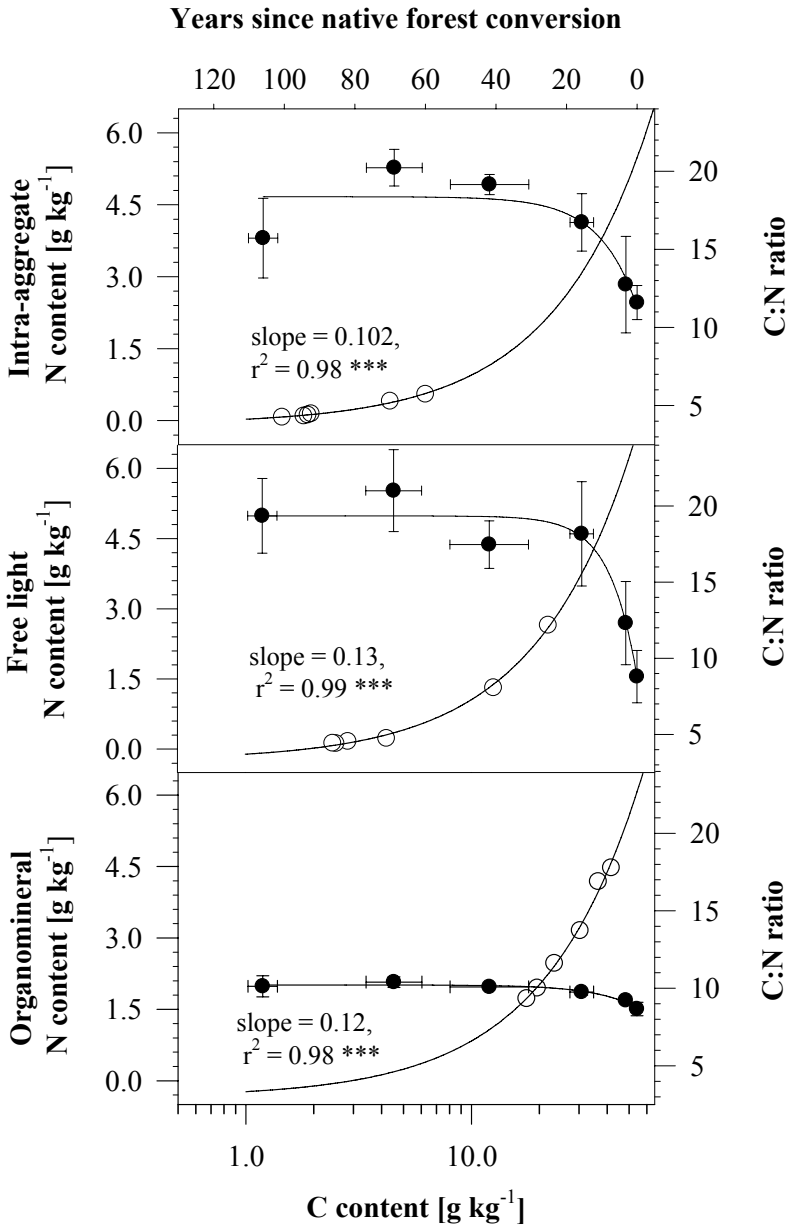

Figure. 3-6. Semi-log plot of soil C and N losses and the equilibrium C:N ratio of organic matter fractions from forest (0-0.12 m) and agroecosystem sites (0-0.11 m, 0-0.10 m), western Kenya.

Previously Kinyangi et al., (unpublished data) found that nearly half of the total C is from new input but after correcting for respiration losses, actual C incorporated is about one third of new crop C

A small isotopic enrichment to the $\delta^{15}N$ composition reflected the unchanged N input sources in the unstable and stable aggregate pools of the degrading soil. In comparison the largest positive shift of up to 1.3‰ in $\delta^{15}N$ occurred in the organomineral fraction. This confirmed that most of the N loss at all sites was from the stable organomineral C pool which may lead to N limitation at the agroecosystem sites. Agricultural soils derived from tropical forests are known to sustain large N losses during slash and burn practices (Danuse et al., 2002; Houghton, 2005) and the large enrichment in the $\delta^{15}N$ often indicates not only N loss (Högberg, 1990) but also the progressive development of N limitation (Murty et al., 2002).

4.4 Thresholds of soil C and N loss

Rapid C and N losses during the initial rapid decline phase, together with the subsequent development of agroecosystem equilibrium were clear indicators sudden changes in the property of organic matter. Two forms of functional threshold behavior (Brisket et al., 2006) can be applied to explain the long-term C and N decline and relationships between organic matter pools in forest and agriculture ecosystem sites. Upon agricultural conversion, the rapid and abrupt change in the C and N contents of the unstable and stable aggregate organic fractions leads to a large shift in the soil total C and N (Figure 6). Using both fractions we can sum each stock decline and calculate a threshold loss equilibrium deficit ratio (EQD). At this point, the C reference to C equilibrium value of 1.0 (C_{ref}/C_{eq}) represents a one half reduction in the initial C and N conetnt of the forest ecosystem sites. From this approach, the C ratio EQD was 8.1, 4.8 and 4.4 for north Nandi, south Nandi and Kakamega sites respectively. From this

ratio, we can deduce that higher C inputs are required to address the deficit at north Nandi than for south Nandi and Kakamega sites, even though the initial C contents at north Nandi (71.8 g kg^{-1}) were nearly similar to south Nandi (83.9 g kg^{-1}). The N ratio EQD was 15.5, 9.4 and 9.0 for north Nandi, south Nandi and Kakamega sites respectively. These threshold loss EQDs are much wider and approach twice the range of those estimated for C. Wide EQDs suggest that N inputs in organic matter fractions would need to be furnished at more than twice the C input rate in order to sustain the deficit and recovery. One of the feasible ways to address the deficit is through increasing n inputs from N fixing crops such as legumes (Thies et al., 1991), cover crops (Doran and Jones, 1996) and agroforestry tree species (Lehmann et al., 2001) at much larger biomass input rates than would be feasible under most current agricultural practices. In the agroecosystem sites, threshold loss EQD represents a critical point of deflection (May, 1977) below which agroecosystem functions with respect to C stabilization and N conservation appear greatly diminished and difficult to recover.

Secondly, C and N changes in the stable organomineral pool without loss approaching equilibrium was an order of magnitude higher compared to changes in the smaller unstable and stable aggregate pools. These differences in organic matter pool equilibrium and non-equilibrium behavior resulted in a significant alteration to the rate processes of C and N transfer between organic matter pools. The overall C:N rate of decline was similar for all pools (slope = 0.102, 0.13 and 0.12 for stable aggregate, unstable and stable organomineral). Given the fraction quality, the C:N ratio of the unstable and stable aggregate pools appeared to suggest that these pools immobilize N (Figure 6). Opposite changes in C:N ratio has sometimes been used to give inconsistent assertions about C and N decline during land use change (Pineiro et al., 2006).

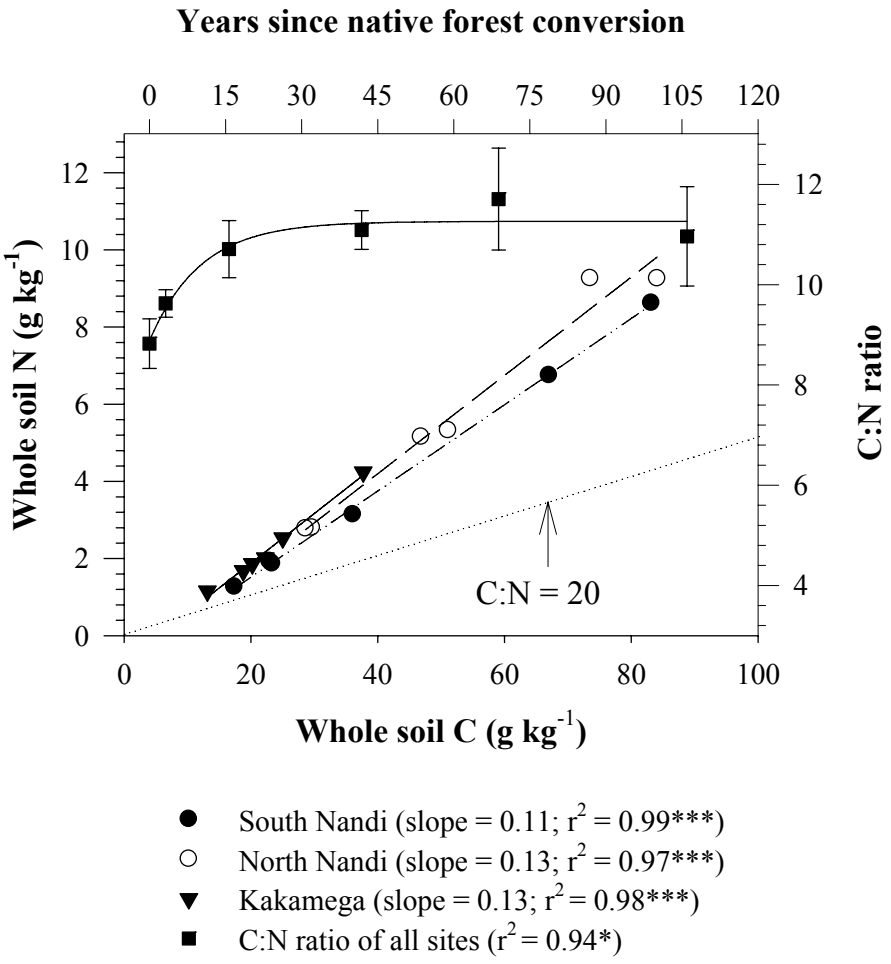

Figure. 3-7. Declining total soil C and N concentration (g kg^{-1}) in whole soil of forest (0-0.12 m) and agroecosystem sites (0-0.11 m, 0-0.10 m), western Kenya.

In our study C:N changes in decomposing organic matter caused differences in the rate of decay between pools without affecting the long-term decline in C and N content (Figure 6) from all agroecosystem sites.

4.5 Thresholds: Implications for soil function

Thresholds may be defined as ecosystem discontinuities (May, 1977; Groffman et al., 2006) where a deflection in the response indicates loss of key ecosystem properties (Briske et al., 2006). These points can be determined by formulating indicators that correlate well with agroecosystem function (Herrick et al., 2002). In the western Kenya agroecosystems, loss of C and N leads to a sharp decline in energy sources for microbial growth, which in turn causes a reduction in nutrient transformation. Other agroecosystem soil health and soil quality attributes whose properties may change or be modified include, C stabilization due to alteration in litter quality and diversity (Joffre et al., 2001), N sources particularly N fixation (Cleveland et al., 1999; Pons et al., 2007), and N availability (Högberg, 1990; Pineiro et al., 2006). At the agroecosystem loss equilibrium, some functions of these key processes may be lacking or are permanently removed. For instance, the litter quality and diversity contributes to a large N pool in the forest but during the rapid C loss phase is gradually replaced by crop litter from cereal monoculture. This results in severe N limitation (Figure 7) during the agroecosystem equilibrium phase. From the isotopic data in Figure 3, C_4 crop C inputs would need to be increased substantially in order to match flows into the organomineral pool. In this case, crop C additions to agricultural fields would increase two times at north Nandi, four times at Kakamega and up to eight times at south Nandi. While the first two to four fold increases can be addressed through mineral fertilization (Dalal and Mayer. 1986) and improved crop management (Batjes and Sombroek, 1997), it is unlikely the 8-fold increase can be met under crop

agriculture alone. For degrading tropical soil, these limitations present a threshold level where only a drastic change to the farming system, such as the incorporation of tree-crop and fallow rotations (Lehmann et al., 2001) along with a modified tillage regime (Six et al., 2004) would lead to a C and N recovery trajectory. Changing organic matter quality does not influence C and N losses but it is unclear what effects this would have on soil health and soil quality. In part, this is due to the fact that these agroecosystems are constantly adjusting towards loss equilibrium of C and N where the C:N ratio is near 10 for a very wide range of C and N contents in whole soil (Figure 7).

5. Conclusions

We have determined that C and N loss upon forest conversion represents a rapid and abrupt change, causing a large shift in the total soil C and N. Slow persistent changes in the stable organomineral pool occurs at an order of magnitude higher than C and N losses sustained in the unstable and stable aggregate soil C pools. By using a threshold loss equilibrium indicator (EQD) we argue that only recoveries matching the loss and input stocks into the stable organomineral fraction can shift the soil degradation threshold in response to organic matter inputs under cultivation agriculture. Continuing C and N decline at equilibrium was linear and the severe loss of stable aggregate C and N is an indicator of poor physical protection of organic matter. One of the key agroecosystem quality attributes whose functioning is likely impaired due to low C and N equilibrium content is the role of biota in nutrient transformations and this largely arises from irreversible loss in litter and litter diversity given monoculture inputs. Therefore these agroecosystem changes coupled with reduced N fixation under cereal cropping appear permanent. Non-linear changes in soil organic matter pools suggest thresholds which are indicators of changing

ecological processes. For all sites, a C and N loss in the organomineral associated organic matter was not stabilized over a longer time scale of 100 years. Unstable and stable aggregate pools accounted for a small fraction of the total C in soil and their low equilibrium indicates that their functional recovery is dependent on drastic change in inputs and management

REFERENCES

Anderson J. M., John Proctor; H. W. Vallack 1983. Ecological studies in four contrasting lowland rain forests in Gunung Mulu national park, Sarawak: III. Decomposition processes and nutrient losses from leaf litter. Journal of Ecology 71: 503–527.

Andrews, S.S., D.L. Karlen, and C.A. Cambardella. 2004. The Soil Management Assessment Framework: A quantitative evaluation method with case studies. Soil Sci. Soc. Am. J. 68:1945–1962.

Batjes, N.H., and W.G. Sombroek. 1997. Possibilities for C sequestration in tropical and subtropical soils. Global Change Biology 3:161–173.

Bernoux, M., C.C. Cerri, C. Neill, and J.F.L. De Moraes. 1998. The use of stable carbon isotopes for estimating soil organic matter turnover rates. Geoderma 82:43–58.

Blanco-Canqui, H., and R. Lal. 2004. Mechanisms of carbon sequestration in soil aggregates. Crit. Rev. Plant Sci. 23:481–504.

Briske, D.D., S.D Fuhlendorf, F.E Smeins. 2006. A unified framework for assessment and application of ecological thresholds. Rangeland Ecology & Management. 59: 225–236.

Bronick, C.J., and R. Lal. 2005. Soil structure and management: A review. Geoderma 124:3–22.

Brown, J.R., Herrick J, Price D. 1999. Managing low-output agroecosystems sustainably: The importance of ecological thresholds. Can. J. For. Res. 29:1112–1119

Carter, M.R., 2002. Soil quality for sustainable land management: Organic matter and aggregation interactions that maintain soil functions. Agron. J. 94:38–47.

Cleveland, C.C., A. R. Townsend, D. S. Schimel, H. Fisher, R. W. Howarth, L. O. Hedin, S. S. Perakis, E. F. Latty, J. C. Von Fischer, A. Elseroad, and M. F. Wasson. 1999. Global patterns of terrestrial biological nitrogen (N-2) fixation in natural ecosystems. Global Biogeochem. Cycles 13:623-645.

Collins, H.P., R.L. Blevins, L.G. Bundy, D.R. Christenson, W.A. Dick, D.R. Huggins, and E.A. Paul. 1999. Soil carbon dynamics in corn based agroecosystems: Results from carbon-13 natural abundance. Soil Sci. Soc. Am. J. 63:584–591.

Dalal, R.C., and R.J. Mayer. 1986. Long-term trends in fertility of soils under continuous cultivation and cereal cropping in Southern Queensland: II. Total organic carbon and its rate of loss from the soil profile. Aust. J. Soil Res. 24:28–292

Danuse, M., M. U. F. Kirschbaum, R. E. Mcmurtrie, and H. Mcgilvray. 2002. Does conversion of forest to agricultural land change soil carbon and nitrogen? a review of the literature. Global Change Biology 8:105-123.

Del Galdo, I., J. Six, A. Peressotti, and M.F. Cotrufo. 2003. Assessing the impact of land-use change on soil C sequestration in agricultural soils by means of organic matter fractionation and stable isotopes. Global Change Biology 9:1204–1213.

Doran, J.W., and A.J. Jones. 1996. Methods for assessing soil quality. SSSA Spec. Publ. 49. SSSA, Madison, WI.

FAO-UNESCO-ISRIC (1988), Revised legend, FAO-Unesco soil map of the world, World Soil Resources Reports 60: 119.

Glenday, J. 2006. Carbon storage and emissions offset potential in an East African tropical rainforest Forest Ecology and Management 235: 72–83.

Gregorich, E.G., M.H. Beare, U.F. McKim, J.O. Skjemstad. 2006. Chemical and biological characteristics of physically uncomplexed organic matter. Soil Sci. Soc. Am. J. 70:975–985.

Groffman, P. M., J. S. Baron, T. Blett, A. J. Gold, I. Goodman, L.H. Gunderson, B. Levinson, M. Palmer, H.W. Paerl, G.D. Peterson, N. LeRoy Poff, D.W. Rejeski, J.F. Reynolds, M.G. Turner, K.C. Weathers, and J. Wiens. 2006. Ecological thresholds: the key to successful environmental management or an important concept with no practical application? Ecosystems 9:1–13.

Herrick, J.E., J.R. Brown, A.J. Tugel, P.L. Shaver, and K.M. Havstad. 2002. Application of soil quality to monitoring and management: Paradigms from rangeland ecology. Agron. J. 94:3–11.

Högberg, P. 1990. Forests losing large quantities of nitrogen have elevated 15N: 14N ratios. Oecologia 84: 229–231.

Högberg, P. 1997. 15N natural abundance in soil–plant systems. New Phytologist 137: 179–203.

Houghton, A R. 2005. Aboveground forest biomass and the global carbon balance. Global Change Biology 11: 945–958.

Jaetzold, R., and H. Schmidt. 1983. Farm management handbook of Kenya. Natural conditions and farm management information. Vol. II. Part A. Ministry of Agric. Nairobi, Kenya

Joffre, R.J., G.I. Ågren, D. Gillon, and E. Bosatta. 2001. Organic matter quality in ecological studies: theory meets experiment. Oikos 93, 451–458.

Kettler, T.A., J.W. Doran, and T.L. Gilbert. 2001. Simplified method for soil particle-size determination to accompany soil-quality analyses. Soil Sci. Soc. Am. J. 65:849–852.

Kramer, M.G., P Sollins, R.S Sletten, and P.K. Swart. 2003. N isotope fractionation and measures of organic matter alteration during decomposition. Ecology 84:2021–2025.

Krull, E.S., E.A. Bestland, and W.P. Gates. 2002 Soil organic matter decomposition and turnover in a tropical Ultisol: Evidence from 13C, 15N and geochemistry. Radiocarbon 44:93–112.

Lehmann, J., M.S. Cravo, and W. Zech. 2001. Organic matter stabilization in a Xanthic Ferralsol of the central Amazon as affected by single trees: chemical characterization of density, aggregate and particle size fractions. Geoderma 99:147-168.

Leifeld, J., and I. Kögel-Knabner. 2004. Soil organic matter fractions as early indicators for carbon stock changes under different land-use? Geoderma 124:143–155.

Martinelli, L. A., M. C Piccolo, A. R Townsend, P. M.Vitousek, E. Cuevas, W. McDowell, G. P Robertson, O. C Santos, and K. Treseder. 1999. Nitrogen stable isotopic composition of leaves and soil: tropical versus temperate forests. Biogeochemistry 46: 45– 65.

May, R. M. 1977. Thresholds and breakpoints in ecosystems with a multiplicity of stable states. Nature 269:471–477.

Murty, D., M.U.F. Kirschbaum, R.E. McMurtrie, and H. McGilvray. 2002. Does conversion of forest to agricultural land change soil carbon and nitrogen? A review of the literature. Glob. Change Biol. 8:105–123.

Piñeiro, G., M. Osterheld, W. Batista, and J.M. Paruelo. 2006. Opposite changes of whole-soil vs. pools C:N ratios: A case of Simpson's paradox with implications on nitrogen cycling. Global Change Biol. 12:804–809.

Pons, T.L., K. Perreijn, C. van Kessel, M. J. A. Werger. 2007. Symbiotic nitrogen fixation in a tropical rainforest: 15N natural abundance measurements supported by experimental isotopic enrichment New Phytologist 173: 154–167.

Six, J., R.T. Conant, E.A. Paul, and K. Paustian. 2002a. Stabilization mechanisms of soil organic matter: Implications for C-saturation of soils. Plant Soil 241:155–176.

Six, J., H. Bossuyt, S. De Gryze, and K. Denef. 2004. A history of research on the link between (micro) aggregates, soil biota, and soil organic matter dynamics. Soil Till. Res. 79:7-31.

Smith, J.U., P. Smith, R. Monaghan, and J. MacDonald. 2002. When is a measured soil organic matter fraction equivalent to a model pool? European Journal of Soil Science. 53:405–416.

Sohi, S.P., N. Mahieu, J.R.M. Arah, D.S. Powlson, B. Madari, and J.L. Gaunt. 2001. A procedure for isolating soil organic matter fractions suitable for modeling. Soil Sci. Soc. Am. J. 65:1121–1128.

Soil Survey Staff. 2003. Keys to soil taxonomy. 9th ed. USDA-Soil Conservation Service, Pocahontas Press, Blacksburg, VA.

Sollins, P., Swanston, C., Kleber, M., Filley, T.R., Kramer, M., Crow, S., B.A. Caldwell, K. Lajtha and R. Bowden. 2006. Organic C and N stabilization in a forest soil: evidence from sequential density fractionation. Soil Biology & Biochemistry 38: 3313–3324.

Sollins, P., P. Homann, and B.A. Caldwell. 1996. Stabilization and destabilization of soil organic matter: Mechanisms and controls. Geoderma 74:65–105.

Solomon D., F. Fritzsche, J. Lehmann, M. Tekalign, and W. Zech. 2002. Soil organic matter dynamics in the sub-humid agroecosystems of the Ethiopian highlands:

Evidence from natural 13C abundance and particle-size fractionation. Soil Sci Soc Am J. 66: 969-978.

Solomon, D., J. Lehmann, J. Kinyangi, W. Amelung, I. Lobe, S. Ngoze, S. Riha, A. Pell, L. Verchot, D. Mbugua, J. Skjemstad and T. Schäfer. 2007. Long-term impacts of anthropogenic perturbations on the dynamics and speciation of organic carbon in tropical forest and subtropical grassland ecosystems. Global Change Biol. 13: 511–530.

SPSS Inc. 2004. Sigma Plot 9.01. Chicago, IL.

Thies, J. E., P. W. Singleton, and B. B. Bohlool. 1991. Influence of the size of indigenous rhizobial populations on establishment and symbiotic performance of introduced rhizobia on field-grown legumes. Appl. Environ. Microbiol. 57: 19–28.

Tisdall, J.M., and J.M. Oades. 1982. Organic matter and water-stable aggregates in soils. J. Soil Sci. 33: 141–163.

Trumbore, S.E. 1993. Comparison of carbon dynamics in tropical and temperate soils using radiocarbon measurements. Global Biogeochem. Cycles 7: 275–290.

Wander, M.M. 2004. Soil organic matter fractions and their relevance to soil function, p. 67–102. In F. Magdoff and R. Weil (ed.) Advances in agroecology. CRC Press, Boca Raton, FL

Werner, C., R. Kiese, and K. Butterbach-Bahl. 2007. Soil-atmosphere exchange of N2O, CH4, and CO2 and controlling environmental factors for tropical rain forest sites in western Kenya. Journal of Geophysical Research 112, D03308, doi:10.1029/2006JD007388.

Witkamp, M. 1971. Soils as components of ecosystems. Annu. Rev. Ecol. Sys. 2: 85–110.

Zingore, S., C. Manyame, P. Nyamugafata, and K. E Giller. 2005. Long-term changes in organic matter of woodland soils cleared for arable cropping in Zimbabwe. European Journal of Soil Science 56: 727-736.

CHAPTER 4

MOLECULAR ALTERATION OF MICROAGGREGATE ORGANIC MATTER AND MINERAL FORMS IN LONG-TERM CULTIVATED SOIL

Abstract

In situ organic matter transformations involving carbon (C) and nitrogen (N) molecular changes modify the geochemistry of soil under long-term agriculture. Using bright light synchrotron infrared and X-ray photo-electron spectroscopy, we probed C and N molecular alterations in order to understand their chemical evolution in a kaolinitic soil. After deforestation, long-term cultivation over a 104–year period caused a 2-3-fold depletion in the microaggregate surface C and N atomic mass. Evaluations of C1s, O1s and N1s by XPS revealed the degradation of aromatic C and pyridinic N from aromatic amines. On the basis of wide scan XPS, microaggregate surface C and N changes were accompanied by depletion of Mg and Ca salts originating from native forest soil. In forest soil, gibbsite formations were associated with a disordered kaolinite mineral phase. For areas consisting of organic matter "hot spots", μ-FTIR chemigram profiles showed that the molecular enrichment ratio of –COH (1000 cm^{-1} to 1085 cm^{-1}) to amide N–C=O (1635 cm^{-1}), was negatively correlated to a linear dehydroxylation of kaolinite –OH at 3695 cm^{-1} upon cultivation ($r^2 = 0.72$, $p = 0.0038$). In turn, kaolinite dehydroxylation was poorly related to the ratio of –CH (2923 cm^{-1}) to amide N–C=O ($r^2 = 0.107$, $p = 0.355$), for aliphatic C forms associated with amide I and II loss under cultivation. This implied that organomineral interactions in cultivated kaolinitic soil were driven by hydroxylated mineral surfaces through H–bonding and ligand exchanges with –OH termini of carbohydrate (–COH) derivatives and amide (N–C=O) functional forms of microaggregate organic matter.

1. Introduction

Internal pore configurations of oxide-rich kaolinitic mineral soil, affects the molecular chemistry of organic matter within their microstructural assemblage (Six et al., 2004). Such configurations confer the basic form and function of carbon (C) in relation to its long-term turnover (Mayer et al., 2004; Kleber et al., 2005). Although microaggregates constitute the primary repository for soil C (Horn and Smucker, 2005), the environmental consequences of accelerated loss in their capacity to store C and nitrogen (N), emanates from their mineral-pore microstructure (Sollins et al., 1996). Organic matter consists of spatially non-ordered, structural as well as non-structural C of varying chemical composition (Zang et al., 2000) and degree of oxidation (Kögel-Knabner, 2002). The capacity of clay minerals to bind C and organic N (Knicker, 2004; Zimmerman et al., 2004) largely depends on their specific surface area which increases from 1:1 to 2:1 clay mineral type (Chorover et al., 2004) and its soil textural content (Hassink, 1997).

Infra red spectroscopy is widely used as a tool to reveal the specific molecular structure of mineral surfaces (Johannson et al., 1998) and particularly to discriminate the vibrational mode of kaolinite inner and outer sphere hydroxyl –OH ions (Farmer, 1964; Ledoux and White, 1964; Wieckowski and Wiewiora, 1976; Madejova, 2003; Guan et al. 2005 and Lehmann et al., 2007). Furthermore, clay minerals form polyvalent cation bridges with portions of organic matter, including stable molecules that differ in biochemical accessibility. This chemical interaction may render not only resistance to microbial attack (Kaiser and Guggenberger, 2007), but also chemical stabilization to those microaggregate organic matter (MOM) forms that are of plant and microbial origin (Ellerbrock and Gerke, 2004; Lehmann et al., 2007). In soil microaggregates, these compounds primarily consist of microbial polysaccharides,

proteins, lipids and their residual mixtures (Kögel-Knabner, 2002; Gleixner et al., 2002).

Current soil aggregation models explain organomineral interaction through correlation between mineral surface area (Petersen et al., 1996) with organic C forms of varying reactivity, which are partitioned through conceptual SOM pool descriptions (Paul et al., 2006). The usefulness of such correlations in predicting the functional distribution of soil C remains undemonstrated. Some studies of bulk soil aggregates separated after concentric erosion (Santos et al., 1997) and X-ray photo-electron spectroscopic (XPS) evaluations show that C and mineral ions preferentially accumulate on the outer surfaces of microaggregates (Santos et al., 1997; Amelung et al., 2002; Gerin et al., 2003). Since organic matter is only contained in a small fraction of the soil matrix, and much of the mineral surface remains free of organic matter (Mayer, 1999), we require better resolution of C and its chemical nature in order to predict its functional distribution (Strong et al., 2004), as well as its stability in soil (Kögel-Knabner, 2002; Solomon et al., 2007b).

Using bright source synchrotron infrared microspectroscopy (μ-FTIR), the carbon chemistry and its spatial molecular evolution can be probed with 5 μm resolution for biological specimens (Miller et al., 2002) and environmental samples (Lehmann et al., 2005, 2007). For this measurement scale, it should be assumed that microaggregate carbon forms, in part constitute organic matter restricted within μm-size mineral pores. Its mobilization and turnover are therefore controlled by the mineral-pore infrastructure (Ellerbrock and Gerke, 2004). We hypothesize that the molecular-level function of these organic forms is altered through geochemical reactions during long-term cultivation. In our study, we examined molecular alterations to the nature of C and N functional forms in MOM, including their

chemical evolution in kaolinitic soil from native tropical forest and long-term agricultural cultivation.

2. Materials and methods

2.1 Site and sample description

We obtained soil aggregates from forest and agricultural sites in medium textured soils adjacent to the eastern margin of Kakamega forest (34º, 57′, 14″E; 00º 14′ 20″N; 1733 m above sea level) in western Kenya. The Kakamega forest soils are Acrisols developed from granitic rock (Jaetzold and Schmidt, 1983). Their high ratio of aluminum to iron content (Al:Fe = 1.6) suggested that these soils contain large proportions of alumino-silicate clay minerals. The soils are well-drained, extremely deep dark reddish brown soils with friable clay and a thick humic top soil (Jaetzold and Schmidt, 1983). The forest site experiences a mean annual temperature of 21.0 °C and mean annual precipitation of ~ 2040 mm. The chemical properties of the undisturbed forest soil were: 80.7 g C kg^{-1}; 8.0 g N kg^{-1} and pH_{water} of 6.5. Soils from the cultivated agricultural fields were: 60.9 g C kg^{-1}; 5.7 g N kg^{-1} and pH_{water} of 6.3, for 2-yr short-term and 18.2 g C kg^{-1}; 0.98 g N kg^{-1} and pH_{water} of 5.5 for 104–yr old long-term cultivated soil (Kinyangi et al., unpublished data).

2.2 Sample procurement and preparation,

Soil microaggregate samples were identified and hydrated in a pre-treatment step according to the procedure described by Kinyangi et al. (2006). Briefly, a 1-g sub-sample obtained from 100 g bulk soil was sieved to pass a 250-µm screen to obtain microaggregates, then sprinkled on a glass fiber filter (Whatman GF/A, 47mm 1.6 µm opening), mounted onto a sieve surface. The sieve was then connected to a chimney funnel which directed warm mist from the humidifier (Ultra-violet light, Slant/Fin;

7.5L capacity). The humidifier chamber was filled with water dispensed from a Barnstead NanoPure Diamond water purification system. Excess water droplets on the glass fiber filter were drained off prior to freezing microaggregates. Individual microaggregate sub-samples were selected and embedded in an ice block that was set onto the cryo-microtome stage for sectioning (Ultracut UTC, Leica Microsystems Inc. Bannockburn IL, USA). Since this pre-treatment stage resulted in frozen samples, sectioning at -55 °C yielded the most stable thin sections. Further detailed descriptions of the cryo-microtome features and thin section sample operations for C measurements, have been reported by Lehmann et al. (2005) and Kinyangi et al. (2006). After sectioning, several microaggregate thin sections were mounted on Cu grids (200 mesh, no 53002, Ladd Research, Williston, VT, USA) that were impregnated with silicon monoxide (SiO) substrate. The Cu grids were transferred onto a stainless steel sample stage-holder (46 mm diameter) and secured onto the center pinholes with scotch tape.

2.3 X-ray photoelectron spectroscopy

Surface analysis of 20 microaggregates was conducted by XPS from dry sieved aggregates (53-250 μm). The XPS measurements can probe a maximum sampling depth of ~ 10 nm and therefore provide a value for surface properties. Both narrow and wide scan XPS measurements were conducted at the Wiley Environmental Molecular Sciences Laboratory using a Physical Electronics Quantum 2000 scanning ESCA Microprobe (Physical Electronics GmbH, Ismaning, Germany) employing a focused monochromatic Al Ka x-ray (1486.7 eV) source for excitation and a spherical section analyzer. The 98-W, 107-μm diameter X-rays were rasterized over a 1.4 × 0.2 mm rectangle on the sample. Survey scan spectra in the 0-1000 eV binding energy range were recorded with pass energy of 50 eV. High-energy resolution scan spectra

of C 1s and O 1s were recorded in 0.2 eV steps with pass energy of 20 eV. Low energy electrons and Ar ions were conducted for specimen neutralization in each measurement. Wide scan and difference wide scan spectra were processed using Omnic 7.2 (Thermo Electron Corp., Waltham, MA) after cropping to a spectral region from 0 to 500 eV. Following automatic baseline correction, electron count data were normalized to scale the peak intensities. The peak subtraction function was used to generate difference spectra so as to reveal molecular changes in the XPS binding energy (eV) states.

2.4 μ-FTIR spectroscopy

Spectroscopic μ-FTIR data were collected from beam line U10B of the NSLS facility at Brookhaven National Laboratory. The beam line is equipped with a Spectra Tech Continuum IR microscope fitted with 32× transmission/reflection and FTIR step-scan spectrophotometer (Nicolet Magna 860, Thermo Nicolet Corporation Wisconsin, USA). It uses a KBr beam splitter and mercury-cadmium-telluride (MCT) detector with 500 - 4000 cm^{-1} frequency range and 1.0 cm^{-1} spectral resolution. Spectra were recorded with a 7-μm aperture from 4000 to 650 cm^{-1} with a resolution of 4 cm^{-1}. Each spectrum was composed of 256 scans co-added before Fourier transform processing. The background spectrum was collected from a clean SiO surface on the grid, adjacent to the edge of the mounted thin section. Recorded spectra were analyzed using Omnic 7.2 software (Thermo Electron Corp., Waltham, MA) after cropping to a frequency region from 4000 to 830 cm^{-1}. Automatic baseline corrections were applied following normalization of the absorbance in order to scale the peak intensities.

For the molecular assessments, chemigram profiles were extracted from the map spectral data at defined absorbance peak frequencies. Changes in the spectral intensity of kaolinite outer –OH (3695 cm^{-1}) and inner –OH (3622 cm^{-1}) surface

hydroxyls were used to calculate a mineral hydroxylation/dehydroxylation ratio (Frost and Vassallo, 1996). Correlation of organic matter dependent hydroxylation involved spectral assessments from target "hot spots" of high organic absorbance intensity, both inside the mineral matrix (A) and from the microaggregate cross-sectional area (B) proximal to the surface. Target "hot spots" provided enriched regions of organic molecular forms, where reactions with hydroxylated mineral surfaces were probed, after splitting the map data to extract recorded infrared spectra.

2.5 Statistical analysis

We used linear regression analysis to relate the kaolinite hydroxylation absorbance ratio to the enrichment of aliphatic (–CH) and carbohydrate (–COH) derivatives associated with amide I and II, N–C=O decomposition. The linear model tested the hypothesis whether a change in the ratio of outer to inner sphere kaolinite –OH was dependent on the alteration of amide I and II, N–C=O forms. The p-value was reported at $\alpha = 0.05$

3. Results and discussion

3.1 Narrow and wide scan X-ray photoelectron spectroscopy

High resolution XPS narrow scan showed that surface regions of microaggregates were enriched in the elemental composition of C, N and O compared to their bulk (Table 1). The atomic ratios of O to C and C to N increased under long-term, 104 yr-long cultivation. These chemical species were inferred from the integrated peak areas for C 1s, N 1s and O 1s (Figure 1a, 1b and 1c). No differences were observed in the electron binding states of the C signal (Figure 1a) from 1s electron transitions. Although the surface C and N forms existed in similar atomic ratios, during long-term cultivation, there was a 2-3-fold reduction in their atomic

mass (Table 1). The highest electron count intensity of the C 1s signal arose from resonance around 284.6 eV in C–C, –CH, 286.4 eV in C–N, C–O and 287.6 eV in C=O groups (Gerin et al., 2003; Arnarson and Kiel, 2001). In agricultural soil, surface O 1s transitions were strongly dominated by alteration to C=O molecular bonds whose intensity increased in the recent 2-year cultivated soil but declined after 104-yr long-term agriculture (Figure 1b). Although interactions between Fe and Al contributed to the O 1s binding energy, at pH 6.0, kaolinite O 1s could be traced since it is shifted to 531.9 eV (Koppelman et al., 1980). Additionally, microaggregate surface composition of organic matter was dominated by C–C and –CH rather than C–O forms of C.

Peak shift in the N 1s spectra pointed to a transition towards 399.8 eV, which showed the existence of hetero-aromatic N forms after short-term cultivation. Under long-term 104-yr cultivation, the N 1s signal nearly disappeared. This diminished signal intensity (399.8 eV) represents a loss of N from aggregate surfaces through decomposition of peptide linkages from amide N–C=O (Barr et al., 1999). In the process, there was a retention of aromatic bound pyridinic N including imine, pyridine and aromatic amines (Abe and Watanabe, 2004; Maie et al., 2006). The chemical nature of the residual N in organic matter may therefore arise from biologically-derived aromatic amine and nucleic acid fractions (Omoike and Chorover, 2004) as well as abiological pyrole N (Knicker, 2004) at those sites which were only recently burned such as the 2-yr cultivation.

Microaggregate surface wide scan XPS pass spectra exhibited multiple peaks in the binding energy states of mineral Si, Fe, Al, Ca and auger Mg electron transitions (Gerin et al., 2003). Since alumino-silicates were dominant in the kaolinitic soil, Al2p, Al2s, Si2p and Si2s electron transitions did not change with continuing long-term cultivation (Figure 2a).

Table 4-1. X-ray photoelectron spectroscopy (XPS) elemental composition, atomic mass ratios of aggregate surface and bulk soil

Years	C	N	O	O:C	C:N
		-------(%)-------			
Bulk soil					
0, Forest	25.1	1.5	55.7	1.0	16.4
2, cultivated	19.1	1.4	59.4	1.3	13.4
104, cultivated	9.2	1.0	65.8	2.6	9.7
Aggregate surface					
0, Forest	26.2	1.8	53.1	0.8	14.2
2, cultivated	19.3	2.0	58.7	1.3	9.5
104, cultivated	8.3	0.8	65.6	2.6	10.0

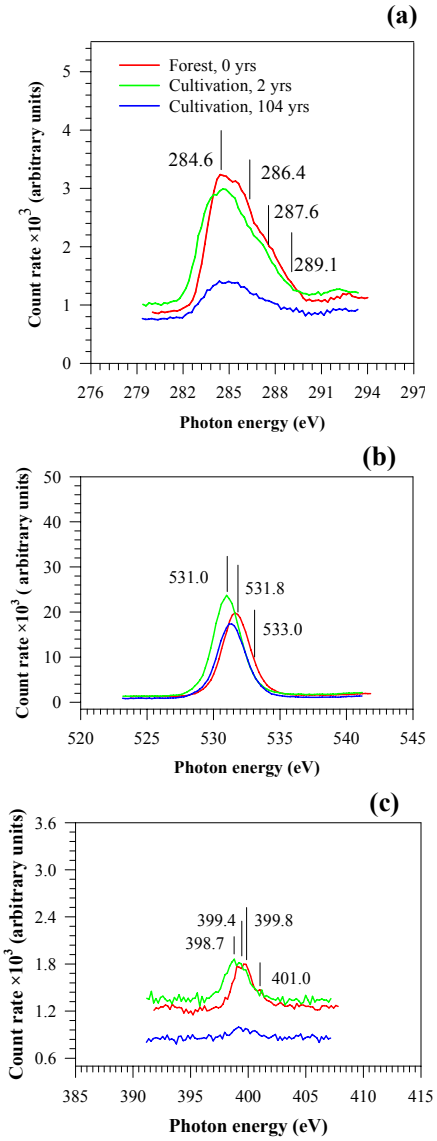

Figure 4-1. Electron transitions in the molecular functional forms; (a), C 1s binding energy for C–C, C–H (284.6 eV), C–N, C–O (286.4 eV), C=O (287.6 eV) and COOH (289.1 eV); (b) O 1s binding energy for C=O interaction with kaolinite (531.8 eV) and (c) N 1s binding energy of aromatic amide (398.7 eV, 399.4 eV) and peptide N (399.8 eV).

The noticeable enrichment of alumino-silicate transitions in the difference spectrum (Figure 2b) was the direct consequence of molecular alteration to C1s (285.5 eV) and N1s (399.8 eV) arising from a loss in C–C/–CH and pyridinic N, as well as peptide linked N–C=O functional groups. Significant Ca2p (347.9 eV; 352.3 eV) and the unique auger MgKLL (306.5 eV; 310 eV) electron modes exhibit a peak doublet after 2 years of cultivation and the split in the peaks of the difference spectrum is lost upon long-term 104-yr cultivation (Figure 2b). We found this peak split to imply that Mg (Amelung et al., 2002) and Ca (Boyd et al., 2003) salts were present on the microaggregate surface only in forest and recently cultivated kaolinitic soil. No molecular changes occurred to the Ca3p (25.0 eV) transition attributed to CaO.

3.2 μ-FTIR imaging of C and N chemical alteration to microaggregate organic matter

Soil aggregate organic matter was dominated by four distinct regions in the spectral range 4000 – 800 wave numbers cm^{-1}. These regions revealed multiple infrared vibrational mode features that were unique to C bonding with N, O and H in the soil organomineral assemblage, together with molecular transformation of the C and N functional group chemistry (Table 2). Gerzabek et al. (2006) asserted that three absorbance regions around 2900 cm^{-1}, 1600 cm^{-1} and 1450 cm^{-1} contribute substantially to molecular changes to organic C in soils. For MOM, chemigram profiles of four regions were mapped (Figure 3) and their chemical images summarized for absorbance intensity from μ-FTIR peak frequencies as:

3.2.1 Molecular signature of organic –OH and amide A –NH

In all soils (Figure 3), the broad nature of the peak around 3200 cm^{-1} was assigned to C functional groups containing –OH (Olk et al., 2000).

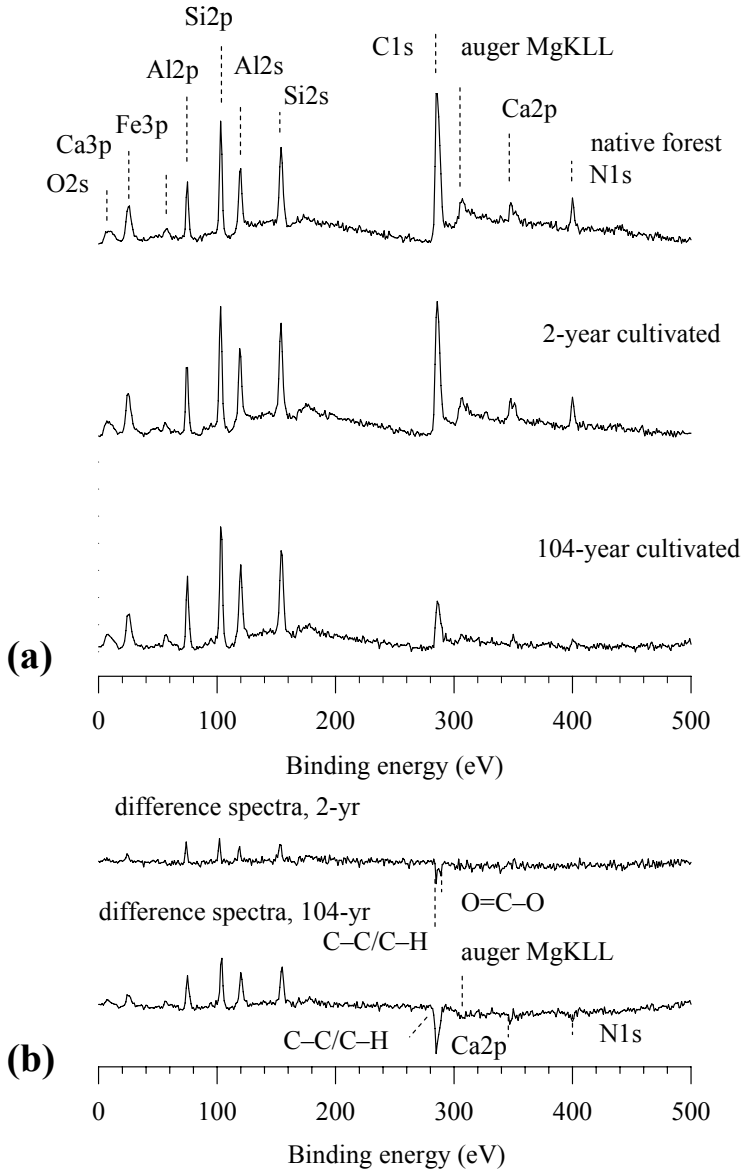

Figure 4-2. Wide scan spectra of the surface electron transition in the binding energy of mineral elements, Al2p, Al2s, Si2p and Si2s of kaolinite. (a). The auger MgKLL and Ca2p transitions exhibit a double peak feature especially after 2 years of cultivation (b). Microaggregate surface Mg and Ca forms appear to be of organic origin as they are almost entirely degraded after 104-yr long-term alteration.

Resonance of amide–A, arising from –NH vibrations was present when the peak features were sharp. Amide–A molecular signature is supported by additional amide I absorbance between 1600-1700 cm^{-1} (Figure 4a & 4b). For this area, absorption spectra showed a broad but high absorption peak centered around 3300 cm^{-1}, which indicated that both –OH and –NH groups dominate the chemigram profile of MOM. In this study, their significant occurrence will later be considered in the context of development of kaolinitic mineral hydroxylation and organic matter reactions.

3.2.2 Molecular alteration of aliphatic –CH, $–CH_2$, and $–CH_3$

Absorption bands from the aliphatic C components gave rise to –CH stretching resonance and bending motions (Figure 3a–v, 3b–v). The two peaks at 2938 cm^{-1} and 2878 cm^{-1} were assigned to the –CH stretching mode of the aliphatic C and particularly the symmetric (2938 cm^{-1}) and asymmetric (2878 cm^{-1}) resonance of the $–CH_3$ (Solomon et al 2007b). An additional peak at 2923 cm^{-1} originated from vibrational absorbance due to aliphatic –CH (Lehmann et al., 2007; Solomon et al., 2007a, 2007b) and more specifically to methylene $–CH_2$ of saturated aliphatic C (Heraud et al., 2005). The deformation mode of the $–CH_3$ showed strong absorption peaks due to the asymmetric (1466 cm^{-1}) and symmetric (1379 cm^{-1}) vibrations. Under native forest soil (Figure 2a–v), the dominant $–CH_3$ aliphatic absorbance intensity around 2931 cm^{-1} rather than $–CH_2$ at 2923 cm^{-1} signals symmetric stretching vibrations of plant (Wilson et al., 2000; Gressel et al., 1995) or microbial derived –CH (Naumann et al., 2005). In recently cultivated soil, increased decomposition causes a significant shift in absorbance to 2923 cm^{-1} (Figure 2b –v). This signal shift represents molecular alteration to (un) saturated long chain aliphatic C (Zaccheo et al., 2002; Heraud et al., 2005), likely of microbial membrane residues (Parikh and Chorover, 2006).

Table 4-2. Infrared (FTIR) peaks for carbon (C) and nitrogen (N) forms in soil

FTIR peaks (wave nos. cm^{-1})	Assigned molecular bonds of kaolinite clay mineral–OH[a] and organic matter[b] C and N
3695, 3622; [§]3526, 3446	Outer and inner surface –OH in kaolinite and [§]gibbsite –OH
3339, 3300	–NH stretches of amide A
3262	stretching vibrations of H-bonded –OH
2938, 2937, 2878	stretching vibrations of –CH, $–CH_3$
2923	asymmetric stretching vibrations of –CH, $–CH_2$
1655, 1635, 1614	amide I N–C=O stretch of COOH and H–C=O of conjugated quinone/ketone
1581	C=C in aromatic rings; pyrole, furan, thiophenes
1530, 1515	amide II N–C stretch and side chain vibration of –NH, tyrosine band and C=C stretch of aromatic C in lignin
1466, 1451	Weak CH_2 stretch vibrations of [φ]amino acid side chains
1410	C=O stretching of carboxylic C and traces of ketone
1400, 1388	C=C of aromatic-C, symmetric stretching of COOH, and H–C=O of conjugated ketone
1347, 1320, 1304	deformation of –CH aliphatic C, aromatic –NH and some stretching of C–O from phenolic –OH
1240, 1233	asymmetric stretching of phosphates in phosphodiesters
1109[†], 1081, 1078, 1077	[†]Si–O–Si, C–O of aliphatic ether, C–OH of alcohols
1051, 1037	C–O stretching and –OH deformations of COOH, Si–O
912[#] 931	Al–OH[#] of Gibbsite, P–O–P at ~pH 6.0
~880	C=C, C=N, –CH in ring structures

[a]Peak assignment for hydroxyl –OH vibrations of clay minerals according to Farmer (1964); Ledoux and White (1964); Wieckowski and Wiewiora (1976); Johannson et al. (1998); Frost (1998); Madejova and Komadel (2001); Madejova (2003); Guan et al. (2005).

[b]Peak assignment for organic molecular functional groups according to: Gressel et al. (1995); Haberhauer et al. (1998); Kansiz et al. (1999); Olk et al. (2000); Barth & Zscherp (2002); Zaccheo et al. (2002); Smidt et al.(2002); Solomon et al. (2005); Miller & Dumas. (2006); He et al. (2006); Lehmann et al. (2007).

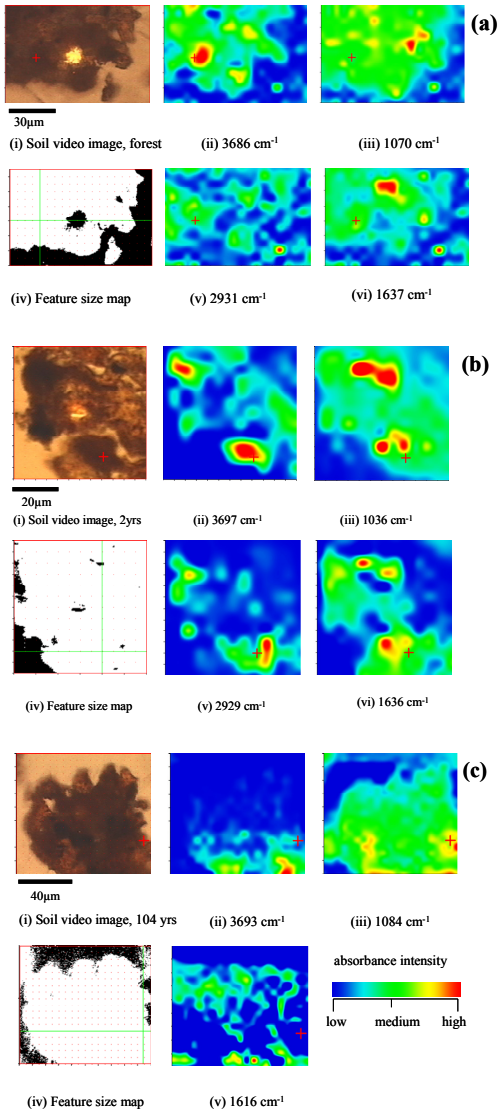

Figure 4-3. Absorbance chemigrams of infrared vibrational mode features unique to C bonding with N, O and H in kaolinitic mineral soil. Soil microaggregate physical video image (3a –iv, 3b –iv, 4c –iv) and chemical profile mapping (3a –ii, iii, v & vi; 3b –ii, iii, v & vi; and 3c –ii, iii, & v) show the distribution of C, N and kaolinite –OH forms. Figures correspond to (a) forest (b) 2-yr cultivation and (c) 104-yr old kaolinitic soil after long-term cultivation. The red (+) sign is a visual reference for organic matter "hot spots"

3.2.3 Molecular alteration of C=C, phenolic –OH, amide I –C=O, amide II H–N–C

Strong absorptions at 1581 cm^{-1} and its associated N shoulder at 1614 cm^{-1} were attributed to the C=C in-plane skeletal vibrations from aromatic compounds (Naumann et al., 2005) and para-substituted benzene rings (Yu et al., 2003). Only MOM from forest and 2-yr cultivated soil exhibited some aromatic C=C molecular absorption at 1581 cm^{-1}, (Figure 4a & 4b). When the lignin absorbance peak is present at 1515 cm^{-1} (Naumann et al., 2005; Heraud et al., 2007) these vibrations are strong evidence for the existence of wood polymers (Pandey, 1999) as well as conjugated quinone and/or ketone in structural litter fractions (Zaccheo et al., 2002; Smidt et al., 2002). Because these bands appeared to contribute little to the absorbance intensity of this aromatic region, and the–OH stretching of phenolic C ~1370 cm^{-1} was clearly absent, we postulated that the aromatic MOM was primarily from non-structural molecular frequencies associated with amide N–C=O (Schmidt-Rohr et al., 2004; Lehmann et al., 2007). This was confirmed by amide II resonance shoulders at 1530 cm^{-1}, which are N–C and N–H bending vibrations from side chains in peptide linkages of aliphatic and aromatic amino acids (Helm and Naumann, 1995; Butler et al., 2002). These N–C linkages in polypeptides arise from amide–protein conformation especially because the forest and 2-yr cultivated soils were highly enriched in total N content (8.0 g N kg^{-1} and 5.7 g N kg^{-1} soil respectively). In addition, amide I peaks around 1635 cm^{-1} (Figure 3a–vi, 3b–vi) are fingerprint for the secondary nature of protein arising from N–C=O molecular stretching of carboxylic C (Schmidt-Rohr et al., 2004; Surewicz et al., 1993; Orsini et al., 2000; Barth and Zscherp, 2002). The soil pH was near neutral (6.5) and the carboxylic (COOH) resonance around 1700 cm^{-1} was markedly absent. Therefore, the stretching vibrations at 1414 cm^{-1} arise more from the symmetric mode of carboxylate COO^{-} rather than aromatic C=C (Filip and Kubat, 2003; Omoike and Chorover, 2004).

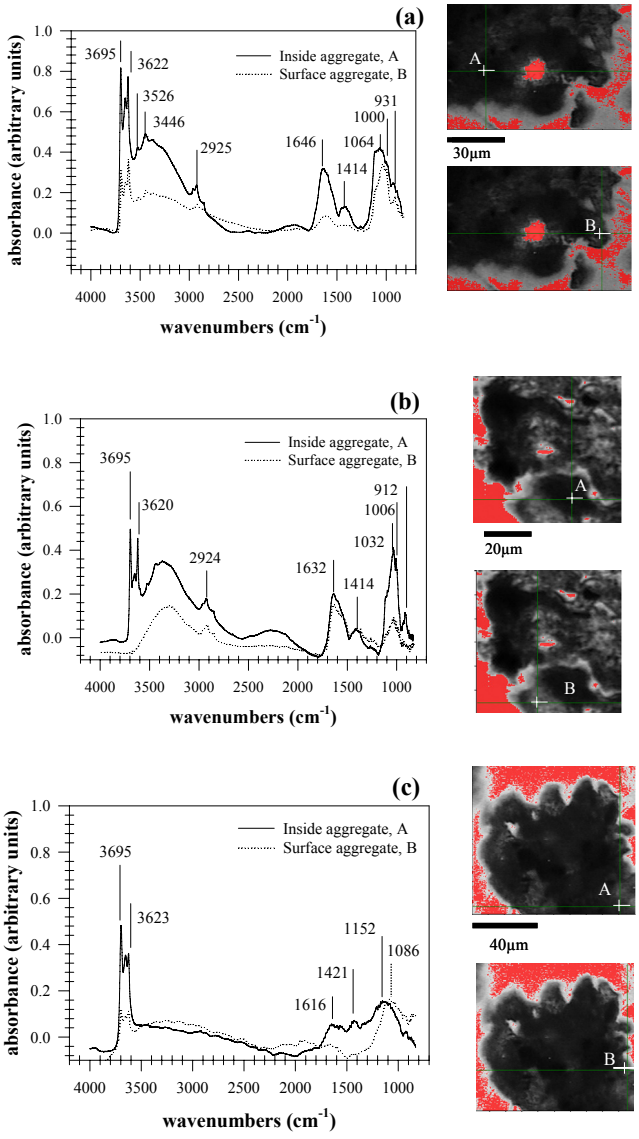

Figure 4-4. Infrared absorption bands assigned to organic matter and kaolinite –OH vibrations from the inner matrix (A) and outer surfaces (B) of microaggregates in kaolinite soil. Figures correspond to (a) forest (b) 2-yr cultivation and (c) 104-yr old kaolinitic soil after long-term cultivation.

Amide I and II molecular alterations support the presence of α–helical secondary structures from the folding nature of protein (Byler and Susi, 1986; Miller and Dumas, 2006). In MOM, amide N–C=O peak frequencies were noticeable in forest and 2-yr cultivated soil but entirely absent in long-term 104-yr cultivated soil. Such peak patterns were unique. Based on the assumption that organic N exists in predominantly amide molecular form (Arnarson and Keil, 2001), we concluded that alterations in microaggregate N evolved from molecular depolymerization (Kögel-Knabner, 2000; Sutton and Sposito, 2005) and the subsequent decomposition of N–C=O from amide N functional forms of organic matter (Knicker, 2004; Schmidt-Rohr et al., 2004).

3.2.4 Molecular alteration of oxidized C–O, C–O–C, C–O[H]

The region 1100 cm^{-1} to 1000 cm^{-1} contained absorbance bands for multiple oxidized functional forms including C–O–C of aliphatic ether, C–O stretching and C–O[H] deformations of alcohols. In MOM, there can be uncertainties regarding molecular assignments of peaks after 1100 cm^{-1} due to phosphate P–O^{-} (Guan et al., 2005; He at al., 2006) and before 1000 cm^{-1} for vibrations due to Si–O (Bertaux et al., 1998) and Al–OH (Wang and Johnston, 2000) stretching. We restricted interpretation of organic signatures to the 1085 cm^{-1} to 1000 cm^{-1} peak area which spans the entire oxidized C–O absorption region. Even though some mineral Si–O bonds absorb in this region, examination by difference spectra (not shown) of organomineral and non-mineral absorbance of MOM confirmed that C–O[H] vibrations accounted for nearly all of the peak frequencies between 1085 cm^{-1} to 1000 cm^{-1} (Figure 4a, 4b & 4c). This was particularly the case when Si–O and Al–OH absorbance appeared weak or missing at ~1110 cm^{-1} and ~912 cm^{-1} respectively (Specht and Frimmel, 2001; Wieckowski and Wiewiora, 1976; Madejova, 2003).

Profound alterations occurred not only from overall reduced intensity of molecular absorbance between short-term 2-yr and long-term 104-yr soil cultivation histories, but also from changes in the peak bandwidth. Peak shifts represented a reduction in the molecular forms of C–O hydrolysis products among both primary and secondary alcohol (–COH) functional groups and this reduction has also been used to demonstrate deformation in plant cell walls (Wilson et al., 2000). As a result of their hydrolysis and oxidation reactions (Gallo et al., 2005), these primary and secondary alcohols appear to be derivatives of carbohydrate C which dominate molecular alteration in forest (Figure 4a) and long-term (Figure 4c) 104-yr cultivated soil. Another observation supporting their oxidation was that chemical absorbance from dominant molecular C forms was consistently more intense for C–O[H] when compared to –CH vibrations.

3.3 Molecular interaction of microaggregate organic matter and hydroxylated mineral surfaces

The infrared absorption bands in the range 3700-3500 cm^{-1} were assigned to –OH vibrations (Table 2) from the outer and inner surfaces of kaolinite clay mineral (Farmer, 1964; Madejova and Komadel, 2001) and gibbsite (Bertaux et al., 1998; Wang and Johnston, 2000). For target organic matter "hot spots", the mineral absorbance ratio of kaolinite –OH (3695 cm^{-1} to 3622 cm^{-1}) was correlated to the molecular enrichment ratio of C–O[H] and –CH (Figure 5). This approach tested the hypothesis whether a shift in the chemical environment of both C–O[H] (1000 cm^{-1} to 1080 cm^{-1}) and –CH (~2930 cm^{-1}) partially originated from hydrolysis of the amide N–C=O with –NH side chains (1610 cm^{-1} to 1670 cm^{-1}), in addition to oxidation of methylated –CH radicals (~2930 cm^{-1} to 2922 cm^{-1}).

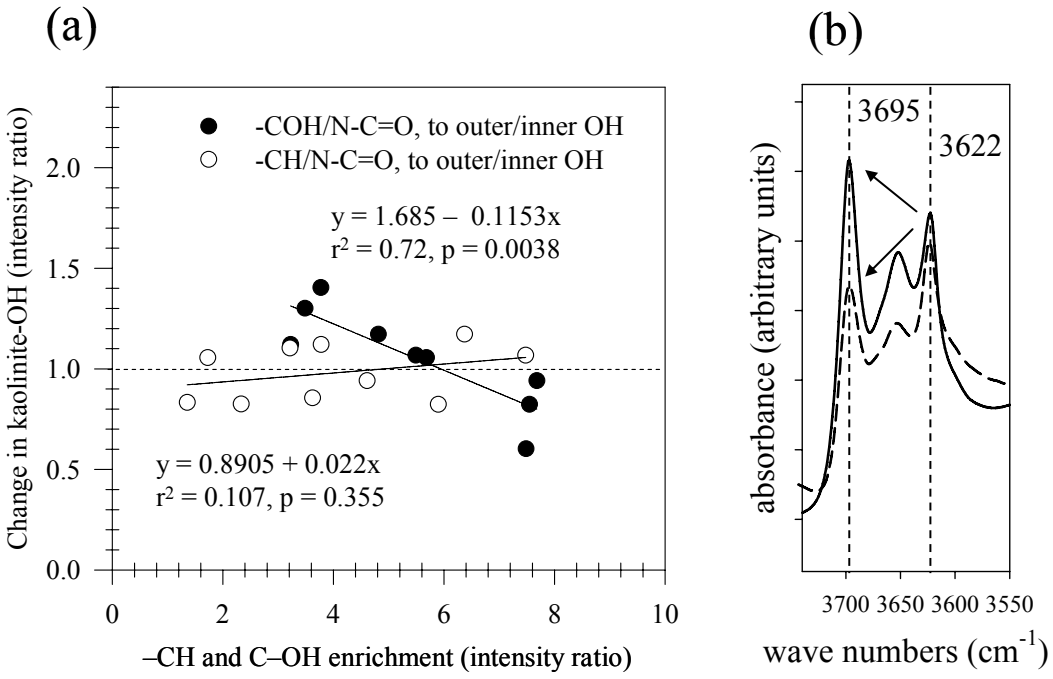

Figure 4-5. Effect of long-term cultivation on kaolinite –OH outer to inner surface absorbance near 3695 cm^{-1} and 3622 cm^{-1} in relation to enrichment of C–OH (n = 9) and –CH (n = 10) molecular forms of MOM from "hot spots" mapped in Figure 4. Dotted line represents changes to outer to inner kaolinite –OH surface ratio of 1.0

Previous work by Frost el al. (1999) examined the intercalation of kaolinite with acetamide and concluded that, H–binding occurs not only with siloxane O but also through exchange of C=O to inner surface –OH. Hence the absorbance from amide I peak was no longer present as a result of H–binding to kaolinite. For our work, the initial absorbance intensity with an intercept of 1.8 explained 72 % of the variation in the increasing oxidation from amide I decomposition, which was well correlated to the reduction in the intensity of the kaolinite surface hydroxylation of cultivated soil (Figure 5a). In effect, increasing organic C–O[H] suppressed the activity of the hydroxyl –OH on the surface of the mineral layer because interactions occurred with the kaolinite –OH. In contrast, increasing –CH was poorly correlated to kaolinite –OH activity. And between the two C functional forms, C–O[H] had a higher intercept and the negative slope increased 5-fold compared to the positive slope for –CH enrichment (Figure 5a) This suggests that mineral-organic surface reactions may be dependent on hydroxylation potential which is generated from C–O[H] rather than–CH enrichment of MOM.

The nature of hydroxyl positioning on kaolinite clay surface and its access to interactions with C–O[H] and –OH of organic matter has been examined by Specht and Frimmel (2001). These authors postulate the interaction of dicarboxylic molecules with the –H or –OH of the mineral surface to occur on the gibbsite Al–OH. Johannson et al. (1998) show that isotopic exchange for the –H in inner surfaces of kaolinite –OH, occurs after treating samples with up to 100 ºC heat. Lehmann et al. (2007) found that the ratio of 2922 cm^{-1} to that of 1589 cm^{-1} is well correlated to kaolinite 3695 cm^{-1}, suggesting a possible role for –CH molecules in mineral stabilization of entire MOM C in forest two tropical soils. Earlier studies as well by Murphy et al. (1992) showed that the sorption of humic matter to mineral as ligand exchange depends on the level of hydroxylation. In our study, the ratio of C–O[H] to N–C=O and –CH to

amide N–C=O ranges from 1.5-3 to 8, which means there is a 5-fold increase in –CH and 2-fold enrichment in C–O[H] molecular alteration related to the decomposition of amide I. In effect, hydroxylation reactions involving carboxyl and amide hydrolysis provide sites for ligand exchange and H–binding to mineral soil.

In soil ligand exchange reactions, the –H associated with hydroxyl –OH may substitute more readily (Yoon et al., 2004) than –H contained in –CH structures of recalcitrant organic matter (Solomon et al., 2007a). In the native forest, intense hydroxylation C–O[H] related to 1070 cm^{-1} seemed to occur alongside a disordered kaolinite phase (Figure 3a-ii; absorbance intensity shift to 3686 cm^{-1}) and gibbsite Al–OH formations (Figure 4a; peak at 3520 cm^{-1}). Upon 2-yr cultivation, the kaolinite was better ordered (3697 cm^{-1}) as the C–O absorbance intensity shifts to 1036 cm^{-1}. In studying kaolinite deformation modes, Frost (1998) suggested that the (dis)ordered kaolinite structure is detected through coupled (3695 cm^{-1}) and uncoupled (3685 cm^{-1}) stretching of –OH vibrations. In forest soil, vibrations near 3685 cm^{-1} (Figure 4a) are due to the disordered –H in the –OH oriented in the same direction as the O–Si of the adjacent kaolinite sheet (Johansson et al., 1998). Furthermore gibbsite –OH resonance at 3526 cm^{-1} and 3446 cm^{-1} is now clearly absent due to dehydroxylation from loss of its weak amorphous crystalline structure (Frost and Vasallo, 1996; Kleber et al., 2005). These changes to the orientation of the clay structural –OH appear to cause some reduction to surface hydroxylation, which is determined from –OH loss of intensity (Frost and Vasallo, 1996) for clay minerals such as kaolinite in Oxisols (Chorover et al., 2004). In this study, gibbsite Al–OH mineral formations and the disordered kaolinite structure in forest soil were lost upon cultivation. This evolution in the mineral molecular form was the probable cause for a reduction in kaolinite hydroxylation after long-term cultivation (Figure 3c-ii). In a previous investigation of two tropical native forest soils, Lehmann et al. (2007) found that –CH organic forms

were positively associated with clay mineral surfaces but in this study, their enrichment upon cultivation is not correlated to hydroxyl variation of well ordered kaolinite clay. This means that $–CH_x$ may interact via H-binding with the poorly crystalline mineral phase in organic matter-rich soil (Torn et al., 1997; Kleber et al., 2005). Unlike organic-rich native forest soils which contain large labile carbon fractions consisting $–CH_x$ (Kögnel-Knabner, 2000, 2002), cultivated soils retain $–CH_x$ molecular forms largely in recalcitrant organic structures (Gleixner et al., 2002; Solomon et al., 2005). These stable $–CH_x$ structures appear to persist in poor association with mineral surfaces of well ordered kaolinite in cultivated soil.

4. Conclusions

Both XPS narrow and wide scan measurements showed that the long term molecular alteration from cultivation agriculture causes a near 8-fold increase in organic C oxidation. Based on examination of both XPS and μ-FTIR map data, we were unable to conclude whether elevated surface concentrations of organic matter detected by XPS were a reflection of C and N occluded in low intensity porous surface breaking pores or a true mass accumulation in the microaggregate surface mineral matrix. In this case, random locations of organic matter and its distribution in microaggregates found by μ-FTIR appeared inconsistent with nanoscale surface XPS atomic mass accumulation. Also, our previous nanoscale C 1s NEXAFS assessments exhibit chemical differences in organic matter of the interior mineral matrix and exterior surface pore regions without noticeable surface C accumulation. Chemigram profiles point to the fact that, a large fraction of the mineral assemblage may not be associated with C but rather, these patchy “hotspots” were both organic and organomineral forms embedded in pore spaces. Kaolinite mineral and organic C reactions were controlled by hydroxylation. Therefore molecular interaction depended

on the –OH hydroxylation sphere potential. Overall, long-term cultivation, involved the enrichment of aliphatic –CH as well as the depolymerization of aromatics and hydrolysis of amide N–C=O alongside the oxidation of C–O[H] forms of carbohydrate derivatives and amide I protein mixtures of MOM. We also posit that compounds rich in aliphatic $–CH_x$ forms bind to amorphous crystalline and poorly ordered clay mineral phases due to their high surface hydroxylation potential. In contrast, carbohydrate and amide mixtures appear to bind through ligand exchange reactions from low hydroxylation of well ordered kaolinite in cultivated soil. These hypotheses can only be tested in forest and cultivated soils known to have developed across a mineralogical gradient.

REFERENCES

Abe, T., Watanabe, A., 2004. X-ray photoelectron spectroscopy of nitrogen functional groups in soil humic acids, Soil Science 169: 35–43.

Amelung, W., K.Kaiser, G.Kammerer, and G Sauer. 2002. Organic carbon at soil particle surfaces-evidence from X-ray photoelectron spectroscopy and surface abrasion. Soil Science Society of America Journal 66: 1526–1530.

Arnarson, T. S., and R.G.Keil. 2001. Organic-mineral interactions in marine sediments studied using density fractionation and X-ray photoelectron spectroscopy. Organic Geochemistry 32: 1401–1415.

Baldock, J. A., and J.O Skjemstad. 2000. Role of soil matrix and minerals in protecting natural organic materials against biological attack. Organic Geochemistry 31 697–710.

Barr, T. L., E.E Hoppe, S.Hardcastle, and S.Seal. 1999. X-ray photoelectron spectroscopy investigations of the chemistries of soils. Journal of Vacuum Science and Technology A: Vacuum Surfaces and Films 17: 1079–1085.

Barth, A., and C.Zscherp. 2002. What vibrations tell us about proteins. Quarterly Reviews of Biophysics 35: 369–430.

Bertaux, J., F.Froehlich, , and P.Ildefonse. 1998. Multicomponent analysis of FTIR spectra; quantification of amorphous and crystallized mineral phases in synthetic and natural sediments. Journal of Sedimentary Research 68: 440–4472.

Boyd, A., M.Akay, , and B.J Meenan. 2003. Influence of target surface degradation on the properties of r.f. magnetron-sputtered calcium phosphate coatings. Surface and Interface Analysis 35: 188–198.

Byler, D.M., and H.Susi. 1986. Examination of the secondary structure of proteins by deconvolved FTIR spectra. Biopolymers 25: 469–487.

Cheng, C.H., J.Lehmann, J.E.Thies, S.D Burton, and M.H Engelhard. 2006. Oxidation of black carbon by biotic and abiotic processes. Organic Geochemistry 37: 1477–1488.

Chorover J., M.K Amistadi, and O.A Chadwick. 2004. Surface charge evolution of mineral–organic complexes during pedogenesis in Hawaiian basalt, Geochimica et Cosmochimica Acta 68: 4859–4876.

Ellerbrock, R. H., and H.H.Gerke. 2004. Characterizing organic matter of soil aggregate coatings and biopores by Fourier transform infrared spectroscopy. European Journal of Soil Science 55: 219–228.

Farmer, V.C., 1964. Infrared absorption of hydroxyl groups in kaolinite. Science 145: 1189–1190.

Farmer, V.C., and J.D Russell. 1964. The infrared spectra of layer silicates. Spectrochimica Acta 20: 1149–1173.

Filip, Z., and J.Kubat. 2003. Aerobic short-term microbial utilization and degradation of humic acids extracted from soils of long-term field experiments. European Journal of Soil Biology 39: 175–182.

Frost, R. L. 1998. Hydroxyl deformation in kaolins. Clays and Clay Minerals 46: 280–289.

Frost, R. L., J.Kristof, , G.N Paroz, and J.T Kloprogge. 1999. Intercalation of kaolinites with acetamide. Physics and Chemistry of Minerals 26: 257–263.

Frost, R. L., and A.M Vassallo. 1996. The dehydroxylation of the kaolinite clay minerals using infrared emission spectroscopy. Clays and Clay Minerals 44: 635.

Gallo, M.E., C.L Lauber, S.E Cabaniss, M.P Waldrop, R.L Sinsabaugh, and D.R Zak. 2005. Soil organic matter and litter chemistry response to experimental N deposition in northern temperate deciduous forest ecosystems. Global Change Biology 11: 1514–1521.

Gerin, P.A., M.J Genet, A.J Herbillon, and B.Delvaux, 2003. Surface analysis of soil material by X-ray photoelectron spectroscopy. European Journal of Soil Science 54; 589–604.

Gerzabek, M.H., R.S Antil, I.Kögel-Knabner, H.Knicker, H.Kirchmann, and G.Haberhauer. 2006. How are soil use and management reflected by soil organic matter characteristics: a spectroscopic approach. European Journal of Soil Science 57: 485–494.

Gleixner, G., N.Poirier, R.Bol, and J.Balesdent. 2002. Molecular dynamics of organic matter in a cultivated soil. Organic Geochemistry 33: 357–366.

Gressel, N., Y.Inbar, A.Singer, and Y.Chen. 1995. Chemical and spectroscopic properties of leaf litter and decomposed organic matter in the Carmel range, Israel. Soil Biology & Biochemistry 27: 23–31.

Guan, X. H., Q.Liu, G. H Chen, and C.Shang. 2005. Surface complexation of condensed phosphate to aluminum hydroxide: an ATR-FTIR spectroscopic investigation, Journal of Colloid and Interface Science 289: 319–327.

Haberhauer, G., B. Rafferty, F.Strebl, and M.H Gerzabek. 1998. Comparison of the composition of forest soil litter derived from three different sites at various decompositional stages using FTIR-spectroscopy. Geoderma 83: 331–342.

Hassink, J. 1997. The capacity of soils to preserve organic C and N by their association with clay and silt particles. Plant and Soil 191: 77–87.

He, Z., T.Ohno, , B.J.Cade-Menun, M.S.Erich, and C.W. Honeycutt. 2006. Spectral and chemical characterization of phosphates associated with humic substances. Soil Science Society of America Journal 70: 1741–1751.

Heraud, P., B.R Wood, M.J. Tobin, J.Beardall, and D.McNaughton. 2005. Mapping of nutrient-induced biochemical changes in living algal cells using synchrotron infrared microspectroscopy. FEMS Microbiology Letters 249: 219–225.

Heraud, P., S.Caine, G.Sanson, R.Gleadow, B.R.Wood, and D.McNaughton. 2007. Focal plane array infrared imaging: a new way to analyse leaf tissue New Phytologist 173: 216–225.

Horn, R. and A.Smucker. 2005. Structure formation and its consequences for gas and water transport in unsaturated arable and forest soils. Soil and Tillage Research 82: 5–14.

Jaetzold, R., and H.Schmidt. 1983. Farm management handbook of Kenya Vol. II Natural conditions and farm management information, Part A. west Kenya. MALD, Kenya

Johansson, U., A.Holmgren, W. Forsling, and R.Frost. 1998. Isotopic exchange of kaolinite hydroxyl protons: a diffuse reflectance infrared Fourier transform spectroscopy study. Analyst 123: 641–645.

Johnston, C.T., D.L Bish, J. Eckert, and L.A. Brown. 2000. Infrared and inelastic neutron scattering study of the 1.03- and 0.95-nm kaolinite-hydrazine intercalation complexes. Journal of Physical Chemistry B 104: 8080–8088.

Kaiser, K., and G. Guggenberger. 2007. Sorptive stabilization of organic matter by microporous goethite: sorption into small pores vs. surface complexation. European Journal of Soil Science 58: 45–59.

Kansiz, M., P.Heraud, B.Wood, F.Burden, J.Beardall, and D.McNaughton. 1999. Fourier transform infrared microspectroscopy and chemometrics as a tool for the discrimination of cyanobacterial strains. Phytochemistry 52: 407–417.

Kinyangi, J., D.Solomon, B.Liang, M.Lerotic, S.Wirick, and J.Lehmann. 2006. Nanoscale biogeocomplexity of the organomineral assemblage in soil: Application of STXM microscopy and C 1s-NEXAFS spectroscopy. Soil Science Society of America Journal 70: 1708–1718.

Kleber, M., R.Mikutta, M.S Torn, and R.Jahn. 2005. Poorly crystalline mineral phases protect organic matter in acid subsoil horizons. European Journal of Soil Science 56: 717–725.

Knicker, H. 2004 Stabilization of N-compounds in soil and organic-matter-rich sediments—what is the difference? Marine Chemistry 92: 167–195.

Kögel-Knabner, I. 2000. Analytical approaches for characterizing soil organic matter. Organic Geochemistry 31: 609–625.

Kögel-Knabner, I. 2002. The macromolecular organic composition of plant and microbial residues as inputs to soil organic matter. Soil Biology and Biochemistry 34: 139–162.

Koppelman, M.H., A.B Emerson, and J.G Dillard. 1980. Adsorbed Cr(III) on chlorite, illite, and kaolinite; an X-ray photoelectron spectroscopic study. Clays and Clay Minerals 28: 119–124.

Ledoux, R.L., and J.L.White. 1964. Infrared study of the OH groups in expanded kaolinite. Science 143: 244–246.

Lehmann, J., B.Liang, D.Solomon, M.Lerotic, F.Luizão, J. Kinyangi, T.Schäfer, S.Wirick, , and C. Jacobsen. 2005. Near-edge X-ray absorption fine structure (NEXAFS) spectroscopy for mapping nano-scale distribution of organic carbon forms in soil: Application to black carbon particles. Global Biogeochemical Cycles 19: 1013–1025.

Lehmann, J., J. Kinyangi, and D.Solomon. 2007. Organic matter stabilization in soil microaggregates: implications from spatial heterogeneity of organic carbon contents and carbon forms. Biogeochemistry doi: 10.1007/s10533-007-9105-3

Madejova, J., P.Komadel. 2001. Baseline studies of the clay minerals society source clays: Infrared methods. Clays and Clay Minerals 49: 410–432.

Madejova, J. 2003. FTIR techniques in clay mineral studies. Vibrational Spectroscopy 31: 1–10.

Maie, N., K.J.Parish, A.Watanabe, H.Knicker, R.Benner, T Abe, K.Kaiser, R.Jaffé. 2006. Characterization of dissolved organic nitrogen in an oligotrophic subtropical coastal ecosystem. Geochimica et Cosmochimica Acta 70: 4491–4506.

Mayer, L.M. 1999. Extent of coverage of mineral surfaces by organic matter in marine sediments. Geochimica et Cosmochimica Acta 6: 207–215.

Mayer, L.M., L.L Schick, K.Hardy, R.Wagai, and J. McCarthy. 2004. Organic matter content of small mesopores in sediments and soils, Geochimica et Cosmochimica Acta 68: 3863–3872.

Miller, L.M., P.Dumas, N.Jamin, J.L Teillaud, J.,Miklossy, and L.Forro. 2002. Combining IR spectroscopy and fluorescence imaging in a single microscope: biomedical applications using a synchrotron infrared source. Review of Scientific Instruments 73: 1357–1360.

Miller, L.M., and P.Dumas. 2006. Chemical imaging of biological tissue with synchrotron infrared light. Biochimica et Biophysica Acta 1758: 846–57.

Murphy, E.M., J.M.Zachara, S.C. Smith, and J. L Phillips. 1992. The sorption of humic acids to mineral surfaces and their role in contaminant binding. Science of the Total Environment 118; 413–423.

Naumann, A., M.Navarro-Gonzalez, S.Peddireddi, U.Kues, and A.Polle. 2005. Fourier transform infrared microscopy and imaging: Detection of fungi in wood. Fungal Genetics and Biology 42: 829–835.

Olk, D.C., G.Brunetti, and N.Senesi. 2000. Decrease in humification of organic matter with intensified lowland rice cropping: A wet chemical and spectroscopic investigation. Soil Science Society of America Journal 64: 1337–1347.

Omoike, A., and J.Chorover. 2004. Spectroscopic study of extracellular polymeric substances from Bacillus subtilis: aqueous chemistry and adsorption effects. Biomacromolecules 5: 1219–1230.

Pandey, K.K. 1999. A study of chemical structure of soft and hardwood and wood polymers by FTIR spectroscopy. Journal of Applied Polymer Science 71: 1969–1975.

Parikh, S.J., and J.Chorover. 2006. ATR-FTIR spectroscopy reveals bond formation during bacterial adhesion to iron oxide. Langmuir 22: 8492–8500.

Paul, E.A., S.J.Morris, R.T.Conant, and A.F.Plante. 2006. Does the acid hydrolysis-incubation method measure meaningful soil organic carbon pools? Soil Science Society of America Journal 70: 1023–1035.

Petersen, L.W., P.Moldrup, O.H.Jacobsen, and D.E. Rolston. 1996. Relations between specific surface area and soil physical and chemical properties. Soil Science 161: 9–21.

Santos, D., S.L.S.Murphy, H. Taubner, A.J.M Smucker, and R.Horn. 1997. Uniform separation of concentric surface layers from soil aggregates. Soil Science Society of America Journal 61; 720–724.

Schmidt-Rohr, K., J. D.Mao, , and D. C. Olk. 2004. Nitrogen-bonded aromatics in soil organic matter and their implications for a yield decline in intensive rice cropping. Proceedings of the National Academy of Sciences USA 101: 6351–6354.

Six, J., H. Bossuyt, S.,Degryze, and K.Denef. 2004. A history of research on the link between (micro) aggregates, soil biota, and soil organic matter. Soil and Tillage Research 79; 7–31.

Smidt, E., P.Lechner, M.Schwanninger, G.Haberhauer, and M.H.Gerzabek. 2002. Characterization of waste organic matter by FT-IR spectroscopy: Application of waste science. Applied Spectroscopy 56; 1170–1175.

Solomon, D., J. Lehmann, J. Kinyangi, B. Liang, and T. Schäfer. 2005. Carbon K-edge NEXAFS and FTIR-ATR spectroscopic investigation of organic carbon speciation in soils. Soil Sci. Soc. Am. J. 69:107-119.

Solomon, D., J. Lehmann, J. Kinyangi, W. Amelung, I. Lobe, S. Ngoze, S. Riha, A. Pell, L. Verchot, D. Mbugua, J. Skjemstad and T. Schäfer. 2007a. Long-term impacts of anthropogenic perturbations on the dynamics and speciation of organic carbon in tropical forest and subtropical grassland ecosystems. Global Change Biol. 13: 511–530.

Solomon, D., J. Lehmann, J.Thies, T.Schafer, B.Liang, J.Kinyangi, E.Neves, J.Petersen, F.Luizao, J.Skjemstad. 2007b. Molecular signature and sources of biochemical recalcitrance of organic C in Amazonian Dark Earths. Geochimica et Cosmochimica Acta 71: 2285–2298.

Sollins, P., P. Homann, and B.A. Caldwell. 1996. Stabilization and destabilization of soil organic matter: mechanisms and controls. Geoderma 74: 65–105.

Specht, C. H., and F. H.Frimmel. 2001. An in situ ATR-FTIR study on the adsorption of dicarboxylic acids onto kaolinite in aqueous suspensions. Physical Chemistry Chemical Physics 3: 5444–5449.

Strong, D.T., H.D.E Wever, R.Merckx, and S.Recous. 2004. Spatial location of carbon decomposition in the soil pore system. European Journal of Soil Science 55: 739–750.

Surewicz, W.K., Mantsch, H.H., Chapman, D., 1993. Determination of protein secondary structure by Fourier transform infrared spectroscopy: a critical assessment. Biochemistry 32: 389–394.

Sutton, R., and G.Sposito. 2005. Molecular structure in soil humic substances: the new view. Environment Science and Technology 39: 9009–9015.

Torn, M.S., S.E Trumbore, O.A Chadwick, P.M.Vitousek, and D.M Hendricks. 1997. Mineral control of soil organic carbon storage and turnover. Nature 389: 170–173.

Wang, S.L., and C.T Johnston. 2000. Assignment of the structural OH-stretching bands of gibbsite. American Mineralogist. 85: 739–744.

Wieckowski, T., and A.Wiewiora. 1976. New approach to problem of interlayer bonding in kaolinite. Clays and Clay minerals 24: 219–223.

Wilson, R.H., A.C Smith, M Kacuráková, P.K Saunders, N.Wellner, and K.W Waldron. 2000. The mechanical properties and molecular dynamics of plant cell wall polysaccharides studied by Fourier-Transform infrared spectroscopy. Plant Physiology 124: 397–405.

Yoon, T.H.; S. B Johnson, and G.E Brown Jr. 2004. Adsorption of Suwannee river fulvic acid on Aluminum Oxyhydroxide surfaces: An in situ ATR-FTIR study. Langmuir 20: 5655–5658.

Yu, P., J.J McKinnon, C.R Christensen, and D.A Christensen. 2003. Chemical imaging of micro-structures of plant tissues within cellular dimension using synchrotron. Journal of Agriculture and Food Chemistry 51: 6062–6067.

Zaccheo, P., G. Cabassi, G.Ricca, and L.Crippa. 2002. Decomposition of organic residues in soil: experimental technique and spectroscopic approach. Org. Geochem. 33: 327–345.

Zang, X., J.Van Heemst, D.H. Jasper, K.J. Dria, and P.G.Hatcher. 2000. Encapsulaation of protein in humic acid from Histosols as an explanation for the occurrence of organic nitrogen in soil and sediment. Organic Geochemistry 31: 679–695.

Zimmerman, A.R., K.W. Goyne, J. Chorover,. S. Komarneni, and S.L Brantley. 2004. Mineral mesopore effects on nitrogenous organic matter adsorption. Organic Geochemistry 35: 355–375.

CHAPTER 5

NANOSCALE BIOGEOCOMPLEXITY OF THE ORGANO-MINERAL ASSEMBLAGE IN SOIL: APPLICATION OF STXM MICROSCOPY AND C 1s-NEXAFS SPECTROSCOPY

Abstract

Methodological constraints limit the extent to which existing soil aggregation models explain carbon (C) stabilization in soil. We hypothesize that the physical infrastructure of microaggregates plays a major role in determining the chemistry of the occluded C and intimate associations between particulate C, chemically stabilized C and the soil mineral matrix. We employed synchrotron-based scanning transmission x-ray microscopy (STXM) coupled with near-edge x-ray absorption fine structure (C 1s-NEXAFS) spectroscopy to investigate the nano-scale physical assemblage and C chemistry of 150 μm microaggregates from a Kenyan Oxisol. Ultra-thin sections were obtained after embedding microaggregates in a sulfur block and sectioning on a cryo-microtome at -55 °C. Principal component and cluster analyses revealed four spatially distinct features: pore surfaces, mineral matter, organic matter and their mixtures. The occurrence of these features did not vary between exterior and interior locations; however, the degree of oxidation decreased while the complexity and occurrence of aliphatic C forms increased from exterior to interior regions of the microaggregate. At both locations, compositional mapping rendered a nano-scale distribution of oxidized C clogging pores and coating pore cavities on mineral surface. Hydrophobic organic matter of aromatic and aliphatic nature, representing particulate C forms appeared physically occluded in 2-5-μm pore spaces. Our findings demonstrate that organic matter in microaggregates may be found as either oxidized C associated with mineral surfaces or aromatic and aliphatic C in particulate form. Using STXM and C 1s-

NEXAFS we are for the first time able to resolve the nano-scale biogeocomplexity of unaltered soil microaggregates.

1. Introduction

Long-term stabilization of soil organic matter (SOM) is controlled by structural configurations in the organo-mineral assemblage of soil microaggregates (Tisdall, 1996; Bronick and Lal, 2005). Several processes combining knowledge of soil parent material, microaggregate structures and biogenic feedback mechanisms are suggested to explain the form and function of soil aggregates as well as the existence of an aggregate hierarchy in soil (Tisdall et al., 1982; Oades et al., 1991). Many studies apply model experiments to evaluate the effects of cultivation on soil aggregation (Six et al., 2004) and C stabilization in various fractions of SOM (Guggenberger et al., 1994; Kaiser et al., 2002). In a review, Blanco-Canqui and Lal (2004), discuss how the development of such models will facilitate better understanding of C sequestration in soils. Since most conceptual models are built on evidence collected from destructive SOM tests, they fail to explicitly provide a linkage to spatial functionality of C stabilization occurring in microaggregate pore regions. This shortcoming is attributed in part to the slow advancement of methodological approaches addressing the functional relevance of SOM (Elliot et al., 1996; Sohi et al., 2001; Wander et al., 2004). Although progress in scanning electron microscopy (Mikutta et al., 2005), computer microtomography (Albee et al., 2000) and X-ray scattering techniques (Amelung et al., 2002; Leifeld et al., 2003) now render images of internal microaggregate porosities and their intra-aggregate attributes, the spatial interrelationships between soil C forms and aggregate stability is still largely unknown.

Application of microspectroscopy to study the structure of biomaterials (Warwick et al., 1998; Hitchcock et al., 2002), now affords the opportunity to adapt novel techniques to investigate nano-scale processes in the C chemistry and structural assembly of soil aggregates. Recent attempts by Schmidt et al. (2003) show that microspectroscopy can be used to capture the microscale variability of SOM in hydrated soil samples dispersed in aqueous media. In an attempt to elucidate the surface C functional characteristics of 5-80 μm size black carbon (BC) particles, Lehmann et al. (2005) succeeded to prepare 200-nm thin BC sections for X-ray microscopy and spectroscopic imaging. In this approach, a combination of scanning and transmission x-ray microscopy (STXM) is accomplished in conjunction with near-edge x-ray fine structure (NEXAFS) to study the nano-scale distribution of C forms on particle surfaces in soil. Incident photon energy is increased throughout a C absorption K edge (280 eV), beyond the ionization threshold (290 eV) causing excited core electrons to be removed from the core hole and promoted to a continuum. The excited phase of the inner-core electron (1s) is characteristic of the structure of the C molecular bonding and can be correlated to specific C forms (Ade et al., 1992; Stöhr et al., 1992). Multiple C 1s electron transitions in the NEXAFS region (284 eV-290 eV) reveal the presence of C moieties such as aromatic-C (C=C), aliphatic-C (C−H), carboxyl-C (COOH) and carbonyl-C (C=O).

Synchrotron STXM and C 1s-NEXAFS are widely used to resolve nanostructures of polymers (Smith et al., 2001) and to fingerprint C in biological materials (Lerotic et al., 2004; Hitchcock et al., 2005), where radiation exposure is controlled to avoid damage to the susceptible C=O bond (Rightor et al., 1996; Braun et al., 2005). High concentrations of C (>700 g C kg^{-1}) in uniform polymer layered samples (Ade and Urquhart, 2002) and BC (Lehmann et al., 2005) permit NEXAFS data filtering, thereby improving the signal-to-noise ratio of the images. Solomon et al.

(2005) also showed that processing extracts through a 2-μm pore membrane to trap mineral particles enhances C spectral signal response from humic substances containing 300-500 g C kg^{-1}. Currently, it is difficult to examine organic matter in soils which contain minerals and low amounts of C (5-150 g C kg^{-1}) because its micro-scale spatial distribution is highly heterogeneous. In this case, the C 1s signal response is significantly masked by absorbance interferences from mineral matter. We attempted to use STXM and C 1s-NEXAFS to investigate C chemical forms in mineral-pore structures after modifying the data background correction. In applying STXM and C 1s-NEXAFS, our objectives were: (i) to examine structural features that confer stabilization of C in the microaggregate soil assemblage; and (ii) to determine the spatial distribution of C chemical functional forms on surfaces and interior regions of unaltered soil microaggregates.

2. Materials and methods

2.1 Site and soil sample background

We obtained soil aggregate material from an agricultural field located on a heavy textured Oxisol (Soil Survey Staff, 2003) dominated by 1:1 kaolinite clays adjacent to Kakamega forest (34º, 57′, 14″E; 00º 14′ 20″N; 1733 m above sea level) in western Kenya. The site is part of a chronosequence experiment, investigating the long-term effects of cultivation agriculture on soil organic matter degradation. The area receives 2080 mm annual rainfall in a bimodal distribution with a mean annual temperature of 19.0°C. One kilogram soil sample from a cultivated maize field that had recently (2001) been converted from natural primary forest was collected from 0.1 m depth using a core sampler with a diameter of 0.1 m. Prior to sampling in June 2003, the site had been tilled for five seasons and planted to maize (*Zea mays* L.) and bean (*Phaseolus vulgaris* L.) crops. The soil was air-dried, crushed and passed through

a 2-mm sieve, packed and submitted to the laboratory. Soil properties for the soil sample were: 85.6 g C kg^{-1}; 9.8 g N kg^{-1} and 1.9 g S kg^{-1}, and pH_{KCL} of 5.3. Other soil chemical and mineralogical properties for Kakamega forest are reported in a study by Krull et al. (2002). They characterize these soils to be dominated by silica, Fe and Al, with low base status (Ca, K, and Mg) due to intense weathering and confirmed the absence of calcite by XRD analysis.

2.2 Preparation of microaggregate thin sections

In our previous work (Lehmann et al., 2005), we reported a procedure for identifying and ultra-sectioning (Ultracut UTC, Leica Microsystems Inc. Bannockburn, IL, USA) 5-80 µm BC particles embedded in preheated (220°C) and super-cooled (in liquid N_2) elemental sulfur prior to sample image and spectroscopic analysis. Several attempts to apply this protocol to section soil aggregates <250 µm were unsuccessful, partly due to the collapse of the crumb structure of soil aggregates under the pressure of the microtome knife. We modified the sectioning protocol to include soil aggregate pre-treatment. Specifically, a 1-g soil sample was sieved to pass a 250-μm screen to obtain microaggregates, then sprinkled on a glass fiber filter (Whatman GF/A, 47mm 1.6 µm opening), mounted onto a sieve surface and fixed to a chimney funnel that transferred warm mist from a humidifier (Ultra-violet light, Slant/Fin; 7.5L capacity). The humidifier chamber was filled with water dispensed from a Barnstead NanoPure Diamond water purification system. After eighteen hours of continuous misting, the microaggregates were considered to be water saturated. Excess droplets on the glass fiber filter were drained off prior to freezing microaggregates. A 150-µm microaggregate sub-sample was selected, embedded in a sulfur block and submitted to the cryo-microtome for sectioning. Since the pre-treatment resulted in a frozen sample, sectioning was accomplished at -55°C. For a

detailed description of the cryo-microtome features and thin section sample operations, see Lehmann et al. (2005).

After sectioning, several microaggregate thin slices were mounted on Cu grids (200 mesh, no 53002, Ladd Research, Williston, VT, USA) impregnated with silicon monoxide (SiO) substrate. The grid was mounted onto the center pinhole of stainless steel sample stage plates (46 mm diameter) with tape to hold the edge. The microaggregate was secured in the crystalline structure of sulfur which was then sublimed in a vacuum oven (1 hr, 40 °C, -31 bar), prior to measurement. Because specificity of the C chemistry relies on the contrast in absorption between successive features of the sample images, the section thickness must be controlled to minimize error. To optimize the signal to noise ratio, Ade et al. (1992) recommend that C-based material (1 g cm^{-3}) be sectioned between 40-800 nm thick, whereas Boese et al. (1996) estimate 1 μm to be the typical thickness of biological samples prepared for spectromicroscopy. In this study, microaggregates were sectioned to ~800 nm thickness. The C content was low (<100 g C kg^{-1} soil) because aggregates also consist of dense mineral matter (>2 g cm^{-3}). For comparison, protein density is about 1.35 g cm^{-3} (Boese et al., 1996).

2.3 STXM and C 1s NEXAFS data acquisition

Scanning transmission X-ray microscopy and C 1s-NEXAFS spectroscopic measurements were completed at beamline X1A1 of the National Synchrotron Light Source, Brookhaven National Laboratory. This light source produces a soft X-ray beam from the 2.8 GeV electron storage ring which illuminates a monochromator that is tunable over 250 eV to 800 eV, operated in synchrony with the sample z-stage. The z-stage was adjusted to focus the X-rays through the microaggregate sample section. Slit openings were set at 25/30/25 μm giving an energy resolution of 0.1 eV. When

combined, the slit settings and zone plate provided scanning spatial resolution of 50 nm. The monochromator energy was increased from 280 eV to 282.5 eV in 0.3 eV increments (scan time 1 msec), from 282.5 eV to 292 eV in 0.1 eV steps (scan time 3 msec), and from 292 to 310 eV in 0.3 eV steps (scan time 3 msec). Smaller energy steps of 0.1 eV were chosen in the spectroscopic regions where C 1s core electron excitation is indicative of sharp 1s $\rightarrow\pi^*$, and broad 1s, 3p $\rightarrow\sigma^*$ transitions. The scan time was increased to reduce error and improve recorded data. Single images were recorded from succeeding photon energy levels and built into a stack using the program Stack Analyze 2.6.1 (Jacobsen et al., 2000). Alignment was completed from a constant reference energy level at 280 eV using the cross-correlation matrix, constrained to a shift limit of 30 pixels, after sobel routine adjustment for edge enhancement. Further stack image processing software and data analyses instructional manuals can be accessed on the website at http://xray1.physics.sunysb.edu/data/software.

2.4 Principle component analyses

We used the program PCA_GUI 1.1.1 (http://xray1.physics.sunysb.edu/data/software) to orthogonalize and noise-filter data. X-ray image data were separated into 3 significant components (s = 1, 2, 3) describing the main features in the microaggregate sample because prior knowledge of such features was unknown. Significant components were determined based on observations of the eigenvalues, eigenimage and eigenspectra (Beauchemin et al., 2002; Lerotic et al., 2004). The goal was to select components due to systematic variations of spectral signals from pixel to pixel and to discard random fluctuations of signal beyond which noise effects will occur. The eigenspectra of the component would be flat, implying lack of variation due to chemical speciation (Lerotic et al.,

2004). The eigenimage scaling factor was adjusted between 0.3-0.6 to increase sensitivity only when additional cluster searches did not control high OD signal responses from pixel classification of minerals.

2.5 Cluster pixel classification

In PCA_GUI 1.1.1, we performed cluster analyses to classify regions in the sample according to spectral similarities of pixel groupings. Using the intensity values from the background (I*o)* histogram, a region of high flux indicated by the brightest surface in the image was selected (PS-I*o*). Several iterated runs improved the accuracy of I*o* region selection through observing the optical density of the designated I*o* surface, adjusted to near 0. Since our sample contained minerals, organic matter and their mixtures, we found strong interference on the filtering of spectral signals which could in part be attributed to ultra-thin regions of optically less dense mineral flakes that are detached from the assemblage. Such regions were classified more due to their OD than spectral characteristics. This resulted in a large pre-edge absorbance as previously noted by Smith et al. (2001), during their examination of polymer material with high chloride contents. Because mineral and pore space pixels occupy the vast majority of the spectral signal search space, pixels due to organic matter were grouped most distant away from their cluster centers. This grouping indicated poor classification by the euclidean algorithm, thereby rendering average cluster spectra that were poorly resolved in definition, whose energy peak positions were difficult to assign.

2.6 Composition thickness maps

Subsequent to principal component and cluster analyses, singular value decomposition (SVD) was calculated, providing compositional thickness maps from

corresponding fitted data. Because SVD is computed from matrix inversion procedures (Kopranirov et al., 2002; Lerotic et al., 2004), it is possible to derive equivalent thickness maps leading to variation in sample mineral and C pseudo-thickness. Optical density is a distinct feature of NEXAFS which is calculated from the transmitted X-ray intensities where sample scan images (I) are normalized from an I*o* scan event recorded without the sample (Jacobsen et al., 2000). The Beer-Lambert law is used to quantify absorption (A) where:

$$\mathrm{A}=\mathrm{OD}=\mu(E)\rho T=-\ln(\mathrm{I}/\mathrm{I}o), \quad (1)$$

with $T = OD / \mu(E)\rho$,(2)

given that μ is a mass absorption coefficient at energy level E, ρ is the material density and T is the sample thickness.

This composition permits construction of thickness maps (Koprinarov et al., 2002; Lerotic et al., 2004), which represent cluster spectra of C forms and those that define regions of mineral and pore spaces. Maps that were uncorrelated with spatial features and only exhibited random patterns were removed from the analysis. Map elimination was based on dissimilarity in classified pixels obtained from cluster analyses. The most contrasting cluster pixel groupings were identified and only these were sought in the composition thickness maps. Because boundary regions are indiscrete (Lerotic et al., 2004), we argue that spectral composition areas must always be viewed as spatial gradations where C forms transition in functional characteristics. During map elimination, care must be taken to retain such overlay regions because they certainly correspond to unique C chemical features.

Table 5-1. Relationships between aggregate features, optical densities (OD) and the C compositional expression from spectral signal dominance of the interior and exterior regions of a soil microaggregate

Feature	OD†	C 1s binding energy transition					C bond
		π* C=C	π* C=N	π* C-H	π* COOH	σ* C=O	
Pore space	< 0.5	-	-	-	-	-	none (OD near 0)
Organic	0.5 – 1.0	+++	++	++	+++	++	C=C, C−H, C=O
Organomineral	1.0 - 1.8	++	-	-	+++	++	COOH, C=N, C=O
Mineral	> 1.8	-	-	-	-	-	none(OD near 2.5)

†Optical density.
No detectable C functional form (-).
Carbon functional form less dominant (+), dominant (++) and most dominant (+++) in the absorption spectrum.

In order to further interpret structural features in the STXM image and associated NEXAFS data, a direct linear relationship was assumed between absorbance in photon energy (OD) and sample material density (Eq. 1). When sample section thickness T for a given density ρ varied in optical depth with respect to the incident soft X-ray beam, we expected OD in the energy absorbance to change. We interpreted this change of variation in the signal response to denote unique sample density characteristics (Koprinarov et al., 2002). We used knowledge of the conceptual features in the microaggregate assemblage (Figure. 1), absorbance characteristics (Eq. 1, Eq. 2) and the cluster display of all spectra (not shown) to approximate the OD ranges that correspond to organic matter, minerals and their mixtures (Table 1).

3. Results and Discussion

3.1 STXM microscopy

Microaggregate regions showed much variation in their material density of C and mineral matter. However, the presence of visible internal mesopore networks permitted transmission of the soft X-ray beam and C density maps (Figures. 2c and 3c) were inferred from the resulting –log ratio of the images (Figures. 2a, 2b, 3a and 3b)**.** Optical densities in the resolved spectral regions for mineral and organomineral matter were elevated, not so much due to sample physical thickness (T), but rather in response to variation in the material density (ρ). Such density heterogeneity is not uncommon in complex biological material (Smith et al., 2001; Hitchcock et al., 2005). By combining STXM and NEXAFS measurements, we were able to extract micro variation in order to map C molecular composition with high spatial resolutions of up to 50 nm. In addition, C, mineral and pore assemblage features were resolved without altering the physical structure of the microaggregate.

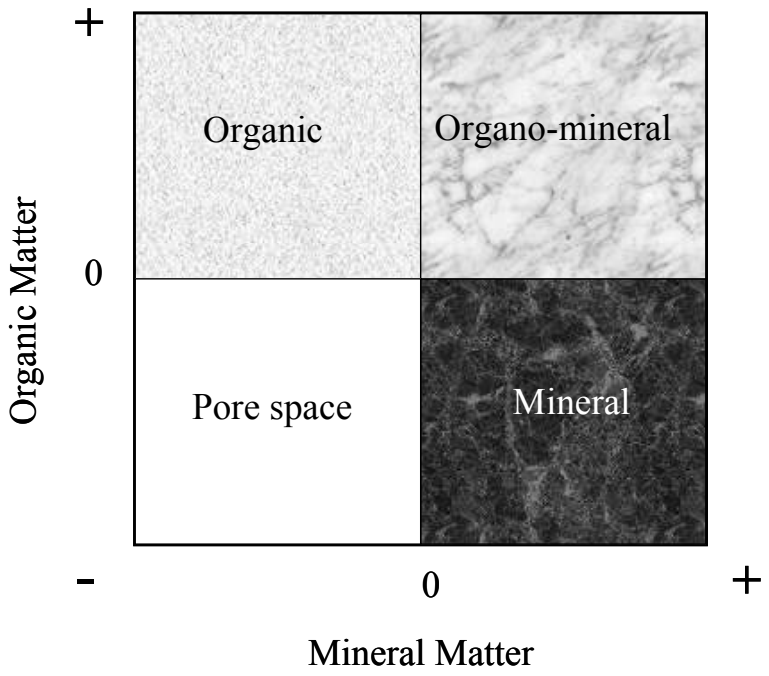

Figure 5-1. Conceptual framework for the interplay between minerals, organic matter, and pore space determining the C stabilization in the soil organo-mineral assemblage.

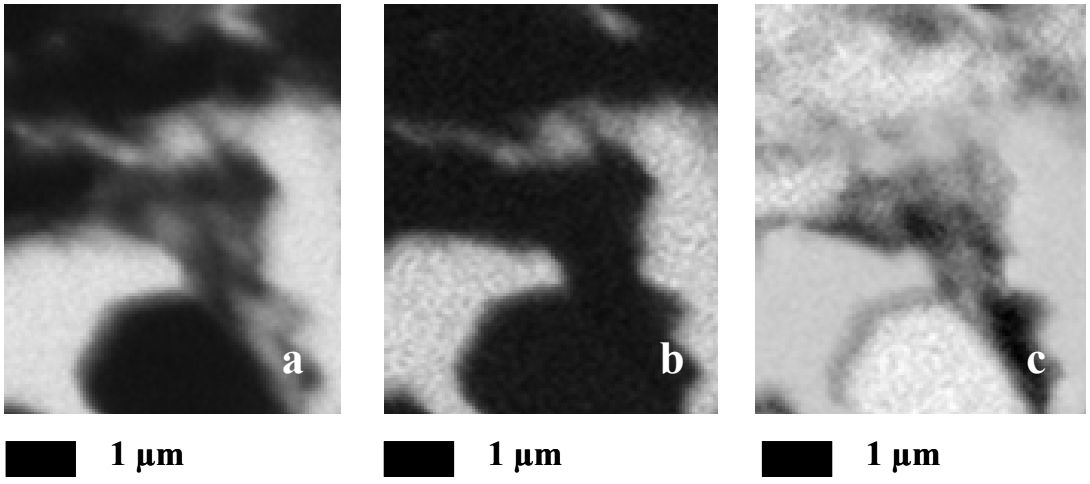

Figure. 5-2. STXM micrographs for an interior aggregate region taken below 281 eV (a) and above 290 eV (b) the carbon absorption edge. Contrast in the C and mineral density is shown in the ratio micrographs (c) calculated from –log [I/I*o*] where I = Σ (281 eV-282 eV) and I*o* = Σ (290 6 eV-291.5 eV).

3.2 NEXAFS Io background correction

We classified spectral regions by varying the ratio of significant components to cluster search by a factor of 3-4 (2/3-2/12 for PS-I*o* and 2/6-2/18 for CM-I*o*), where I*o* background regions correspond to pore space (PS) or mineral matter (CM). This search was combined with cluster composition mapping to investigate variations in the C chemistry and mineral composition. When PS-I*o* was selected for correction, the pixel population was tightly anchored around clusters of mineral absorbance that contain OD values >2.0 (Table 1). Pixels that represent mixtures of mineral and organic matter were distinctly clustered further away from clay and separated from pixel clusters of organic matter. Lerotic et al. (2004) have suggested the use of angle rather than euclidian distance measure algorithm to improve clustering where physical thickness variations interfere with composition resolution. Because we find both physical thickness and density variations to be inherent properties of organomineral interactions, an algorithm that suppresses density variations would almost lead to loss in optical compositional prediction. Instead, we used the euclidian distance measure approach to classify the microaggregate sample pixel population in order to capture both density and C chemical variations that result from organomineral associations.

Given that a slight energy shift in peak position can mean a complete alteration in the C chemistry (Scheinost et al., 2001), we sought alternative analyses to correct for poor peak definition arising from large background interference by mineral matter. We used a pixel classification that instead designates mineral absorbance regions of high OD as the I*o*, without masking expression of mineral or organomineral pixels. This approach is a modification to cluster data filtering for those biological and environmental samples that not only contain low C contents, but also include areas

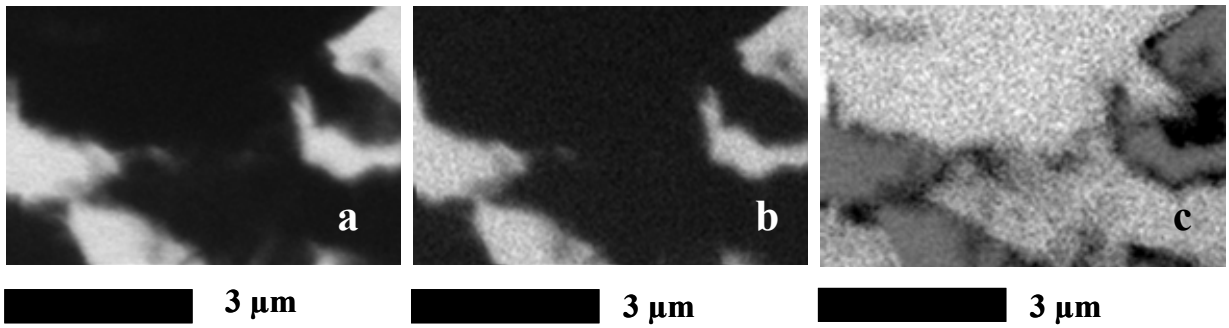

Figure. 5-3. STXM micrographs for an exterior aggregate region taken below 281 eV (a) and above 290 eV (b) the carbon absorption edge. Contrast in the C and mineral density is shown in the ratio micrographs (c) calculated from –log [I/I*o*] where I = Σ (281 eV-282 eV) and I*o* = Σ (290 6 eV-291.5 eV).

where C is occluded in dense non-C matter. This modification corrects for elevated pre-edge absorbance and minor variations unrelated to OD, which improves cluster centering of carbonaceous pixels from the spectra search space. Although the OD values are now reported on a negative Y-axis scale, we interpret OD related to minerals as less negative (~ 0) and OD related to pore space as more negative (~ -2.5). Following this revised procedure, we repeated cluster analyses on the significant components (s = 2, 3) to test for thematic contrast of the results. Pixels in the resulting plot of components were anchored near a mineral cluster center with clear expression of the contrast between organic matter, organo-mineral and pore structures using both the 18 (Figure. 4a-interior) and 12 (Figure. 4b-exterior) classified regions.

3.3 Cluster composition thickness maps

In the interior region of the microaggregate we completed an extensive evaluation of the cluster indices map (not shown), spectral pixel plots (Figure. 4a) and composition thickness maps (Figure. 5) in order to establish spatial interrelationships in the structural biogeocomplexity of the mineral-pore assemblage. Using NEXAFS, this mapping approach has been shown to reveal protein composition of sperm cells (Zhang et al., 1996) and spatial variations of BC oxidation (Lehmann et al., 2005). Compositional thickness maps displayed bright white regions that were associated with distinct and significant fitted spectra. In Figure 5a, we observe variable nanoscale pore constrictions (>500 nm) and 2-5 μm large pore voids in dense mineral assemblage, stabilized by patchy occurrences of particulate or mineral-bound organic matter in both open and closed orifices. The visible structures in the mineral-pore network and the location of mineral and organic matter

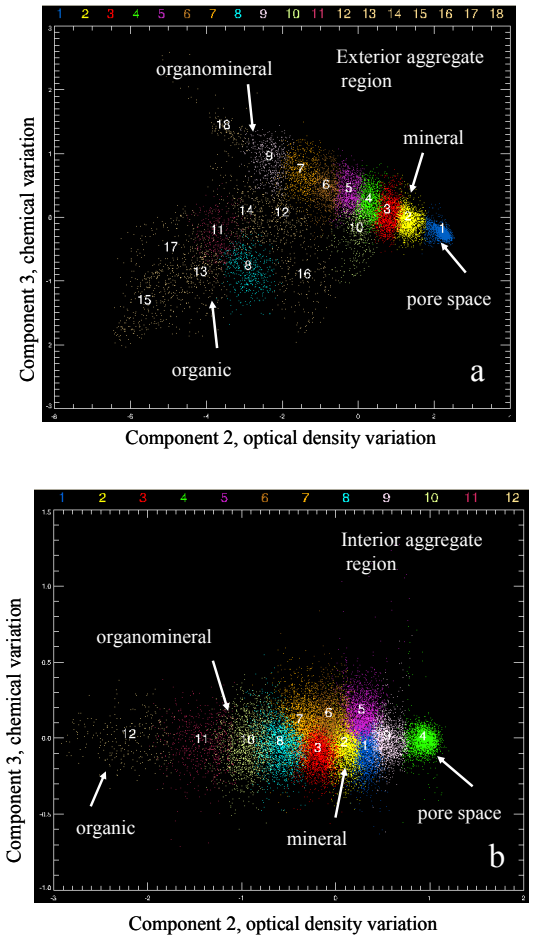

Figure. 5-4. Cluster pixel plots of components 2 and 3 show spectral characteristics of mineral and organic matter, color-coded for each cluster (color legend on top axis). Yellow color represents mineral cluster pixels separated from cluster pixels of organic and organomineral complexes by the blue (a) and green (b) clusters of pore space pixels. Pixel separation with an OD gradient (axis component 2), distinguishes C chemical species in the organic or organo-mineral matter, and is noticeable only in (a) but not (b) on axis component 3.

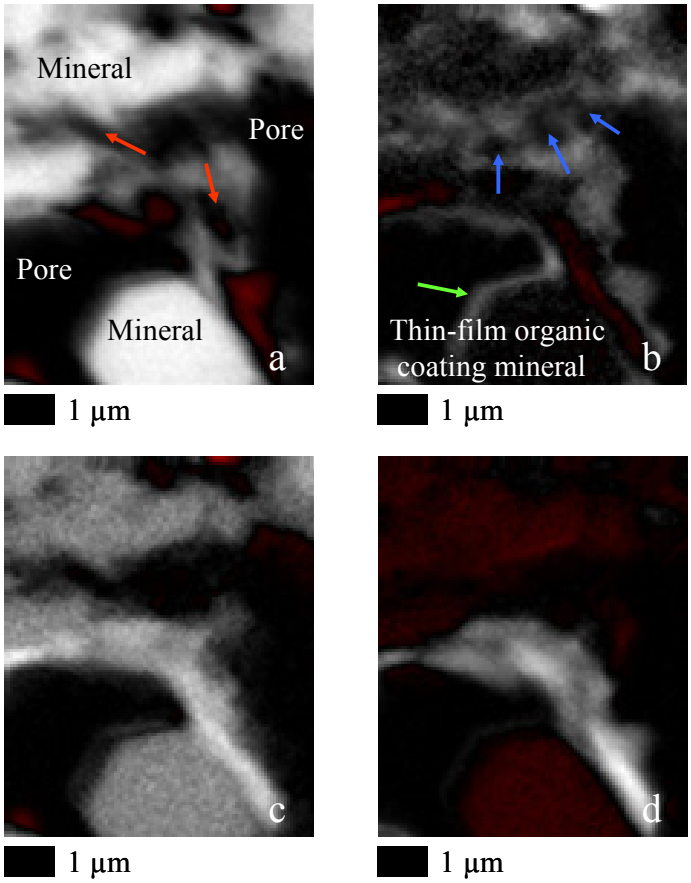

Figure. 5-5. Composition thickness maps of the main thematic regions in the interior of a micro-aggregate. Composition maps show bright white regions of minerals (a), organomineral complexes of carboxylic-C forms (b), organomineral coatings of aromatic, aliphatic-C forms (c), and particulate forms of aromatic-aliphatic-C (d). Red arrows show small nanometer pores in mineral matrix. Blue arrows point at small nanometer pores in organomineral complex.

are already revealed from 12 clusters (Figure. 4b) and these appear similar in their overall geometry to the interior regions of the microaggregate.

3.4 Spatial distribution of carbon forms inferred from cluster pixel classification

C 1s-NEXAFS spectroscopy identified nano variability in mineral and C chemical composition of the mineral-pore assemblage. Gradations of the spectra in the C absorption region were captured by components $s = 2, 3$ after excluding $s = 1$ representing only average sample spectral characteristics and rejecting $s = 4$, when pixel to pixel signals were uncorrelated. From the cluster spectra we were able to distinguish organic matter bound to minerals along cavities, precipitating stable C assemblages which form mineral complexes that are separated by pore connectivity. The STXM images of the C density maps consistently revealed that the brightest image regions, which corresponded to the strongest C absorption signal (Lawrence et al., 2003), occurred within or along pore cavities but not between mineral layers such as may occur in marine environments (Ransom et al., 1997; Mayer et al., 2004). Four dominant thematic features in the microaggregate section were expressed as: (i) minerals, (ii) organo-mineral assemblages of predominantly oxidized C forms, (iii) particulate organic matter of aromatic, amide, aliphatic, carboxyl and carbonyl type C, and (iv) complex surface and internal pore networks (Figures. 5 and 7).

3.5 Organic matter and mineral assemblage

The mineral domain was displayed as a compact matrix consisting of sections that vary in optical density, whose spectral signal in the energy absorbance was ~ 2.5 (Figure. 5a and 7a). We observed mineral flakes that were loosely attached on the broken edges of more compact mineral matter. These assemblages of minerals appeared to bind to the organic matter that covered the compact mineral matter (Figure 5c) providing early evidence for microaggregate formation in nanostructures.

According to Denef et al. (2005), this process leads to abiotic aggregate formation and reformation. Because the section of soil material is from an Oxisol, we further hypothesize that such nano-aggregation is likely initially mediated by abiotic-cationic mineral bonding (Kaiser et al., 2002). Evolving aggregates are then stabilized through geochemical controls such as wetting and drying cycles (Park et al., 2005), salt mobility (Sollins et al., 1996) and pH charge dependence (Bronick and Lal, 2005), or geological time exposure (Trumbore et al., 1993).

Amelung et al. (2002) have examined a 50 nm depth region on soil surface particles using XPS and found organic matter to be concentrated at the particle surface. At 50 nm depth, these authors possibly only measured organic mater bound on the surface as microfilms, excluding organic matter that is sequestered in surface breaking pores or localized by clogging internal connecting pores. Mikutta et al. (2005) reported a "pore-clogging" effect of AlOOH by dissolved organic C and Zimmerman et al. (2004) found large protein macromolecules to be excluded from the mineral surfaces through a "pore-filling" mechanism in marine sediments. Our findings support observations of organic matter stabilization on surface microfilms and in pore structures of the organo-mineral assemblage (Figures. 5b, 5c, 5d, 7b and 7c).

3.6 Carbon chemical forms in microaggregates

C 1s-NEXAFS spectra exhibited multiple peaks in the fine structure of the K-edge absorption region indicating the presence of multiple organic C functional moieties in the mineral-pore structures. Dominant C chemical forms visible in these nanostructures showed absorbance near 285.0 eV, 286.0 eV, 286.6, 287.3 eV, 288.6 eV

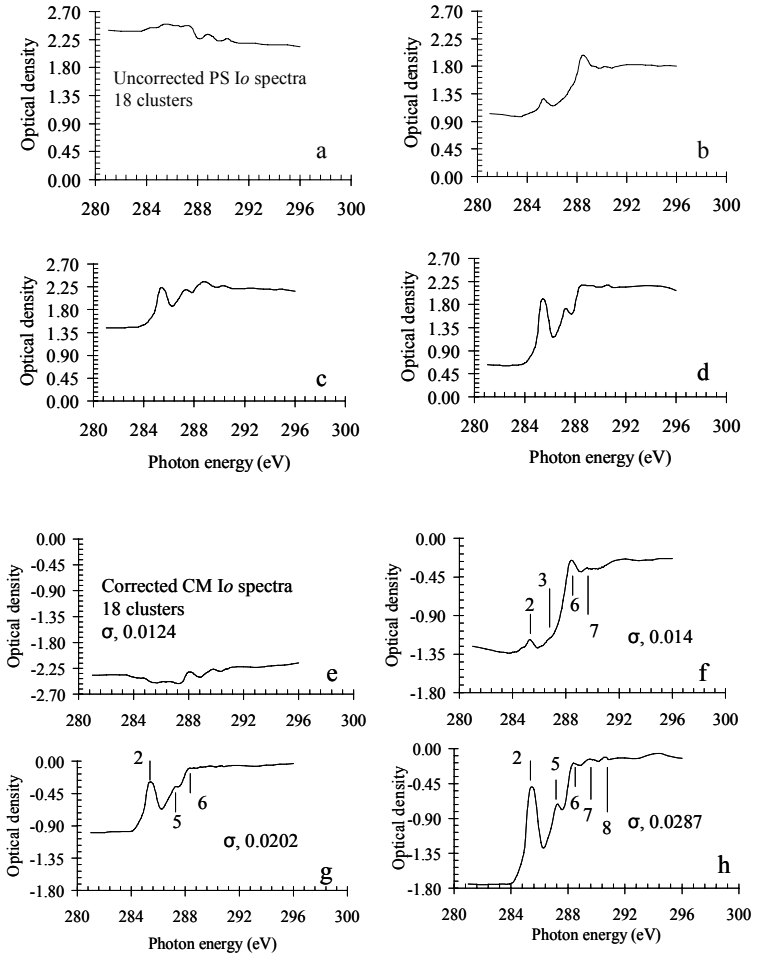

Figure. 5-6. Spectral signatures of the composition thickness maps of the interior area shown in Figure 5, with both uncorrected PS-I*o* (a, b, c, and d) and CM-I*o* corrected spectra (e, f, g, and h). Spectra (a) and (e) refer to mineral and pore space signatures, respectively. Spectra b and c show elevated OD as a result of absorbance by mineral matter. Residual errors for the fitted spectra e, f, g and h are shown with their root variance, σ.

and 289.5eV energy regions. Their peak positions are designated 2, 3, 4, 5, 6 and 7, following spectra assignments published by past NEXAFS studies on known biomaterials (Table 2). Two peaks that appeared to be significant shifts in the absorbance energy attributed to aromatic-C and carbonyl-C, occurred near 286.0 eV and 289.7 eV. No transitions were recorded in the 284.3 eV region of low energy absorbance from saturated quinone type C. Organic matter in the interior region is most complex and required a large cluster search (18) to effectively classify C chemical composition regions (Figure. 4a). In contrast, no C chemical difference in the functional form was observed across spatial regions in the exterior region (Figure. 4b).

3.6.1 Aromatic-C: protonated, alkylated, hydroxylated and amide substituted aromatic C (284.0 eV- 287.1 eV)

According to Table 2, the resonance at energy level 2, near 285.0 eV represents 1s→π* C=C of aromatic C (Boyce et al., 2002; Schäfer et al., 2003, Lehmann et al., 2005). Organic matter in pores inside the aggregate had a strong absorbance due to presence of phenyl rings and may indicate the existence of aromatic protein macromolecules (Brandes et al., 2004; Hitchcock et al., 2005). The peak intensity of aromatic-C declined significantly when organic matter was bound to minerals suggesting a transformation that oxidized C=C to COOH forms. Organic matter in exterior regions of the aggregate showed a weak 1s→π* C=C and no 1s→π* C−H indicating depleted aromatic-C and nearly no aliphatic-C forms. Carbon forms appearing at energy level 3 (Figures. 6f and 8f) suggest excitations due to 1s→π* C=N from N substitution in the phenyl ring (Ade and Urquhart, 2002; Brandes et al., 2004; Hitchcock et al., 2005). This functional form undergoes hydrolysis-reduction reactions to precipitate acidic COOH and basic NH_2 groups. In a study of 20 amino acids commonly occurring in soil biological material, Kaznacheyev et al. (2002) show that

C=N bond structures are only found in histidine, (C=C) and arginine (no C=C). Although the C=N resonance occurs in the 286.0-286.5 eV energy region (Boese et al., 1996; Ade and Urquhart, 2002; Flynn et al., 2003), often overlapping with assignment to R-OH, work by Scheinost et al. (2001) suggests that the 1s→π* transition near 286.1 is not resonance from aromatic C bonded to OH. This resonance may instead originate from unsaturated aromatic-C (Lehmann et al. 2005) or C=O substituted aromatic-C (Cody et al., 1998). Flynn et al. (2003), who studied the C composition of interplanetary dust alluded to the ambiguity in this peak resonance arguing that both C=N and R−OH bonds are feasible assignments. Phenolic-C forms at energy level 4 were assigned 1s→π* C=C transitions of hydroxylated-C on the phenyl ring (Braun et al., 2005; Solomon et al., 2005). The absence of resonance due to phenols (286.6 eV-287.1 eV) and quinone type-C (284.0 eV) may point to evidence for lack of plant derived C from lignin degradation (Solomon et al., 2005).

3.6.2 Aliphatic-C (287.3 eV-287.6 eV)

A pronounced resonance around 287.3 eV was assigned to 1s→π* transitions of C−H and appeared in the image of the interior regions of the aggregate (Figures. 6g and 6h). The presence of resonances in the aliphatic-C chain structure together with oxidized carboxyl and carbonyl-C suggested the occurrence of C forms in phospholipid fatty acids or chitin (Solomon et al., 2005) that may be residues from particulate C. The 1s→π* transition near 287.3 eV is also due to aliphatic-C of CH, CH_2, and CH_3 groups that may form non-polar termini which confer hydrophobic properties. Further experimentation is required to understand how non-polarity establishes mineral coating

Table 5-2. Photon energy (eV) peak resonance assignment for organic C functional forms obtained from near edge absorption fine structure (NEXAFS) spectroscopy

Peak regions	Photon energy	Carbon functional group forms†	References
1	284.3	Quinone-C, protonated aromatic-C	a, b, d, e i
2	284.9-285.5	Alkylated to carbonyl-substituted aromatic-C	a, b c, g, h
3	286.0-286.5	Unsaturated aromatic-C, C−N and C=N of N substitution in phenyl ring	a, d, e
4	286.5-287.1	Phenolic O−H, ketone O−C−O	c, d, e, f, h
5	287.3-287.6	Aliphatic C−H	a, b, i
6	287.7-288.8	Carboxyl-C, split features of C−C, C−H or COOH	a, c, e, g, i
7	289.3-289.8	Carbonyl-C, alcohol-C ether linkage R−O−R	d, e, f, i
8	289.8-290.0	Unassigned but probably organic C−O with traces of inorganic C−O	a

†peak assignments for C 1s NEXAFS according to: a) Brandes et al. (2004); b) Braun et al. (2005); c) Cody et al. (1998); d) Hitchcock et al. (2005); e) Lehmann et al. (2005); f) Scheinost et al. (2001); g) Schäfer et al. (2003); h) Smith et al. (2001); and i) Solomon et al. (2005).

of aromatic-aliphatic structures noticeable in Figure 5c. Schreiber et al. (2000) attributed hydrophobicity in alkyl-thiol-based monolayers to the effect of phospholipid bilayers which in themselves are primary constituents of biological membranes (Benzerara et al., 2004). Therefore, we postulate particulate organic matter exhibiting 1s→π* C=C and 1s→π* C−H to in part, indicate structures and debris of re-synthesized C possibly of microbial membranes, tissue and residues.

3.6.3 Carboxyl-C (287.7 eV-288.8 eV)

The strong absorption band near 288.6 eV was assigned to a 1s→π* COOH transition of carboxylic-C (Cody et al., 1998; Boyce et al., 2002; Schäfer et al., 2003; Lehmann et al., 2005). The characteristic carboxyl phenyl ring manifested a 0.3 eV energy shift on the C=O bond, down to 288.3 eV, which indicates the presence of carboxyamides (Lawrence et al., 2003; Benzerara et al., 2004; Brandes et al., 2004). Carbon chemical forms dominated by oxidized C are characterized by polar carboxyl-C absorption near 288.6 eV representing aliphatic rather than aromatic acids (Kaznacheyev et al., 2002). The peaks in both sections were broad signifying the presence of both amide and polysaccharide carboxyl-C (Benzerara et al., 2004). Oxidized organic matter interacted as a discontinuous thin film-type layer through binding in pore cavity regions on the mineral surface (Figures. 5b and 7c). Transmission electron microscopy has shown the existence of mono-layers to explain the binding of natural organic matter to clay surfaces in marine sediments (Ransom et al., 1997) but further examination (Brandes et al., 2004; Mayer et al., 2004) now highlights a preferential and patchy location of organic matter in the mineral-pore complex. Our findings partly agree with Brandes et al. (2004) and Mayer et al. (2004), supporting observations for a patchy occurrence of organic matter on minerals.

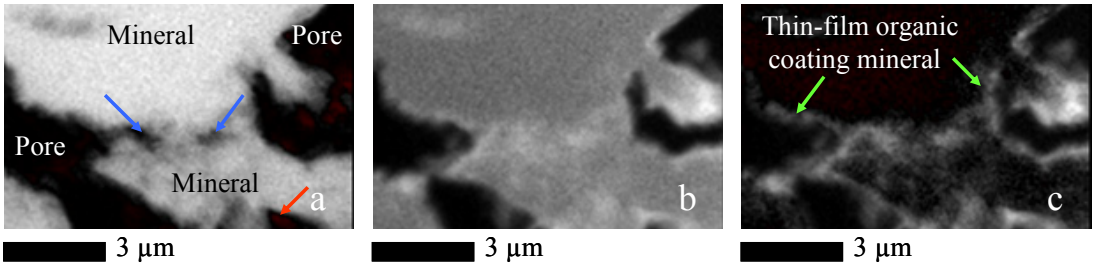

Figure. 5-7. Composition thickness maps of the main thematic regions at the exterior of a micro-aggregate. Composition maps show bright white regions of minerals (a), organomineral complexes of carboxylic-C forms (b) and organomineral coatings of aromatic, carboxylic-C forms (c). Red arrows show small nanometer pores in mineral matrix. Blue arrows point at small nanometer pores in organomineral complex.

In addition to patchy location, we also observed a thin film of organic coating but not uniform mono-layers, confirming that organic matter in soil microaggregates may be stabilized as patchy thin films on surfaces. The functional properties of protonated-deprotonated ($COOH/COO^{-}$) carboxyl termini visible in the spectrum of both regions (Figures. 6f, 8e and 8f) indicates oxidative degradation under acidic conditions. Orientation in C binding, common to self-assembled layers, involving hydroxyl−OH and alkyl−CH groups may confer hydrophilic and hydrophobic termini (Schreiber et al., 2000), causing organic matter to either coat surfaces (Figure. 5c), or clog mineral pores (Figure. 7b).

3.6.4 Carbonyl-C (289.3 eV-289.6 eV)

The sharp absorption band near 289.5 eV corresponds to the 1s→3p, σ* of C=O groups (Cody et al., 1995; Flynn et al., 2003) primarily representing polysaccharides, some aliphatic ethers and alcohol-C (Boyce et al., 2002; Scheinost et al., 2001). There was a visible shift to higher energy absorption resulting in 1s→σ* excitation of C=O (289.8 eV) specifically for organic matter clogging mineral pores or coating pore cavities. This peak shift maybe due to the inductive effect of 2 oxygen atoms adjacent to the carbonyl group (Boese et al., 1997; Smith et al., 2001), whose charge environment shows a band of O-substituted sp^3-hybridized C (Boyce et al., 2002) close to the ionization threshold (290 eV). The presence of the 1s→σ* C=O can be used to distinguish between protein-nucleic acid C=O and polysaccharide C−O in carboxylic groups of organic matter (Benzerara et al., 2004). We therefore find the occurrence of aromatic, aliphatic and acidic carboxyl functional groups to provide evidence that microaggregates may be stabilized by protein (C=C, C=N, C=O), lipid (C−H, COOH) and polysaccharide (C−H, C−OH) organomineral complexes of organic matter in soil.

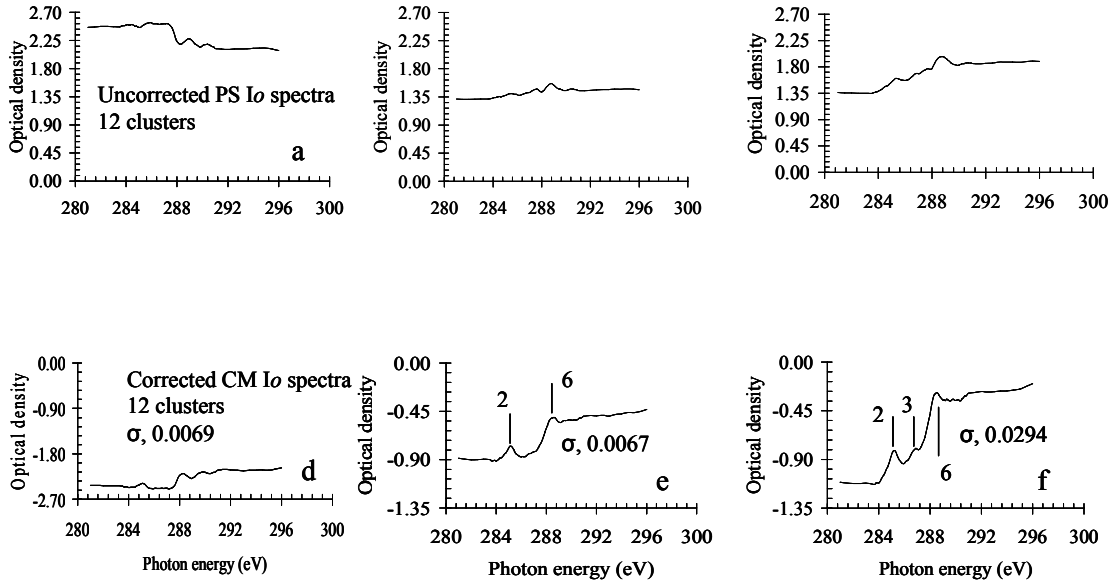

Figure. 5-8. Spectral signatures of the composition thickness maps of the exterior area shown in Figure 7, with both uncorrected PS-I*o* (a, b and c) and CM-I*o* corrected spectra (d, e and f). Spectra (a) and (d) refer to mineral and pore space signatures, respectively. Spectra (b), (c), (e) and (f) show elevated OD as a result of absorbance by mineral matter. Residual errors for the fitted spectra (d), (e) and (f) are shown with their root variance, σ.

3.7 Implications for modeling soil organic matter dynamics

Having examined the nanoscale spatial attributes of the C chemistry in microaggregates, we offer comments that may help to improve current models that describe interrelationships among the structural components in aggregate formation-deformation dynamics: i) there is merit to resolve preference for organic matter binding mainly to pore cavities where current models assume dominance of organic matter-mineral mixing in the organomineral complex; ii) we need to further investigate the relationship between clay contents and pore geometry with respect to C chemical adsorption and microbial access where models draw correlations between organic matter and soil texture as protective capacities; and iii) there is need to elucidate the affinity of polar hydrophilic COOH to complex with minerals while particulate non-polar aromatic and aliphatic-C structures are not complexed but rather coated by minerals, leading to geophysical occlusion of C.

4. Conclusions

Using STXM and C 1s-NEXAFS, we were able to visualize for the first time, an undisturbed intact microaggregate assembly and to resolve C functional forms at spatial resolutions that have not been feasible up to now with established methodological approaches. We have observed oxidized carboxyl-C to coat the mineral surface or clog pores. Hydrophobic aromatic and aliphatic-C was confined between mineral assemblages exhibiting encrustation or geophysical occlusion in 2-5-μm pore spaces. The chemical form of mineral-associated organic matter appeared to be significantly altered between exterior and interior regions. Organic matter in exterior regions was highly processed; containing more carboxyl-C relative to aromatic-C. Organic matter in interior regions was more complex and contained significant amounts of aromatic and aliphatic-C. In this study, it is evident that the role

of chemical adsorption for C stabilization in microaggregates of soils dominated by 1:1 clay minerals may be diminished due to organic matter retention in pores. Mineral surface flaking was noticeable in pore regions and the scale of primary particle intimacy for nano aggregate formation-deformation is below the current scales of 20-250 μm postulated in many of the existing aggregation models. These findings provide only the first insights into C stabilization processes occurring in mineral-pore assemblages. Further STXM and NEXAFS studies incorporating N and O K-edge experiments are necessary in order to gain a complete understanding of the biogeocomplexity of soil microaggregates and their role in global C cycling.

REFERENCES

Ade H., X. Zhang, S. Cameron, C. Costello, J. Kirz, and S.Williams. 1992. Chemical contrast in x-ray microscopy and spatially resolved XANES spectroscopy of organic specimens. Science 258:972–975.

Ade, H., and S.G. Urquhart. 2002. NEXAFS spectroscopy and microscopy of natural and synthetic polymers. *In* T.K. Sham (ed.) Chemical applications of synchrotron radiation. World Scientific Publishing, River Edge, N J.

Albee, P.B., G.C. Stockman, and A.J.M. Smucker. 2000. Extraction of pores from microtomographic reconstructions of intact soil aggregates. ANL/MCS-P791-0200. Mathematics and Computer Sci. Div. Argonne Natl. Lab., Argonne, IL.

Amelung, W., K. Kaiser, G. Kammerer, and G. Sauer. 2002. Organic carbon at soil particle surfaces-evidence from X-ray photoelectron spectroscopy and surface abrasion. Soil Sci. Soc. Am. J. 66:1526-1530.

Beauchemin, S., D. Hesterberg, and M. Beauchemin. 2002. Principal component analysis approach for modeling sulfur K-XANES spectra of humic acids. Soil Sci. Soc. Am. J 66:83-91.

Benzerara, K., T.H. Yoon, T. Tyliszczak, B. Constantz, A.M. Spormann, and G. Brown. 2004. Scanning transmission X-ray microscopy study of microbial calcification. Geobiology 2:249-259.

Blanco-Canqui, H., and R. Lal. 2004. Mechanisms of carbon sequestration in soil aggregates. Crit. Rev. Plant Sci. 23:481-504.

Boese, J.M. 1996. X-ray absorption near edge structure of amino acids and peptides. M. A. thesis. Department of Physics, State University of New York. Stony Brook NY.

Boese, J., A. Osanna, C. Jacobsen, and J. Kirz. 1997. Carbon edge XANES spectroscopy of amino acids and peptides. J. Electr. Spectr. Rel. Phen. 85:9-15.

Boyce, C., G. Cody, M. Feser, C. Jacobsen, A. Knoll, and S. Wirick. 2002. Organic chemical differentiation within fossil plant cell walls detected with x-ray spectromicroscopy. Geology 30:1039-1042.

Brandes, J.A., C. Lee, S. Wakeham, M. Peterson, C. Jacobsen, S. Wirick, and G.D. Cody. 2004. Examining marine particulate organic matter at sub-micron scales using scanning transmission X-ray microscopy and carbon X-ray absorption near edge structure spectroscopy. Marine Chem. 92:107-121.

Braun, A., F.E. Huggins, N. Shah, Y. Chen, S. Wirick, S.B. Mun, C. Jacobsen and G.P. Huffman, 2005. Advantages of soft X-ray absorption over TEM-EELS for solid carbon studies - a comparative study on diesel soot with EELS and NEXAFS. Carbon 43:117-124.

Bronick, C.J., and R. Lal. 2005. Soil structure and management: a review. Geoderma. 124:3-22

Cody, G.D., H. Ade, S. Wirick, G.D. Mitchell, and A. Davis. 1998. Determination of chemical-structural changes in vitrinite accompanying luminescence alteration using C-NEXAFS analysis. Org. Geochem. 28:441-455.

Denef, K., and J. Six. 2005. Clay mineralogy determines the importance of biological versus abiotic processes for macroaggregate formation and stabilization. Eur. J. Soil Sci. 56:469-479.

Elliott, E.T., K. Paustian, and S.D. Frey. 1996. Modeling the measurable and measuring the modelable: A hierarchical approach to isolating meaningful soil organic matter fractionations. p. 161-179. *In* D.S. Powlson, P. Smith, and J.U.

Smith (eds.) Evaluation of soil organic matter models using existing long-term datasets. Springer-Verlag, Berlin. Germany

Flynn, G.J., L.P. Keller, M. Feser, S. Wirick, and C. Jacobsen. 2003. The origin of organic matter in the solar system: evidence from the interplanetary dust particles. Geochim. Cosmochim. Acta 67:4791-4806.

Flynn, G.F., L.P. Keller, C. Jacobsen, and S. Wirick. 2004. An assessment of the amount and types of organic matter contributed to the earth by interplanetary dust. Adv. Space Res. 33:57-66.

Guggenberger, G., B.T. Christensen, and W. Zech. 1994. Land use effects on the composition of organic matter in particle-size separates of soil I. Lignin and carbohydrate signature. Eur. J. Soil Sci. 45:449-458.

Hitchcock, A.P., C. Morin, Y.M. Heng, R.M. Cornelius, and J.L. Brash. 2002. Towards soft X-ray spectromicroscopy of biomaterials. J. Biomat. Sci. Polymer Ed. 13:919-938.

Hitchcock, A.P., H.D. Stöver, L.M. Croll, R.F. Childs. 2005. Chemical mapping of polymer microstructure using soft X-ray spectromicroscopy. Austr. J. Chem. 58:423–432.

Jacobsen, C., S. Wirick, G. Flynn, and C. Zimba. 2000. Soft X-ray spectroscopy from image sequences with sub-100 nm spatial resolution. J. Microsc. 197:173-184.

Kaiser, K., K. Eusterhues, C. Rumpel, G. Guggenberger, I. Kögel-Knabner. 2002. Stabilization of organic matter by soil minerals-investigations of density and particle-size fractions of two acid forest soils. J. Plant Nutr. Soil Sci. 165:451-459.

Kiem, R., and I. Kögel-Knabner. 2002. Refractory organic carbon in particle-size fractions of arable soils II: organic carbon in relation to mineral surface area and iron oxides in fractions <6 μm. Org. Geochem. 33:1699-1713.

Koprinarov, I.N., A.P. Hitchcock, C. McCrory and R.F. Childs. 2002. Quantitative mapping of structured polymeric systems using singular value decomposition analysis of soft X-ray images. J. Phys. Chem. B 106:5358-5364.

Leifeld, J., and I. Kögel-Knabner. 2003. Microaggregates in agricultural soils and their size distribution determined by X-ray attenuation. Eur. J. Soil Sci. 54:167–174.

Lerotic, M., C. Jacobsen, T. Schäfer, and S. Vogt. 2004. Cluster analysis of soft x-ray spectromicroscopy data. Ultramicroscopy 100:35-57.

Lerotic, M., C. Jacobsen, J.B. Gillow, A.J. Francis, S. Wirick, S. Vogt, and J. Maser. 2005. Cluster analysis in soft X-ray spectromicroscopy: finding the patterns in complex specimens. J. Electr. Spectr. Rel. Phen. 144-147C:1137-1143.

Lehmann, J., M.S. Cravo, and W. Zech. 2001. Organic matter stabilization in a Xanthic Ferralsol of the central Amazon as affected by single trees: chemical characterization of density, aggregate and particle size fractions. Geoderma 99:147-168.

Lehmann, J., B. Liang, D. Solomon, M. Lerotic, F. Luizão, J. Kinyangi, T. Schäfer, S. Wirick, and C. Jacobsen. 2005. Near-edge X-ray absorption fine structure (NEXAFS) spectroscopy for mapping nano-scale distribution of organic carbon forms in soil: Application to black carbon particles. Global Biogeochem. Cycles 19:1013-1025.

Mayer, L.M., L.L. Schick, K.R. Hardy, R. Wagai, and J.F. McCarthy. 2004. Organic matter content of small mesopores in sediments and soil. Geochim. Cosmochim. Acta 68:3863-3872.

Mikutta, C., F. Lang, and M. Kaupenjohann. 2004. Soil organic matter clogs mineral pores: evidence from ^{1}H-NMR and N_2 adsorption. Soil Sci. Soc. Am. J. 68:1853-1862.

Oades, J.M., and A.G. Waters. 1991. Aggregate hierarchy in soils. Austr. J. Soil Res. 29:815-828.

Ransom, B., R.J. Bennett, R. Baerwald, and K. Shea. 1997. TEM study of in situ organic matter on continental shelf margins: Occurrence and the "monolayer" hypothesis. Mar. Geol. 138:1–9.

Rothe, J., M.A. Denecke, and K. Dardenne. 2000. Soft X-ray spectromicroscopy investigation of the interaction of aquatic humic acid and clay colloids. J. Coll. Interface Sci. 231:91-97.

Schäfer, T., N. Hertkorn, R. Artinger, F. Claret, and A. Bauer. 2003. Functional group analysis of natural organic colloids and clay association kinetics using C (1s) spectromicroscopy. J. Phys. IV France. 104:409-412.

Scheinost, A.C., R. Kretzschmar, I. Christ, and C. Jacobsen. 2001. Carbon group chemistry of humic and fulvic acid: A comparison of C-1s NEXAFS and ^{13}C-NMR spectroscopies, p. 39-47. *In* E.A. Ghabbour, and G. Davies (eds.) Humic substances: structures, models and functions. Royal Soc. Chem., Gateshead, UK.

Schmidt, C., J. Thieme, U. Neuhäusler, C. Jacobsen, B. Kaulich, M. Salomée, and J. Susini. 2003. Spectromicroscopy of soil colloids. J. Phys. IV France. 104:405-408.

Six, J., H. Bossuyt, S. De Gryze, and K. Denef. 2004. A history of research on the link between (micro) aggregates, soil biota, and soil organic matter dynamics. Soil Till. Res. 79:7-31.

Smith, A.P., S.G. Urquhart, D.A. Winesett, G. Mithchell and H. Ade. 2001. Use of near-edge X-ray absorption fine structure spectromicroscopy to characterize multicomponent polymeric systems. Appl. Spectr. 55:1676-1681.

Sohi, S.P., N. Mahieu, J.R.M. Arah, D.S. Powlson, B. Madari and J.L. Gaunt 2001. A procedure for isolating soil organic matter fractions suitable for modeling. Soil Sci. Soc. Am. J. 65:1121-1128.

Soil Survey Staff. 2003. Keys to soil taxonomy. 9th ed. USDA-Soil Conservation Service, Pocahontas Press, Blacksburg, VA.

Sollins, P., P. Homann, and B.A. Caldwell. 1996. Stabilization and destabilization of soil organic matter: mechanisms and controls. Geoderma 74:65–105.

Solomon, D., J. Lehmann, J. Kinyangi, B. Liang, and T. Schäfer. 2005. Carbon K-edge NEXAFS and FTIR-ATR spectroscopic investigation of organic carbon speciation in soils. Soil Sci. Soc. Am. J. 69:107-119.

Stöhr, J. 1992. NEXAFS spectroscopy. Springer series in surface sciences 25, Springer, Berlin, Germany

Tisdall, J.M., and J.M Oades. 1982. Organic matter and water-stable aggregates in soils. J. Soil Sci. 33:141– 163.

Trumbore, S.E. 1993. Comparison of carbon dynamics in tropical and temperate soils using radiocarbon measurements. Global Biogeochem. Cycles 7:275–290.

Urquhart, S.G., and H. Ade. 2002 Trends in the carbonyl core (C 1s, O 1s) → π*C=O transition in the near-edge X-ray absorption fine structure spectra of organic molecules. J. Phys. Chem. B. 106:8531-8538.

Wander, M.M. 2004. Soil organic matter fractions and their relevance to soil function, p.67-102. *In* F. Magdoff, and R. Weil (eds.) Advances in agroecology. CRC Press, Boca Raton, FL.

Warwick, T., K. Franck, J.B. Kortright, G. Meigs, M. Moronne, S. Myneni, E. Rotenberg, S. Seal, W.F. Steele, H. Ade, A. Garcia, S. Cerasari, J. Denlinger, S. Hayakawa, A.P. Hitchcock, T. Tyliszczak, J. Kikuma, E.G. Rightor, H.J. Shin, and B.P. Tonner. 1998. A scanning transmission X-ray microscope for materials science spectromicroscopy at the Advanced Light Source. Rev. Sci. Instrum. 69:2964.

Zhang, X., R. Balhorn, J. Mazrimas, and J. Kirz. 1996. Mapping and measuring DNA to protein ratios in mammalian sperm head by XANES imaging. J. Struct. Biol. 116:335-344.

Zimmerman, A.R., K.W. Goyne, J. Chorover, S. Komarneni, and S. L. Brantley. 2004. Mineral mesopore effects on nitrogenous organic matter adsorption. Org. Geochem. 35:355-375.

CHAPTER 6

SUMMARY AND CONCLUSIONS

Land use conversion at the Kakamega-Nandi forest sites supported rapid C stock and nutrient loss rates. Soil C and N stocks were uncoupled to soil nutrient contents in cultivated soils of the agriculture ecosystem sites, where differences existed in the lag phase between their losses from surface soil. Close coupling of C and soil nutrients was attributed to organic matter mineralization and immobilization for C and N whereas uncoupling occurred after soil nutrients were released and became leached out of surface soils. For all agroecosystem sites, organic matter dependent charge compensated for the loss in cation charge, providing buffering capacity to reduce soil acidity at heavy-textured North Nandi sites and permitting only gradual modest soil acidity increase at heavy-textured South Nandi and medium-textured Kakamega sites. Although loss pathways differed among organic (C, N) and inorganic elements (P, Ca, Mg, K), the degrading heavy-textured Nandi soils cascade from high to medium and low C stocks and nutrient equilibria, while medium-textured Kakamega soil instead transitions from medium to low equilibrium of C stocks. These data provided important information about biogeochemical characteristics of degrading soil in a highland tropical ecosystem. Our knowledge of these processes should lead to a better understanding of the long-term nutrient losses as well as the nature and timing of C and nutrient repletion required to reverse soil degradation and its implication for global cycles of elements in terrestrial and aquatic ecosystems

After assessing the long-term changes to C and N content in SOM pools as indicators of thresholds, we determined that C and N loss upon forest conversion represented a rapid and abrupt change, causing a large shift in the total soil C and N content. Slow persistent changes in the stable organomineral pool occurred at an order

of magnitude higher than C and N losses sustained in the unstable and stable aggregate soil C pools. By using a threshold loss equilibrium indicator (EQD) we concluded that only recoveries matching the loss and inputs into the stable organomineral fraction can shift the soil degradation threshold in response to organic matter inputs under cultivation agriculture. For all agroecosystem sites, a C and N loss in the organomineral associated organic matter was not stabilized over a longer time scale of 100 years. Unstable and stable aggregate pools accounted for a small fraction of the total C in soil and their low equilibrium indicates that their functional recovery is dependent on drastic change in inputs and management

For the specific assessment of C stabilization in the organomineral assemblage, both XPS narrow and wide scan measurements showed that the long term molecular alteration from cultivation agriculture causes a near 8-fold increase in organic C oxidation. Micro-FTIR chemigram profiles pointed to the fact that, a large fraction of the mineral assemblage may not be associated with C but rather, patchy “hotspots” were both organic and organomineral forms embedded in pore spaces. Kaolinite mineral and organic C reactions were controlled by hydroxylation. We concluded that mineral and C molecular interactions were dependent on the –OH hydroxylation sphere potential. Overall, long-term cultivation, involved the enrichment of aliphatic –CH as well as the depolymerization of aromatics and hydrolysis of amide N–C=O alongside the oxidation of C–O[H] forms of carbohydrate derivatives and amide I protein mixtures of MOM. Using STXM and C 1s-NEXAFS, we were able to visualize for the first time, the undisturbed intact microaggregate assembly and to resolve C functional forms at spatial resolutions that have not been feasible up to now with established methodological approaches.

APPENDIX A

Data table for chapter 2, Figure 2-3

Site	Yrs	C stock kg m^{-2}	stderr
Kakamega	0	6.5	0.7
	3	5.0	0.4
	8	4.2	0.3
	19	3.6	0.4
	31	2.5	0.3
	50	2.0	0.3
	77	1.6	0.1
	104	2.0	0.1
North Nandi	0	7.3	0.7
	3	6.1	0.7
	7	5.0	0.4
	19	5.3	0.3
	25	4.0	0.4
	52	3.7	0.3
	70	3.1	0.3
	111	4.5	0.3
South Nandi	0	4.2	0.9
	4	2.8	0.1
	9	2.5	0.2
	20	2.0	0.3
	28	2.8	0.6
	50	2.0	0.2
	57	1.7	0.3
	71	1.3	0.3
	104	1.6	0.1

Data table for chapter 2, Figure 2-3 contd.

Site	Yrs	N stock kg m^{-2}	stderr
Kakamega	0	0.69	0.1
	3	0.54	0.1
	8	0.40	0.0
	19	0.33	0.1
	31	0.21	0.0
	50	0.18	0.0
	77	0.12	0.0
	104	0.17	0.0
North Nandi	0	0.70	0.0
	3	0.58	0.1
	7	0.49	0.0
	19	0.49	0.0
	25	0.38	0.0
	52	0.37	0.0
	70	0.30	0.0
	111	0.45	0.0
South Nandi	0	0.45	0.1
	4	0.28	0.0
	9	0.22	0.0
	20	0.18	0.0
	28	0.18	0.0
	50	0.19	0.0
	57	0.15	0.0
	71	0.10	0.0
	104	0.14	0.0

Data table for chapter 2, Figure 2-4

Site	Years	Mean 13C	SED 13C
Kakamega	0	-25.3	0.4
	3	-24.3	0.1
	8	-19.8	0.3
	19	-20.8	0.7
	31	-18.6	0.2
	50	-19.4	0.2
	77	-17.7	0.3
	104	-18.1	0.3
North Nandi	0	-25.4	0.2
	3	-24.8	0.2
	7	-23.2	0.9
	19	-21.2	1.2
	25	-19.6	0.8
	52	-18.4	0.4
	70	-18.0	0.3
	111	-17.4	1.1
South Nandi	0	-26.6	0.2
	4	-23.8	0.2
	9	-21.2	0.4
	20	-20.3	0.9
	28	-19.9	1.0
	50	-19.9	0.8
	57	-20.6	0.6
	71	-18.4	0.1
	104	-19.5	0.4

Data table for chapter 2, Figure 2-4

Site	Yrs	15N	stderr
Kakamega	0	5.63	0.2
	3	6.27	0.2
	8	7.02	0.2
	19	6.47	0.0
	31	7.49	0.2
	50	7.28	0.2
	77	7.19	0.6
	104	7.86	0.5
North Nandi	0	4.94	0.3
	3	5.53	0.2
	7	5.60	0.2
	19	6.51	0.4
	25	6.62	0.1
	52	6.69	0.2
	70	6.59	0.3
	111	6.49	0.1
South Nandi	0	5.46	0.1
	4	*	*
	9	6.17	0.2
	20	6.75	0.1
	28	6.99	0.2
	50	6.85	0.5
	57	6.68	0.3
	71	6.56	0.9
	104	6.84	0.1

Data table for chapter 2, Figure 2-5

Site	Years	N (%)	SED N	Years	15N	SED 15N
South Nandi	0	0.70	0.06	0.00	5.60	0.19
	3	0.54	0.07	3.25	6.27	0.16
	8	0.41	0.02	8.00	6.89	0.22
	19	0.33	0.05	18.67	6.39	0.09
	31	0.22	0.03	30.80	7.23	0.20
	50	0.18	0.02	50.00	7.23	0.22
	77	0.12	0.02	77.40	6.64	0.70
	104	0.17	0.01	104.00	8.05	0.46
North Nandi	0	0.75	0.06	0.00	4.67	0.30
	3	0.59	0.05	2.78	5.66	0.27
	7	0.49	0.04	7.00	5.60	0.23
	19	0.49	0.04	19.00	5.34	0.15
	34	0.43	0.04	34.00	6.69	0.12
	53	0.32	0.03	52.86	6.24	0.28
	72	0.30	0.04	71.50	6.75	0.35
	114	0.45	0.03	114.00	6.49	0.10
Kakamega	0	0.45	0.12	0.00	5.46	0.13
	4	0.26	0.04	3.75	6.48	0.81
	9	0.21	0.03	9.00	5.90	0.25
	20	0.21	0.03	19.60	6.71	0.13
	27	0.18	0.01	26.50	6.96	0.22
	50	0.19	0.02	50.00	6.52	0.53
	64	0.16	0.03	63.50	7.18	0.23
	104	0.14	0.01	104.00	6.27	0.34

Data table for chapter 2, Figure 2-7

Kakamega	Years	P mg kg^{-1}	Mg mmolc	K mmolc	Ca mmolc
	2	15.8	45.2	19.0	245.0
	2	9.8	36.1	15.8	180.1
	4	5.4	21.5	10.5	121.6
	5	7.5	9.7	12.1	54.9
	17	5.9	6.6	7.0	35.6
	18	6.0	6.6	5.4	32.8
	18	4.1	8.7	6.4	46.4
	28	2.5	11.3	5.8	39.8
	30	5.4	9.4	6.8	43.5
	31	2.7	20.8	6.0	80.2
	38	2.7	13.1	6.5	44.2
	43	3.7	12.5	2.7	58.4
	45	8.9	4.4	2.4	19.7
	47	*	7.8	3.3	37.9
	53	*	8.6	3.9	39.9
	73	3.8	5.3	4.5	18.2
	73	10.8	1.7	6.6	4.3
	81	8.1	8.2	5.8	28.7
	82	1.3	15.8	6.5	62.3
	104	5.1	6.9	5.5	31.6
	104	2.3	9.4	5.5	35.9
	104	1.5	24.3	10.0	89.0

Data table for chapter 2, Figure 2-7 contd.

North Nandi	Years	P mg kg^{-1}	Mg mmolc	K mmolc	Ca mmolc
	4	29.9	40.8	7.6	116.9
	4	32.9	39.8	6.7	155.6
	4	22.0	26.9	5.1	99.8
	5	9.3	21.7	6.1	88.0
	9	26.7	21.8	5.4	81.5
	19	5.3	16.4	4.1	120.7
	19	6.8	28.0	9.1	152.6
	19	3.1	26.1	8.9	94.2
	19	18.7	28.3	6.5	123.9
	19	16.1	42.6	7.2	149.6
	32	*	40.7	*	88.4
	34	8.0	12.1	8.0	32.4
	34	9.1	24.4	7.4	66.6
	48	11.1	10.8	4.9	39.0
	52	5.5	14.7	7.0	45.1
	54	6.1	17.6	8.0	45.9
	54	8.3	9.0	5.6	23.1
	54	8.8	10.9	5.0	35.9
	54	15.5	16.5	6.9	36.1
	64	10.0	12.9	3.9	27.0
	74	23.4	9.6	5.5	24.3
	74	16.9	18.1	5.6	70.5
	114	13.4	35.1	*	63.5
	114	17.4	23.1	7.1	79.3
	114	7.0	15.0	4.5	49.6

Data table for chapter 2, Figure 2-7 contd.

South Nandi	Years	P mg kg^{-1}	Mg mmolc	K mmolc	Ca mmolc
	4	5.0	3.8	1.3	24.8
	4	8.0	13.3	2.9	23.3
	4	10.6	3.4	1.1	16.5
	9	6.1	6.6	1.3	20.0
	9	4.6	11.2	1.7	23.7
	9	12.3	3.9	0.9	18.4
	9	8.5	*	*	*
	19	3.2	2.1	0.7	13.3
	19	2.0	*	*	*
	19	7.8	4.9	1.1	11.4
	19	8.1	5.3	1.5	24.1
	22	3.5	0.5	0.2	5.4
	27	7.5	3.5	1.4	13.9
	30	8.7	7.9	*	62.2
	44	2.5	0.8	0.3	2.5
	54	7.4	8.6	0.9	23.8
	54	7.6	6.5	1.0	12.9
	54	1.9	1.5	1.2	7.0
	57	5.2	4.3	1.1	12.9
	57	9.8	6.8	1.6	18.5
	74	3.8	0.8	0.5	2.8
	74	16.0	1.2	0.5	4.9
	104	11.7	4.6	1.7	15.0
	104	1.3	*	*	*
	104	7.3	5.8	0.9	11.3
	104	7.4	1.5	0.7	6.0

Data table for chapter 2, Figure 2-8

Kakamega		North Nandi		South Nandi	
Yrs	Soil pH	Yrs	Soil pH	Yrs	Soil pH
0	6.67	0	7.3p	0	6.25
0	6.20	0	7.66	0	6.52
3	6.55	0	7.25	3	5.89
4	6.15	3	7.34	4	5.74
18	5.48	4	6.98	4	6.10
19	5.50	4	7.6	4	6.29
29	6.00	4	7.00	9	5.9
31	5.69	5	6.23	9	5.94
32	6.04	7	7.08	9	6.18
44	5.79	9	6.88	19	6.16
46	5.35	19	*	19	5.87
48	5.54	19	7.16	19	6.18
54	6.05	19	6.35	22	6.03
74	4.99	19	6.5	27	5.61
74	4.61	34	6.21	30	6.28
82	5.69	34	5.76	44	5.51
83	5.90	48	5.97	54	5.57
104	5.33	52	6.25	54	6.10
104	5.37	54	6.29	54	5.59
*	*	54	5.84	57	5.9
*	*	64	5.6	57	5.62
*	*	74	5.97	74	5.28
*	*	74	6.50	104	5.48
*	*	114	6.19	104	5.71
*	*	114	6.28	104	5.54
*	*	114	6.13	104	5.53
*	*	*	*	104	5.77